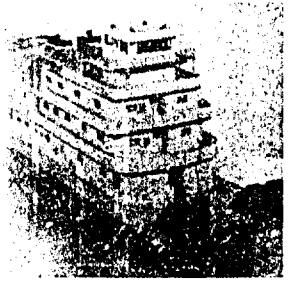


REPAIR, EVALUATION, MAINTENANCE, AND  
REHABILITATION RESEARCH PROGRAM

TECHNICAL REPORT REMR-HY-4

EFFECTS OF GEOMETRY ON THE KINETIC  
ENERGY OF A TOWBOAT AND BARGES  
IN A NAVIGATION LOCK

AD-A207 057



by  
Sandra K. Martin

Hydraulics Laboratory



DEPARTMENT OF THE ARMY  
Waterways Experiment Station, Corps of Engineers  
PO Box 631, Vicksburg, Mississippi 39181-0631



March 1989  
Final Report

Approved For Public Release; Distribution Unlimited

DTIC  
ELECTE  
APR 24 1989  
S E D



Prepared for DEPARTMENT OF THE ARMY  
US Army Corps of Engineers  
Washington, DC 20314-1000  
Under Civil Works Research Work Unit 32922

089 4 24 200

Unclassified

SECURITY CLASSIFICATION OF THIS PAGE

REPORT DOCUMENTATION PAGE				Form Approved OMB No. 0704-0188	
1a. REPORT SECURITY CLASSIFICATION <b>Unclassified</b>			1b. RESTRICTIVE MARKINGS		
2a. SECURITY CLASSIFICATION AUTHORITY		3. DISTRIBUTION / AVAILABILITY OF REPORT Approved for public release; distribution unlimited.			
2b. DECLASSIFICATION / DOWNGRADING SCHEDULE					
4. PERFORMING ORGANIZATION REPORT NUMBER(S) Technical Report REMR-HY-4			5. MONITORING ORGANIZATION REPORT NUMBER(S)		
6a. NAME OF PERFORMING ORGANIZATION USAEWES Hydraulics Laboratory		6b. OFFICE SYMBOL (if applicable) CEWES-HS-L	7a. NAME OF MONITORING ORGANIZATION		
6c. ADDRESS (City, State, and ZIP Code) PO Box 631 Vicksburg, MS 39181-0631			7b. ADDRESS (City, State, and ZIP Code)		
8a. NAME OF FUNDING / SPONSORING ORGANIZATION US Army Corps of Engineers		8b. OFFICE SYMBOL (if applicable)	9. PROCUREMENT INSTRUMENT IDENTIFICATION NUMBER		
8c. ADDRESS (City, State, and ZIP Code) Washington, DC 20314-1000		10. SOURCE OF FUNDING NUMBERS See reverse.			
		PROGRAM ELEMENT NO.	PROJECT NO.	TASK NO.	WORK UNIT ACCESSION NO.
11. TITLE (Include Security Classification) Effects of Geometry on the Kinetic Energy of a Towboat and Barges in a Navigation Lock					
12. PERSONAL AUTHOR(S) Martin, Sandra K.					
13a. TYPE OF REPORT Final report		13b. TIME COVERED FROM _____ TO _____		14. DATE OF REPORT (Year, Month, Day) March 1989	15. PAGE COUNT 109
16. SUPPLEMENTARY NOTATION A report of the Hydraulics Problem Area of the Repair, Evaluation, Maintenance, and Rehabilitation (REMR) research program. Available from National Technical Information Service, 5285 Port Royal Road, Springfield, VA 22161. (Continued)					
17. COSATI CODES			18. SUBJECT TERMS (Continue on reverse if necessary and identify by block number)		
FIELD	GROUP	SUB-GROUP	Attached mass	Lock geometry	
			Kinetic energy	Towboats	
			Lock barriers		
19. ABSTRACT (Continue on reverse if necessary and identify by block number) The structural design of elements such as miter gates or protective barrier systems on locks requires that the total energy expected to be produced by a vessel impacting these structures be known by the engineer. In addition to the simple kinetic energy produced by a vessel's movement as related to its mass and speed, there are complicated hydrodynamic forces, including drag and wave propagation, which can affect the total energy of the moving vessel, especially as it enters or travels through geometrically restrictive areas such as lock chambers. In several previous studies, the mass of the system has been arbitrarily increased to account for the hydrodynamic forces. Specific relationships have not been developed to quantify the effective increase in energy as a function of vessel speed, mass, and surrounding geometry.  (Continued)					
20. DISTRIBUTION / AVAILABILITY OF ABSTRACT <input checked="" type="checkbox"/> UNCLASSIFIED/UNLIMITED <input type="checkbox"/> SAME AS RPT. <input type="checkbox"/> DTIC USERS			21. ABSTRACT SECURITY CLASSIFICATION Unclassified		
22a. NAME OF RESPONSIBLE INDIVIDUAL			22b. TELEPHONE (Include Area Code)	22c. OFFICE SYMBOL	

DD Form 1473, JUN 86

Previous editions are obsolete.

SECURITY CLASSIFICATION OF THIS PAGE

Unclassified

10. WORK UNIT ACCESSION NO. (Continued).

Funding provided by Repair, Evaluation, Maintenance, and Rehabilitation research program Work Unit No. 32322, sponsored by the Headquarters, US Army Corps of Engineers.

16. SUPPLEMENTARY NOTATION (Continued).

Originally submitted in partial fulfillment of the requirements for the degree of Master of Science to Mississippi State University, Mississippi State, MS.

19. ABSTRACT (Continued).

This research defines empirically the hydrodynamic energy produced by a high-mass, low-velocity vessel as it travels into the geometrically restrictive conditions imposed by a lock chamber, and compares it to the theoretical potential energy of an instrumented test cable designed to react equally and opposite to the vessel energy at the moment of peak impact. Specifically, the energy measured in the resisting system was compared to the expected energy of a vessel traveling at a known velocity with a known mass. The empirical tests were conducted in a 1:25-scale physical model of a lock chamber and with a 1:25-scale remote-operated towboat and push barges that replicate a typical size United States navigation lock facility and vessel. As the model tow traveled into the lock chamber and impacted a rigidly affixed test cable placed in the tow's path, impact parameters were monitored including tension in the cable with time, angles formed at the reactions due to deflection with time, and the approaching speed of the tow.

Appendix A presents additional data obtained during testing.

(S)

PREFACE

This study was conducted from October 1984 through January 1988 by personnel of the Locks and Conduits Branch (LCB), Hydraulic Structures Division (HSD), Hydraulics Laboratory (HL), US Army Engineer Waterways Experiment Station (WES), Vicksburg, MS, under the Repair, Evaluation, Maintenance, and Rehabilitation (REMR) research program sponsored by the Headquarters, US Army Corps of Engineers (USACE). Funding was provided under Civil Works Research Work Unit 32322, "Lock Gate Impact Barriers."

The work was conducted by Ms. Sandra K. Martin, LCB, under the general supervision of Messrs. Frank A. Herrmann, Chief, HL; and Richard A. Sager, Assistant Chief, HL; Glenn A. Pickering, Chief, HSD; and John F. George, Chief, LCB. Special guidance was also provided by Dr. Sam Kiger and Mr. Frank Dallriva of the Structures Laboratory (SL) at WES.

The REMR Directorate of Research and Development Coordinator in USACE was Mr. Jesse A. Pfeiffer, Jr., and members of the REMR Overview Committee were Mr. James E. Crews, Chairman, and Dr. Tony C. Liu. Mr. Glenn Drummond, USACE, was Technical Monitor for the Hydraulics Problem Area. The REMR Program Manager was Mr. William F. McCleese, SL, and the Problem Area Leader was Mr. Pickering. This report was written by Ms. Martin and edited by Mrs. Marsha C. Gay, Information Technology Laboratory, WES.

This report was also submitted to the Academic Faculty of Mississippi State University, Mississippi State, MS, in partial fulfillment of the requirements for the degree of Master of Science.

COL Dwayne G. Lee, EN, is the Commander and Director of WES.  
Dr. Robert W. Whalin is the Technical Director.

CG...  
INSPECTE...  
4

Accession For	
NTIS GRA&I	<input checked="" type="checkbox"/>
DTIC TAB	<input type="checkbox"/>
Unannounced	<input type="checkbox"/>
Justification	
By _____	
Distribution/	
Availability Codes	
Dist	Avail and/or Special
A-1	

## CONTENTS

	Page
PREFACE.....	1
CONVERSION FACTOR, NON-SI TO SI (METRIC) UNITS OF MEASUREMENT.....	3
PART I: INTRODUCTION.....	4
Background.....	4
Establishment of Physical Model Criteria.....	5
Physical Model Study Objectives.....	8
PART II: THE TESTING FACILITY.....	9
Physical Model Components.....	9
Testing Apparatus.....	12
In-Place Calibration of the Cable Assembly.....	16
PART III: THEORY.....	21
Dynamics.....	21
Hydrodynamic Theory.....	32
PART IV: TESTING PROGRAM.....	40
Independent Variables.....	40
Operation of the Tow.....	43
Dependent Variables.....	44
Testing Sequence.....	45
PART V: DATA REDUCTION.....	46
Conversion of Data to Engineering Units.....	46
Calculation of Force, Energy, and Impulse.....	48
Sample Data Curves.....	48
Summary Data of Peak Results.....	51
PART VI: COMPARISON OF EXPERIMENTAL DATA.....	54
Force and Energy Versus Velocity for Variable Mass.....	54
Force and Energy Versus Velocity for Variable Barge Widths.....	54
Force and Energy Versus Velocity for Flat Floor and Sill.....	58
Effects of Tow Operation on Velocity.....	58
Results.....	62
PART VII: COMPARISON OF THEORETICAL TO EXPERIMENTAL RESULTS.....	65
Force Comparisons.....	65
Energy Comparisons.....	65
Impulse Comparisons.....	69
Results.....	69
PART VIII: CONCLUSIONS.....	78
REFERENCES.....	81
TABLES 1-5	
APPENDIX A: SUPPLEMENTARY DATA.....	A1
APPENDIX B: NOTATION.....	B1

CONVERSION FACTORS, NON-SI TO SI (METRIC)  
UNITS OF MEASUREMENT

Non-SI units of measurement used in this report can be converted to SI (metric) units as follows:

<u>Multiply</u>	<u>By</u>	<u>To Obtain</u>
degrees (angle)	0.01745329	radians
feet	0.3048	metres
foot-pounds (force)	1.355818	joules
horsepower (550-foot-pounds (force) per second)	745.6999	watts
inches	2.54	centimetres
pounds (force)	4.448222	newtons
pounds (force) per square inch	6.894757	kilopascals
pounds (mass)	0.4535924	kilograms
pounds (mass) per cubic foot	16.01846	kilograms per cubic metre
ounces (mass)	28.34952	grams
square feet	0.09290304	square metres

EFFECTS OF GEOMETRY ON THE KINETIC ENERGY OF  
A TOWBOAT AND BARGES IN A NAVIGATION LOCK

PART I: INTRODUCTION

Background

1. Vessel impact often damages gates at US Army Corps of Engineers navigation locks, necessitating costly repairs to towboats, barges, and cargo, as well as to the gates themselves. Shipping interests incur additional expenses due to delays while waiting for repairs. Property damage resulting from flooding in instances of complete failure of a gate can translate into extensive monetary losses. The objective of this research program currently in progress at the US Army Engineer Waterways Experiment Station is to develop a means to protect lock gates from vessel impact and thereby reduce or eliminate the resulting damage (Martin 1986).

2. The total approach taken to accomplish this objective basically encompassed two tasks: a literature search and a quantitative physical model study. The first task, an extensive literature search, assessed the accidents at Corps inland waterways locks, identified an assortment of impact barriers common to locks abroad, and provided diverse theory relating to the hydrodynamics of vessels in locks. The accident data provided economic criteria with which to evaluate potential benefits of a barrier system. The information regarding barrier types was used to select suitable operational mechanics for possible implementation on United States navigation locks (Martin, in preparation). The literature regarding hydrodynamics established the purpose of this paper: the definition of the relationship between lock geometry and the kinetic energy of a tow and barges.

3. The second task was to quantify the energy produced by a barge train in the restrictive geometry imposed by a lock chamber and compare this energy to variable test conditions and to kinetic energy calculated based on the tow's approach speed and mass. This task was accomplished using a 1:25-scale physical model study in which a typical lock chamber and tow were equipped with a test cable instrumented to measure the actual force produced by several

tow types with differing masses and configurations contacting the test cable at various approach speeds.

4. While the ultimate product obtained for the research program will be design criteria for a structural alternative such as an impact barrier or fendering system, imperative to the successful design of this structure is an accurate determination of the kinetic energy produced by a barge in a lock chamber. This report describes in detail the testing and results, as well as the theory related to this phenomenon.

#### Establishment of Physical Model Criteria

5. The approach taken to perform the model study required that a few fundamental procedures and base assumptions be established. These items include selection of the dimensions of the lock, an operation scheme for the tow, and the creation of a testing procedure with accurate repeatability.

6. A 1:25-scale model of a lock having prototype dimensions of 110 ft\* in width and a nominal chamber length of 600 ft was selected as it is typical of Corps locks found on the Arkansas, Illinois, Upper Mississippi, Tennessee, and Tennessee-Tombigbee waterways. These locks are authorized for 9-ft navigation drafts and vary in lift from approximately 15 ft to 100 ft. Likewise, the prototype towboat, which operates with twin screws rated at 4,300 hp, was selected because it also is typical of those found on these waterways.

7. The tests were conducted under two basic lock floor conditions: either with a flat floor that extended from the downstream miter gate to the upstream approach or with a raised sill placed at the station in which the upstream miter gate would exist in the prototype. The flat floor provided a base condition in which the pool was of sufficient depth so that propellers on the towboat could operate efficiently. The sill was raised to a height at which the ratio of the depth of pool over the sill to the draft of the tow was 1.5. This ratio has been found in literature to be a standard for which channel depths are designed and one in which the tow begins to behave peculiarly (Kooman 1973). Tests conducted with the sill in place were compared to tests conducted with flat floor conditions to measure the effects of sill heights on the energy of the tow.

---

\* A table of factors for converting non-SI units of measurement to SI (metric) units is found on page 3.

8. All tests were conducted as the tow entered from the upstream approach with the upstream gates open, traveled into the chamber, and contacted a test cable approximately 1 ft (25 ft prototype) upstream of the downstream miter gate. Although accidents involving collision of tows with miter gates can occur on either gate from upstream or downstream, testing of the downstream gate by an upstream tow was chosen for several reasons. The most catastrophic scenario was the one chosen for testing because failure of the downstream gate could result in potential loss of pool and flooding downstream. Secondly, literature revealed that this location was the most common for barrier systems. Additionally, systems designed for this location could be readily modified for other locations as well. Finally, the primary reason for performing the testing at this location was that the operational behavior of the tow as it crossed the upstream sill and entered the restrictive width imposed by the chamber walls was drastically different from its characteristic behavior during travel in the open channel and pool approaches. The "behavior" of the tow includes effects of the lock dimensions on tow speed, the tendency of the tow to "push" water at its bow creating a translatory wave, and the phenomenon known as tow squat where the tow lowers in the water (Maynord 1987).

9. The model study was not designed to measure the latter two phenomena directly, but rather to define these effects empirically as a coefficient of kinetic energy or coefficient of attached mass. To simplify the measurement of the kinetic energy, a triangular projection was installed on the lead barge so that contact with the cable occurred at one point instead of being distributed along the length of the cable. The testing was designed to measure the velocity of the tow at midchamber, the velocity of the tow just prior to impact, the tension in the test cable during the impact, the deflection of the cable, and the speed at which the cable moved. After the tension in the cable, the deflection of the cable, and the point at which the tow contacted the cable were determined, the total force applied by the approaching tow and barges was then calculated.

10. The towboat followed the same operation for each test. The bow of the lead barge was placed approximately 35 ft upstream of the downstream miter gate and aligned with the upstream guide wall (Figure 1). At that point, from a dead start, the towboat was turned on and driven at a constant propeller speed until the lead barge was approximately 2.1 ft away from the test cable.

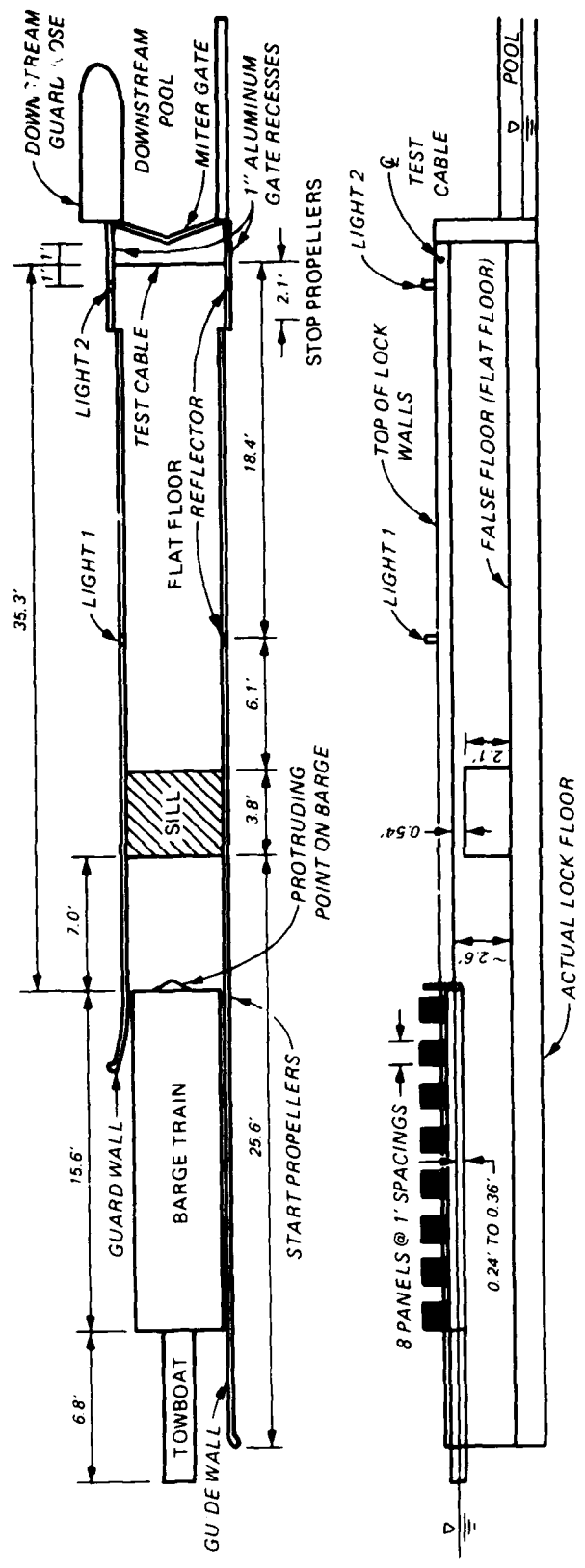


Figure 1. Schematic of model lock

At that time, the propellers were turned off and the boat coasted into the cable. Aligning the barge train along the guide wall not only made it possible to guide the tow uniformly into the chamber from test to test, but also reproduced a prototype condition in which the awaiting tow is typically moored to the upstream guide wall. The boat was allowed to coast into the barrier so that the testing apparatus could measure the deceleration of the tow without the effect of the engine horsepower. In actual situations, when collision with the gates is imminent, it was found that the operator often "kills" the engines or in some instances attempts reversal of the engines to minimize contact. The point at which such prototype tow operations occur is not only variable, but in most cases, unknown. A sensitivity test was performed in which the tow was driven into the chamber at a constant speed (during flat floor conditions), the propellers were turned off, and the tow was allowed to coast. The results indicated that the tow continued to coast at a constant speed for a distance much further than the coasting zone chosen in the model. Also apparent from operation of the tow with the sill in place, for the tow to pass over the sill without completely stopping, the engines had to remain on until the barges cleared the sill. The actual point at which the engines were turned off in the model was arbitrarily chosen to be 2.1 ft from the cable, and this distance remained consistent throughout the testing. In light of these considerations, the general test conditions prescribed are representative of actual locking conditions and tow operations, yet allow consistent replication of test procedures.

#### Physical Model Study Objectives

11. The specific objectives of this physical model effort are summarized as follows:

- a. To quantify an empirical coefficient of mass that lumps hydrodynamic effects into one term by comparing model measurements of force, energy, and impulse to theoretical values of the same.
- b. To assess what effects, if any, that variable geometric conditions of the lock and barges have on the relationship between force, energy, and tow velocity.

## PART II: THE TESTING FACILITY

### Physical Model Components

#### The lock

12. The physical model (Figure 2) replicated at a 1:25 scale the geometric, hydraulic, and operational components of a lock facility including the upstream pool, the guide wall and guard wall approaches, the lock chamber and miter gates, a longitudinal fill and empty system, and a section of the downstream pool. The model chamber dimensions were 4.4 ft wide by 24 ft long. The entire model was contained in a flume approximately 17 ft wide by 90 ft long. The model was equipped with two skimming weirs that maintained constant-level pools in the headbays and tailbays, and was supplied with water from a constant-head tank by a 12-in. valve. Figure 1 shows the basic flume with model dimensions.

#### The towboat

13. The towboat (Figure 3) was a radio-operated replica of the Corps towboat, the *Benyaard*. It was geometrically scaled down to be 6.8 ft long by 1.6 ft wide with a hull thickness of 0.44 ft. The boat was equipped with two 1/4-hp reversible motors that ran twin propellers 4.36 in. in diameter with five blades. There were two steering rudders and four flanking rudders.

#### The barges

14. Jumbo barges used during testing were each 7.8 ft long by 1.4 ft wide by 0.66 ft high (195 ft long by 35 ft wide by 16.5 ft high in the prototype). The barges were made of aluminum and were ballasted with lead ingots. A maximum of nine barges and a minimum of two barges were used during the testing with drafts varying from approximately 0.24 ft to 0.36 ft. Only data from tests with the 0.36-ft drafts will be used in this discussion; data from the tests conducted with a 0.24-ft draft and a nine-barge configuration are presented in Appendix A.

15. Modifications were made to several of the barges to aid in the data acquisition or as a result of the barge's enduring the impact with the test cable. A 1/4-in. aluminum plate the width of the barge by 2 ft in height, securely mounted to the front of the lead barge, provided an ultrasonic target for one of the instrumentation devices. Attached to this plate was the protruding triangular projection to acquire point contact with the cable. The



Figure 2. Lock testing facility

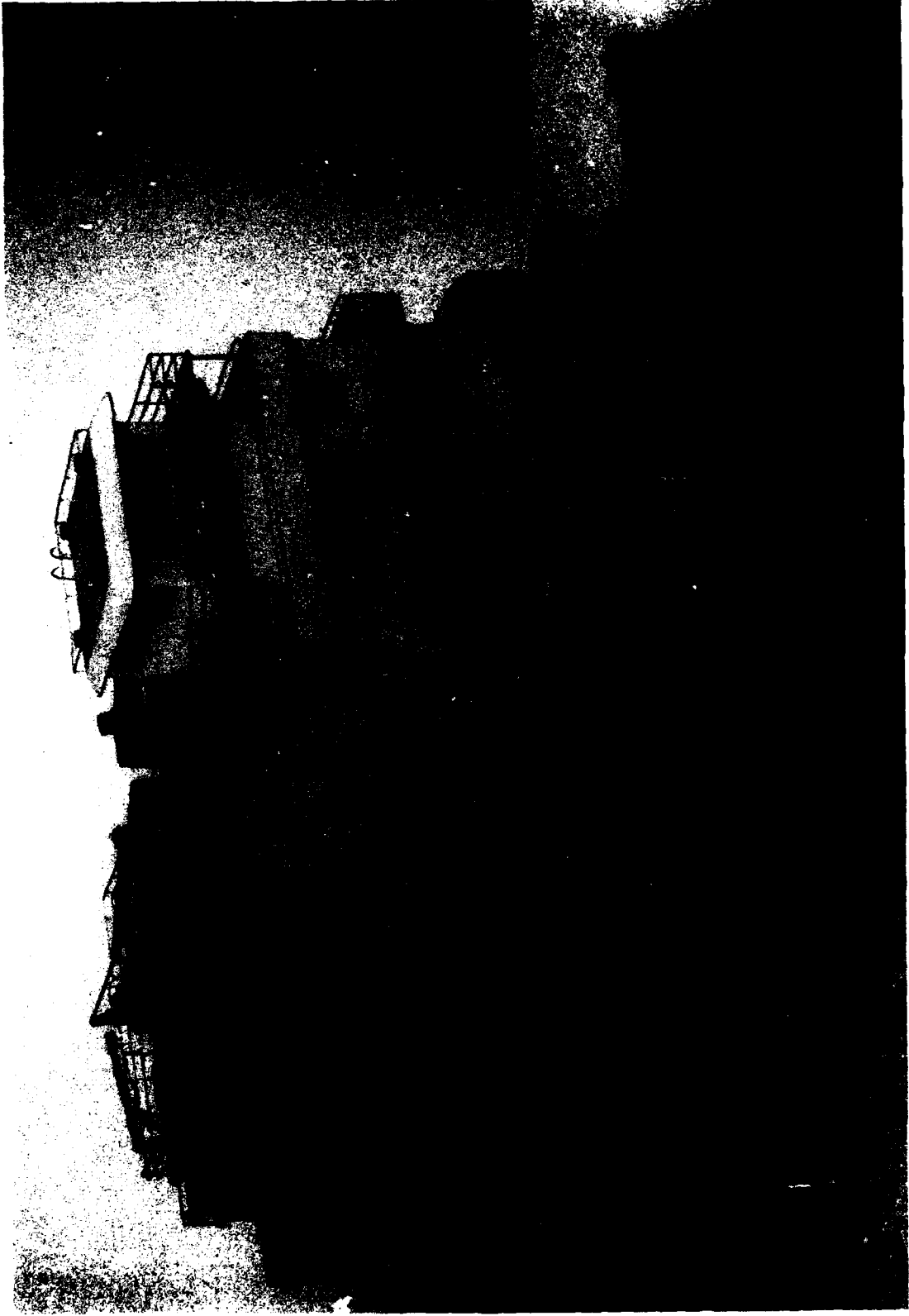


Figure 3. Remote-operated towboat

lead barge also had two aluminum angles attached lengthwise atop its frame and bolted to the plate to ensure rigidity and inhibit deformation upon impact. Two of the six barges had 1-ft-wide, black, sheet metal sections at 1-ft spacings attached to the top of the barges along the length of the barge train. As the tow moved into the lock chamber, these panels intercepted a light beam that was cast perpendicular to the lock walls. (More details on the black panels and the aluminum plate on the lead barge can be found in the section, "Velocity and Position Devices.")

### Testing Apparatus

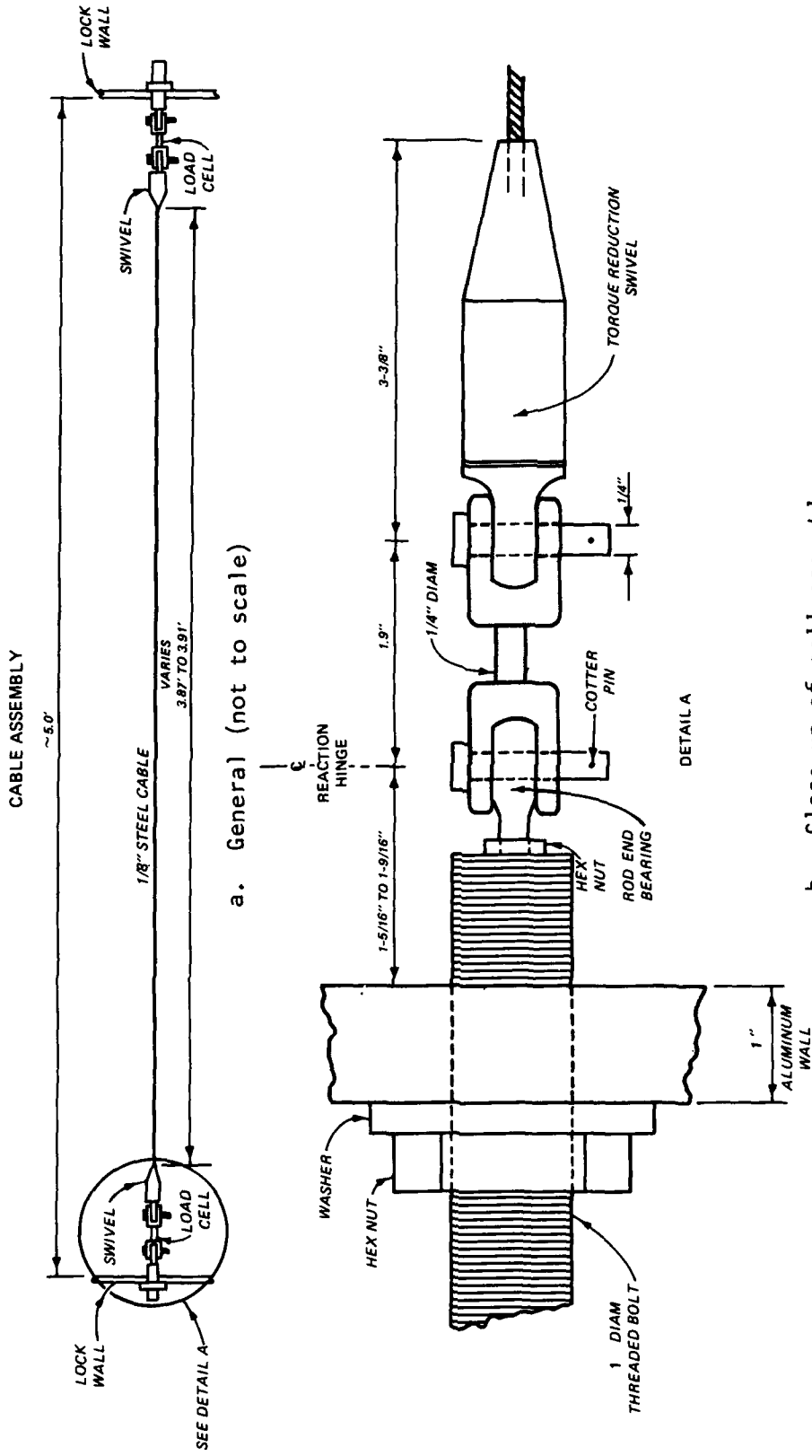
#### Restraining device

16. The restraining device selected for testing was a stainless steel cable with load cells affixed to either end and secured to the miter gate recesses. Specifically, the ends of a 1/8-in.-diam, 7- by 19-strand cable having a breaking strength of 1,760 lb and weighing 29 lb per 1,000 ft, were secured with epoxy into the socket caps of two eye shank torque reduction swivels. The load cells were pinned to the eye shanks of the swivels on one end and to rod end bearings on the other. The rod end bearings were attached to 1-in.-diam threaded bolts, which were in turn secured to the lock walls with washers and nuts. The model walls at the section of the testing apparatus were constructed of 1-in. aluminum plate with external bracing and an internal rod to provide stiffness to the system and prevent movement of the walls during impact of the tow with the cable. Figure 4 provides a sketch of the cable assembly and dimensions.

17. The load cells were calibrated to 2,000 lbs with less than 1 percent error. Each cell consisted of a 1/4-in.-diam steel shank with eight strain gages that compensated for any applied bending moments. The cells, however, were sensitive to torque; therefore, the swivels were added to the assembly. The two analog outputs from the cells were sent through amplifiers before input to the data acquisition system. In-place calibration of this assembly in regard to the cells is discussed in the section, "In-Place Calibration of the Cable Assembly."

#### Velocity and position devices

18. Three types of instruments were used to monitor velocity and position of the towboat and cable: a position/velocity transducer (PVT), an



b. Close-up of cell assembly  
 Figure 4. Cable assembly



with time prior to contact with the cable provided the approach velocity of the tow. Additionally, the ultrasonic readings provided a backup and cross-check measurement of the cable deflection.

21. The two retroreflective light beams sent out a digital pulse when the light beam was broken or reinstated. One light beam was stationed near the upstream end of the lock chamber on the lock wall with a reflector placed directly across from the beam on the opposite lock wall. The other was similarly mounted 1 ft upstream of the test cable. (See Figure 1 for location of these devices.) The light beams had dual purposes. By monitoring the on/off digital bits of the upstream light beam as the black 1-ft sections on the barges moved perpendicularly past the light beam, the midchamber speed of the tow could be determined. Both light beams were also used as digital "triggers" to begin a certain stage of the data acquisition.

#### Data acquisition equipment

22. A microcomputer system was chosen that was equipped with interface hardware and software to streamline data acquisition on the model study. The interface hardware was a plug-in board with eight analog-to-digital (A/D) input channels, two digital-to-analog (D/A) output channels, and eight digital input/output ports. Two software packages were used with this system. One drove the hardware, allowed for real-time display, and saved the data to files; and the other was a spreadsheet software used to analyze and plot the data. The instrumentation devices were wired to an external screw terminal connector, which was then linked to the hardware boards in the microcomputer via ribbon cables.

23. The menu-driven software was set up to perform the data acquisition as follows:

- a. Two channels were sampled at 20 samples a second for a duration of 2 min. One channel monitored the digital input port to which the most upstream light beam was connected. The other channel was a time channel that used the system clock and the demo board provided with the software to record the time at which the samples were taken. At the moment the lead barge broke the light beam, the slow-speed, long-duration data acquisition began; and by monitoring the on/off sequence as each 1-ft section on the barge passed the light beam, the velocity of the tow was determined.
- b. As the lead barge interrupted the light beam near the test cable, six additional channels were triggered to begin data acquisition. These channels collected data at a rate of 200 samples per second for a duration of 6 sec. Five of these

channels monitored the A/D channels, which contained the velocity tachometer, the position potentiometer, the two load cells, and the ultrasonic module. The sixth channel was a time channel corresponding to the higher sampling frequency.

- c. All data were saved into two data files, in a format compatible with the spreadsheet software, for later analysis and reduction.
- d. As the test was being conducted, a real-time display on the color monitor displayed the voltage inputs from the five A/D channels. This allowed immediate review of the test and the capability of deciding to proceed or make corrections to the equipment.

24. Sensitivity tests were performed to optimize efficient selection of sampling frequencies and durations so that all pertinent peaks and data were saved with a minimal amount of unnecessary data collection. The system performed efficiently and with a high degree of accuracy (Martin 1987).

#### In-Place Calibration of the Cable Assembly

25. Initial testing results indicated that some properties unique to the cable and cell assembly required an understanding of the static system. The static tests were conducted to ensure the confidence in the cable system to react equally and opposite to the force applied by the tow during dynamic tests.

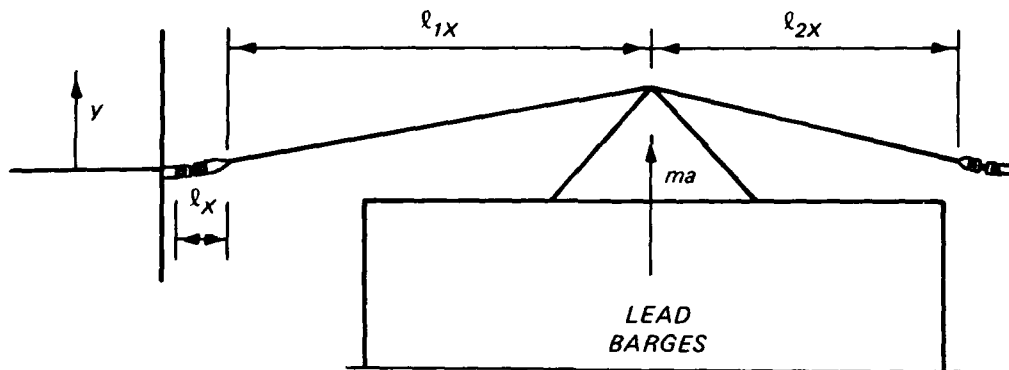
26. One of the properties observed during the initial tests was that the tension in the cable steadily dropped after each impact. Due to the lay of the twisted strands composing the cable, it was found that when the cable was repeatedly exercised, the resulting tension began to level out; that is, the strands seated themselves in a stable arrangement that produced more consistent results. Exercising was accomplished by first applying a pretension to the cable and then applying loads to the cable of up to 60 percent of its breaking strength. For instance, it was discovered that an ultimate pretension value of roughly 350-400 lb could be achieved by first tightening the cable to approximately 500 lb, then exercising it until the drops in tension began to stabilize at around 350 lb. The cable was exercised in both the static and the dynamic tests.

27. A static load-deflection curve was obtained through an in-place calibration test. The test was performed by mounting a steel hook equipped with a third load cell and position potentiometer on an I-beam. The whole

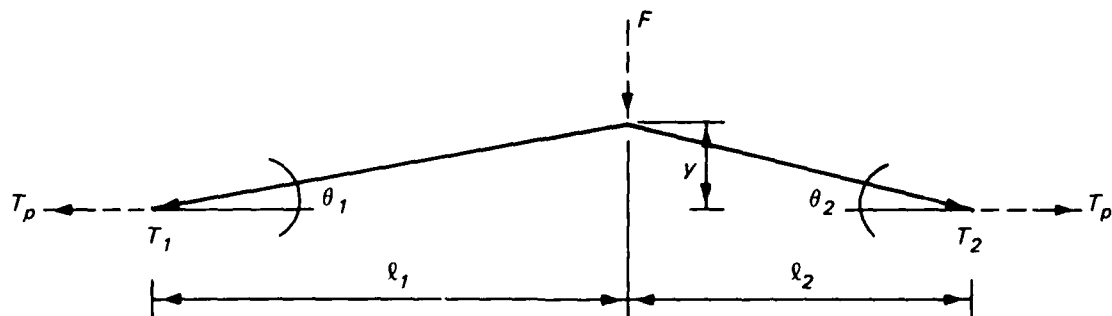
apparatus was supported by the lock walls and positioned such that the hook with load cell was placed directly over the cable and centered between the reaction hinges. (Only one of two test cables that were used in the dynamic tests was calibrated in this manner. The other had been disassembled prior to performance of this test.)

28. The data collected from the static test included the loads in cells 1 and 2 (representing the tension applied to the cable), the load applied at the center line (simulating the approximate location of the dynamic load), and the perpendicular displacement of the cable in the vertical resulting from the applied center-line load. (See Figure 6 for free body diagram.) The testing procedure was as follows:

- a. Prior to any tensioning of the cable, the zero readings of all three load cells were recorded.
- b. The cable was tightened without any center load and the tension in cells 1 and 2 were recorded.



a. TOW IMPACTING CABLE



b. FREE BODY DIAGRAM

Figure 6. Free body diagram

- c. The cable was then exercised by raising and lowering the hook attached to the center load with an electric motor until the two cells stabilized.
- d. The unloaded pretension was recorded. Then the motor raised the hook until 5 lb of force was applied to the center of the cable. Deflection and loads in all cells were recorded. The procedure continued at approximately 5- to 20-lb increments until the center load was approximately 180 lb and the deflection was slightly less than 3 in.

Two static tests were performed on this cable. The results of one test are found in Figure 7.

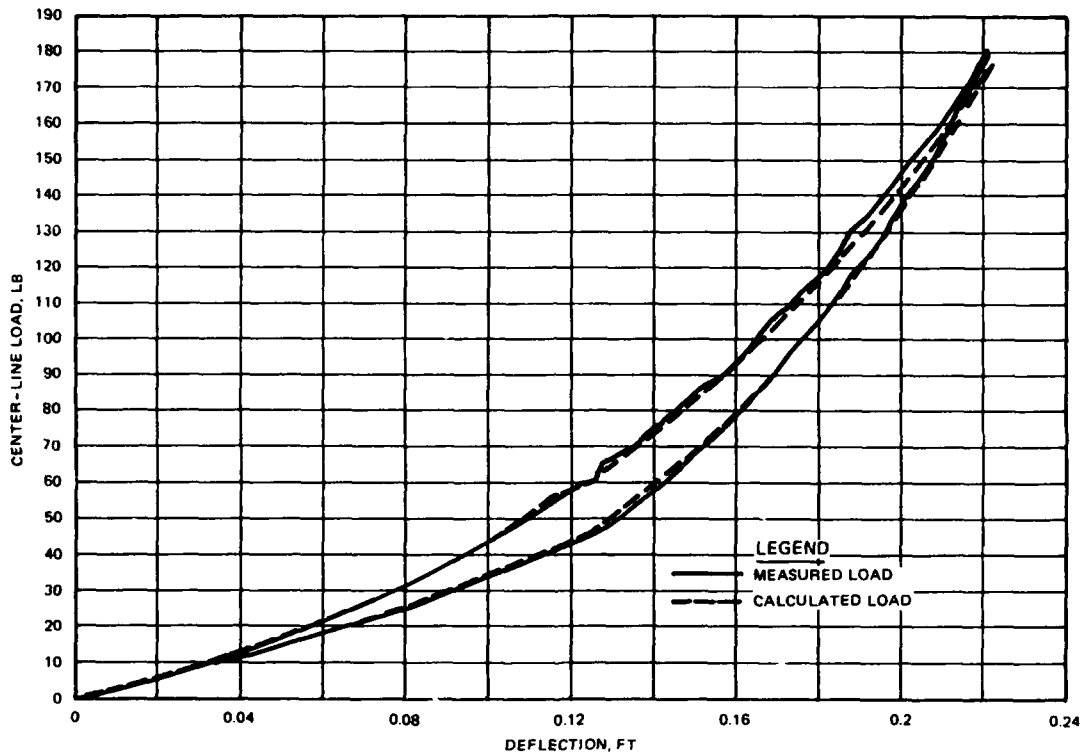


Figure 7. Static load test

29. To check the validity of the cells in the cable, the values obtained from cells 1 and 2 were used with the deflection values to calculate the expected center-line load, such that:

$$F = T_1 \sin \theta_1 + T_2 \sin \theta_2 \quad (1)$$

If  $\theta_1 = \theta_2 = \theta$ , as defined in Figure 6, this reduces to:

$$F = (T_1 + T_2) \sin \theta \quad (2)$$

where\*

$F$  = center-line force, pounds

$T_1$  = total tension recorded in cell 1, pounds

$T_2$  = total tension recorded in cell 2, pounds

$\sin \theta = \tan^{-1} (y/l)$  where  $y$  = deflection, feet

$l_1 = l_2 = l$  = length of cable from contact point to reaction hinge, feet

The values of  $T_1$  and  $T_2$  take into account the pretension  $T_p$  of the cable. By comparing actual center-line loads to calculated loads (see plots, Figure 7), it was concluded that data obtained from the load cells during dynamic tests could be used with reasonable accuracy to calculate the force produced by the impacting tow.

30. Dynamic load-deflection curves were calculated for each impact test. By comparing results from the dynamic and static tests, it was found that the curves were similar in shape, given that the absolute pretension values and the point at which the load was applied to the cable varied between tests. Figure 8 displays results from Test 24 in which the same cable was used, the pretension was 334.6 lb, and the tow contacted the cable such that  $l_1 = 2.42$  ft and  $l_2 = 2.33$  ft. Superimposed on this graph are data from the static test. Although these plots correlate extremely well, direct comparison of the static and dynamic curves is limited since it has been found that often the deflection produced by a dynamic load is greater than that which would have resulted from the static application of the same load. The ratio comparing these deflections is known as the dynamic load factor (DLF) and could account for discrepancies found in similar comparisons (Biggs 1964).

31. It was also discovered during the in-place static tests that there were some discrepancies in the readings of the load cells that were unnoticed during laboratory calibration of the cells. Each cell, in fact, read from 1 to 15 lb difference while in a pretensioned but zero deflection condition. Some of this can be attributed to the twist of the cable applying a torque to the cells. The swivels that were installed did not alleviate this problem, but did minimize it. It was also apparent that in addition to the cable losing tension after impact, the cells displayed similar losses in that an offset

---

\* For convenience, symbols and abbreviations are listed in the Notation (Appendix B).

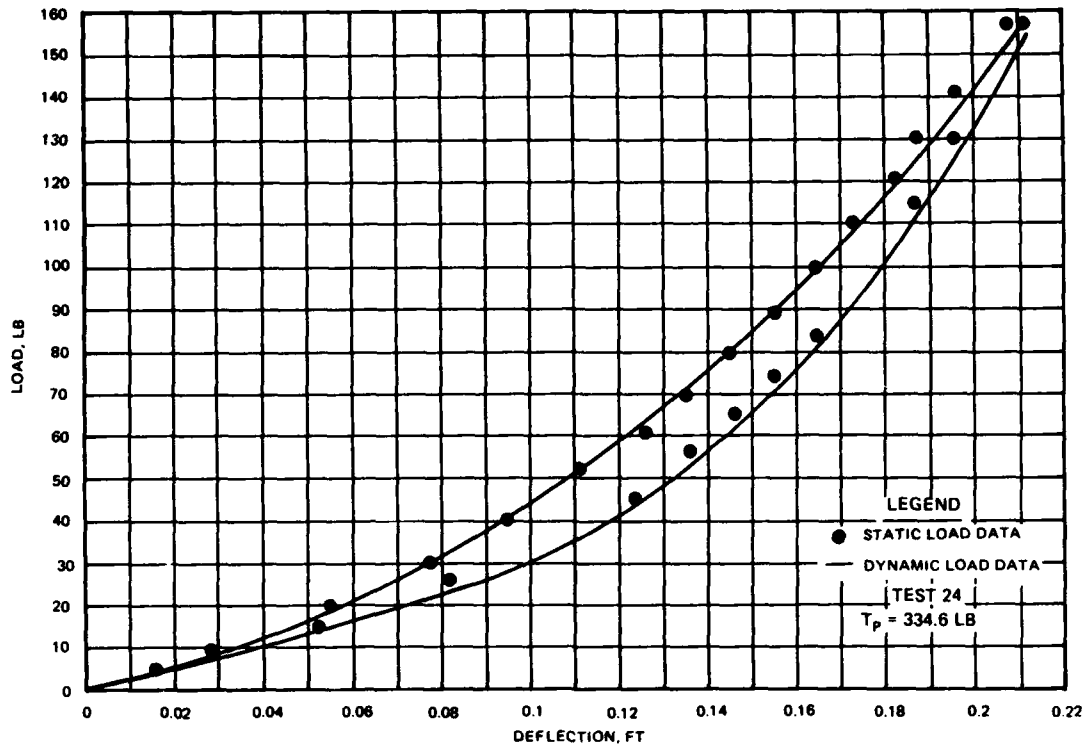


Figure 8. Force-deflection curve, static and dynamic

was exhibited. That is, after 10 to 15 impacts, the cells would have a 10- to 20-lb offset from their original zero readings taken with the cable slack and completely unloaded. This makes the less than 1 percent error found in the laboratory calibration of the cells meaningless when compared to actual test conditions.

32. Given the behavior of the cable and the performance of the cells, values in the load cells before and after each dynamic test were carefully measured and recorded. In the final data used, the before- and after-impact offset of each cell never exceeded 10 lb, and the difference in pretension readings between cells was usually less than 15 lb. The pretension value was used with the change in tension that occurs during an impact test to determine the total tension in the cable and, consequently, the value of the applied load. The sensitivity of the errors in the pretension value on the ultimate force-deflection curve is minimal.

## PART III: THEORY

### Dynamics

#### Kinematics

33. To begin the discussion of dynamics requires the introduction of the fundamental concepts related to kinematic theory. In this application, it regards the rectilinear motion of the tow in the lock chamber prior to and during impact. Instantaneous velocity  $v$  is a function of displacement  $y$  with time  $t$  defined by

$$v = \left( \frac{dy}{dt} \right) \quad (3)$$

Velocity can also be noted as  $\dot{y}$  such that it is the first derivative of displacement with respect to time. Instantaneous acceleration at a time  $t$  is

$$a = \frac{dv}{dt} = \frac{d^2y}{dt^2} \quad (4)$$

where  $\ddot{y}$  (or  $a$ ) is the second derivative of displacement with respect to time. Graphical procedures were used in the data reduction to obtain the velocity of the tow just prior to impact with the cable and the acceleration at maximum deflection or  $v = 0$ . The velocity was obtained graphically as the slope of the  $yt$  curve (displacement versus time) as recorded from the ultrasonic module. The  $vt$  curve (velocity versus time), based on outputs of the velocity tachometer attached to the cable, was used to determine acceleration and in some instances deflection. The slope of the  $vt$  curve at  $v = 0$  represents the acceleration of the cable at peak force. The area under the  $vt$  curve from time of contact to  $v = 0$  is the maximum displacement; that is,

$$\int_{y_0}^{y_{\text{peak}}} dy = \int_{t_0}^{t_{\text{peak}}} v dt \quad (5)$$

or

$$y_{\text{peak}} = \int_{t_0}^{t_{\text{peak}}} v \, dt \quad (6)$$

More on graphical solutions can be found in Hibbeler (1974).

34. The acceleration was determined for all tests by this method except for tests 46-57 in which the velocity tachometer was not sampled. Deflection values were obtained primarily by the position potentiometer and not by integration of the vt curves. In randomly selected tests, integration of the vt curve was used only as a check against results from the position potentiometer and/or ultrasonic device.

#### Force theory

35. The free body diagram in Figure 6 accounts for the dynamic forces acting on the cable, defined by Newton's second law of motion, which states that "a particle acted upon by an unbalanced force F receives an acceleration, a, that is in the direction of the force and has a magnitude which is directly proportional to the force" (Hibbeler 1974).

36. Given that the diagram is in dynamic equilibrium, the principles of statics may be applied such that by summing the forces in the y direction,

$$T_1 \sin \theta_1 + T_2 \sin \theta_2 + ma = 0 \quad (7)$$

where m is the mass of the vessel. This implies that the cable reacted with an equal and opposite force to the force ma produced by the tow. Then, knowing the tension and angles of the reaction, the equation can be solved for ma .

37. This equation assumes several conditions. One assumption is that only the mass and acceleration (or deceleration in this case) of the towboat and barges contributed to the resultant force in the cable, such that frictional forces and system gains in mass were neglected. Specific theory regarding these components is discussed in the section, "Hydrodynamic Theory." This assumption can be corrected by equating the reaction forces to a summation of the mass times acceleration components such that

$$T_1 \sin \theta_1 + T_2 \sin \theta_2 = \Sigma ma \quad (8)$$

38. Another assumption concerns the line of action of the force whereby the tow was assumed to apply a force to the cable in the y-direction only with no translation or rotation and the center of mass was assumed to be in line with the point of contact with the cable.

39. In response to the center of mass, the weights were evenly distributed on either side of the center line of the barge train. Additionally, the protruding point was always centered along this same axis, as was the towboat pushing the barges.

40. Regarding the angle of approach, much was dependent upon the skill of the radio operator to keep the boat aligned parallel to the lock walls. Every effort was made during operation of the tow to drive the tow straight into the chamber. If the tow was not straight, the tests were either repeated or comments to that effect were included in the data record book. Obviously, the least amount of error occurred when the maximum number of barges was used, and more room for error existed during tests of the two-barge configurations.

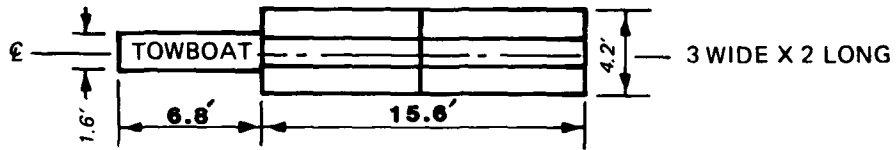
41. The maximum, or worst condition, translation angles that could be obtained are shown in Table 1 for the different types of barge configurations (Figure 9). The maximum angles were derived geometrically based on the relationship of the dimensions of the tows to the chamber width. Provisions to measure the angle formed from the barge train translated from the center line were not made in the model. Ratios of  $F_y$  (the force in the y-direction) to  $F_r$  (actual resultant force formed by the angle) are trigonometric equivalents to the cosine of the angle. Assuming the maximum angle can be obtained, the error was less than 1 percent for configuration Types 1-5 and 2.1 percent for Type 6. Furthermore, in tests where narrow barge trains were used, such that the stern of the tow could move laterally with respect to the bow, causing rotation, the data plots of narrow barge trains showed no signs of deviation from those with wider barge trains (i.e., see Figure 20).

42. Therefore, the validity of the equation, and thereby the free body diagram, remains intact despite assumptions relative to the center of mass and angle of approach.

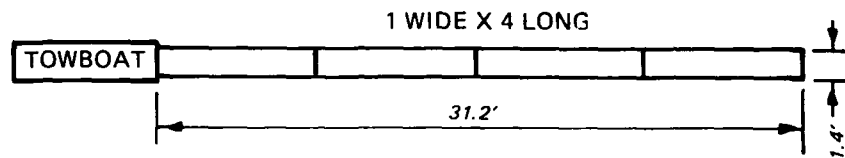
#### Energy and momentum

43. Problems involving Newton's second law concerning force and the kinematic equations of velocity and displacement can also be solved by

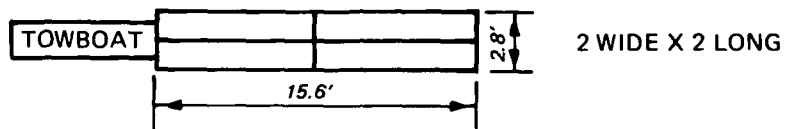
TYPE 1



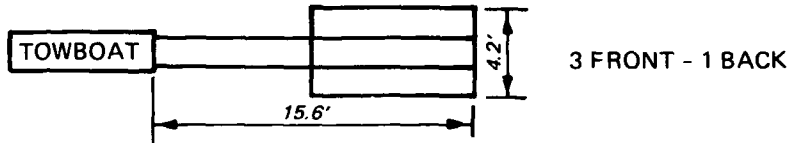
TYPE 2



TYPE 3



TYPE 4



TYPE 5



TYPE 6

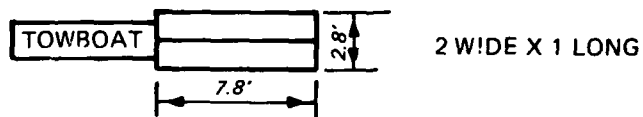


Figure 9. Barge configurations

applying the principle of work and energy. This principle states that the work done by all the forces acting on the body during a given displacement is equal to the change in kinetic energy of the body. If the force undergoes a finite displacement along the path from  $y_0$  to  $y_1$ , then work,  $W$ , done by  $F$  can be determined by integrating the force displacement curve such that:

$$W_{0-1} = \int_{y_0}^{y_1} F \, dy \quad (9)$$

where  $F$  is a function of  $y$ ,  $F(y)$ . Rewriting the equation summing the forces gives the following:

$$ma + F(y) = 0 \quad (10)$$

and

$$-m \left( \frac{dv}{dt} \right) \left( \frac{dy}{dy} \right) = F(y) \quad (11)$$

or

$$m \left( \frac{dv}{dy} \right) \left( \frac{dy}{dt} \right) = F(y) \quad (12)$$

Then multiplying both sides by  $dy$  and substituting  $v$  for  $dy/dt$ :

$$mv \, dv = F(y) \, dy \quad (13)$$

Integrating both sides:

$$m \int_{v_0}^{v_1} v \, dv = \int_{y_0}^{y_1} F(y) \, dy \quad (14)$$

If the definite integral from  $V_0$  to  $V_1 = 0$  at maximum force is evaluated where  $V_0$  is the velocity of the vessel just prior to impact and  $V_1$  is the velocity at peak displacement:

$$\frac{mv^2}{2} \Big|_{V_0}^{V_1} = \int_{y_0}^{y_1} F(y) dy \quad (15)$$

$$\frac{-mV_0^2}{2} = \int_{y_0}^{y_1} F(y) dy \quad (16)$$

Combining the principles of work and energy, the term on the right side of the equation represents the work done by all the forces acting on the body as it moves along the path, and the term on the left represents the kinetic energy of the body at initial and final points on the path.

44. From conservation of energy it is also known that

$$KE_0 + PE_0 = KE_1 + PE_1 \quad (17)$$

where

- $KE_0$  = kinetic energy at  $t = 0$
- $PE_0$  = potential energy at  $t = 0$
- $KE_1$  = kinetic energy at  $t = 1$
- $PE_1$  = potential energy at  $t = 1$

If  $KE_0$  is the kinetic energy of the moving tow just prior to impact,  $PE_1$  is the potential energy of the cable at maximum deflection,  $PE_0$  is zero for the cable, and  $KE_1$  is zero for the tow, then

$$KE_0 = PE_1 \quad (18)$$

where, as stated previously,

$$KE_0 = \frac{mV_0^2}{2}$$

and

$$PE_1 = \int_{y_0}^{y_1} F(y) dy$$

In the model,  $PE_1$  is the area under the load-deflection curve as measured during each model test. Theoretically for  $KE_0$ ,  $V_0$  is the velocity of the tow taken just prior to contact with the cable.

45. Suitable solutions to problems involving impact, where the force can be expressed as a function of time, introduce the principle of impulse and momentum. Momentum of a body is defined as the vector  $mv$  since the scalar  $m$  acts in the same direction as  $v$ .

Given:

$$F = m \left( \frac{dv}{dt} \right) \quad (19)$$

then

$$F dt = m dv \quad (20)$$

Integrating the left side with respect to time (from  $t_0$  to  $t_1$ ) and the right from  $V_0$  to  $V_1$ ,

$$\int_{t_0}^{t_1} F dt = mV_1 - mV_0 \quad (21)$$

If  $V_1$  equals zero at peak displacement of the cable, then

$$\int_{t_0}^{t_1} F dt = -mV_0 \quad (22)$$

The left side of the equation, defined as the impulse of force  $F$ , is simply the area under the  $Ft$  curve (force versus time) from  $t_0$ , where the tow initially contacts the cable, to  $t_1$ , where the peak force occurs. The right side represents the momentum of the tow.

Cable theory as related to force

46. Given the properties of the cable (i.e., cross-sectional area  $A_c$ , modulus of elasticity,  $E$ ), and the geometry of the assembly as described in Figure 6, a theoretical load-deflection curve can be derived as follows.

47. Summing the forces in the y-direction,

$$F = T_1 \sin \theta_1 + T_2 \sin \theta_2 \quad \text{from (1)}$$

where

$$T_1 = T_p + dT_1 \quad (23)$$

$$T_2 = T_p + dT_2 \quad (24)$$

and  $dT$  is the change in tension as a function of cable elongation.

48. From trigonometry,

$$\sin \theta_1 = \frac{y}{\sqrt{y^2 + \ell_1^2}} \quad (25)$$

$$\sin \theta_2 = \frac{y}{\sqrt{y^2 + \ell_2^2}} \quad (26)$$

49. Based on material properties (Timoshenko and Gere 1972), and  $\ell_1 = \ell_2$ , total elongation of the cable assembly  $\delta_t$  due to change in tension is calculated by the following equation:

$$\delta_t = \frac{dT \ell}{AE} = \delta_c + \delta_s = \sqrt{y^2 + \ell^2} - \ell \quad (27)$$

where

T = tension

$\ell$  = half-length of the cable

A = cross-sectional area

and the elongation in the cable only  $\delta_c$  and the elongation in the swivel only  $\delta_s$  are calculated by the following expressions:

$$\delta_c = \frac{dT \ell_{1x}}{A_c E} \quad \text{where } \ell_{1x} = \ell_{2x} \quad (28)$$

$$\delta_s = \frac{dT \ell_x}{A_s E} \quad (29)$$

The variables in Equations 28 and 29 are defined as follows:

$\ell_{1x}$  = length of cable from end of swivel (cell 1) to point of contact, ft

$A_c$  = Cross-sectional area of the cable = 29 lb/1,000 ft divided by  
490 lb/ft<sup>3</sup> = 5.918 × 10<sup>-6</sup> ft<sup>2</sup>

$\ell_{2x}$  = length of cable from end of swivel (cell 2) to point of contact, ft

$\ell_x$  = length of cell and swivel assembly, ft

$A_s$  = Cross-sectional area of the swivel = 5 oz/3.75 in. divided by  
490 lb/ft<sup>3</sup> × 0.0625 lb/oz × 12 in./ft = 0.00204 ft<sup>2</sup>

Assuming  $\delta_s \ll \delta_c$ , such that  $\delta_s = 0$ ,

$$\delta_c = \delta_t \quad (30)$$

Then

$$dT_1 = \delta_{c1} \left( \frac{A_c E}{\ell_{1x}} \right) \quad (31)$$

and similarly,

$$dT_2 = \delta_{c2} \left( \frac{A E}{l_{2x}} \right) \quad (32)$$

Plugging Equation 27 into Equations 31 and 32,

$$dT_1 = \left( \sqrt{y^2 + l_1^2} - l_1 \right) \left( \frac{A E}{l_{1x}} \right) \quad (33)$$

$$dT_2 = \left( \sqrt{y^2 + l_2^2} - l_2 \right) \left( \frac{A E}{l_{2x}} \right) \quad (34)$$

Substituting Equations 23 and 24 into Equation 1,

$$F = (T_p + dT_1) \sin \theta_1 + (T_p + dT_2) \sin \theta_2 \quad (35)$$

Substituting Equations 25-34 into Equation 35 yields

$$F = y \left[ \left( \frac{T_p}{\sqrt{y^2 + l_1^2}} + \frac{A E}{l_{1x}} - \frac{A E l_1}{l_{1x} \sqrt{y^2 + l_1^2}} \right) + \left( \frac{T_p}{\sqrt{y^2 + l_2^2}} + \frac{A E}{l_{2x}} - \frac{A E l_2}{l_{2x} \sqrt{y^2 + l_2^2}} \right) \right] \quad (36)$$

50. Plotting the load-deflection curve based on Equation 36 with that obtained from the static or dynamic load-deflection curves did not result in the same plots. Figure 10 compares the dynamic load-deflection curve from Test 24 data with those of Equation 36. (The values of  $T_p$ ,  $l_1$ , and  $l_2$  taken from the test were plugged into the equation along with incremental values of  $y$  to obtain  $F$ ). There are several explanations for this discrepancy. For one, the exact modulus of elasticity of the cable was unknown and assumed to be that of steel ( $29 \times 10^6$  psi). Also, the area of the cable is estimated from the weight per unit length of cable divided by the specific weight of steel when in actuality the area is a function of the load and elongation of the cable. The diameter of the cable decreases as the cable is stretched. By lumping  $A$  and  $E$  into one term, the value could have been

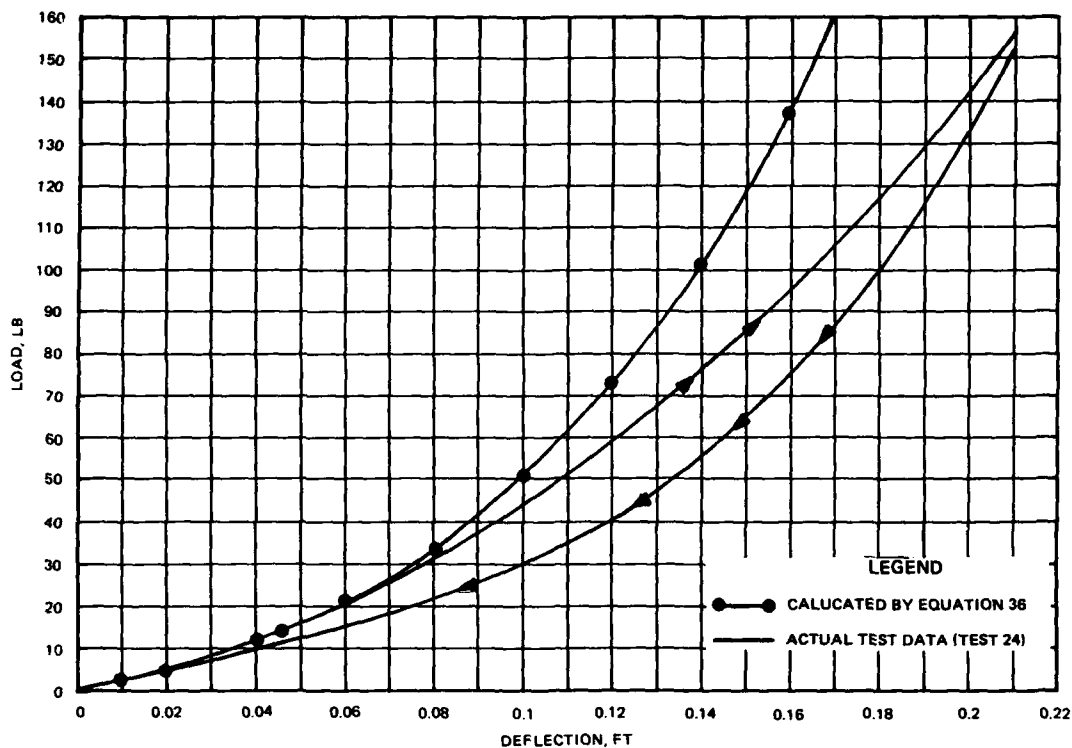


Figure 10. Force-deflection curve, actual test data versus Equation 36

obtained empirically from the static load tests. It was not the intent of this research to define the properties of the cable; therefore, this exercise was not performed.

51. In actual static and dynamic tests where the cable assembly was loaded and unloaded, the recorded data yielded load-deflection curves similar to those in Figure 10, which, unlike those of the theoretical Equation 36, exhibited the presence of a hysteresis loop. This loop may be the result of hysteretic or internal damping. Biggs (1964) states that "all structural dynamic systems contain damping to some degree, but the effect may not be significant if the load duration is short and only the maximum dynamic response is of interest. Damping, in general, is due in part to the internal molecular friction of the material. It is also due to the loss of energy associated with the slippage of structural connections either between members or between the structure and supports." Damping can take any of several forms, the most common being viscous in which the damping force is proportional to velocity. Solid or hysteretic damping is caused by the internal friction or

hysteresis when a solid is deformed. In hysteretic damping, the damping force is proportional to velocity and inversely proportional to frequency. The area enclosed by the hysteresis loop is the energy dissipated during a cycle and can be represented by the formula (Steidel 1971):

$$\Delta U = \pi h X^2 \quad (37)$$

where

$\Delta U$  = energy dissipated over cycle

$h$  = hysteretic damping constant (pounds per inch or pounds per foot)

$X$  = maximum displacement (inches or feet)

Since the peak force and maximum deflection were of primary interest in this study, the damping effects were of little consequence. The damping coefficient was not determined in the analysis, but had it been, the theoretical equation for  $F$  would have included an additional term such that

$$F = kx + \left(\frac{h}{w}\right) \dot{x} \quad (38)$$

The  $kx$  term is the force produced from Equation 36 where  $F$  is a function of  $T_p$ ,  $l_1$ ,  $l_2$ , and  $AE$ . The spring constant  $k$  is nonlinear in this application, and  $x$  is displacement. The second term relates to damping where the force is the hysteresis constant  $h$  divided by the system frequency  $w$  times the first derivative of displacement with time  $\dot{x}$ .

52. A theoretical force-deflection curve was not derived that explicitly represented the actual curves obtained from the data. It was unnecessary to derive such an equation since each different dynamic test produced its own force-deflection curve. Test curves empirically represent all the unknown properties of the cable, any hysteretic damping, and/or other unknown parameters that would be essential to the derivation of an absolute theoretical equation.

#### Hydrodynamic Theory

53. The dynamic equations in the preceding paragraphs were developed neglecting the influences of the hydraulic forces that interact with the tows' movements. To understand these forces, it is necessary to discuss theory and

results obtained from literature regarding attached mass, drag force, limiting velocities, and translatory waves.

Attached mass and drag

54. When flow passes a blunt body, it will separate from the solid surface, causing a resultant downstream "wake." Pressure differences between the upstream and downstream faces of the body produce a net thrust on the body known as the form drag. The form drag is defined by the equation (Henderson 1966):

$$P_f = C_D * A * 1/2\rho v_0^2 \quad (39)$$

where

$P_f$  = drag force

$C_D$  = coefficient of drag

A = frontal area of the body projected normal to flow

$\rho$  = density of water

$v_0$  = free stream velocity

The drag is complicated in this application as flow is permitted to return on either side of the moving tow and along its bottom. Further, the tow is propelled through the water by the engines until it nears the cable. The drag in this equation is more applicable to flow around an obstacle such as a bridge pier.

55. Kapustanskiĭ and Marchenko (1975) performed numerical analysis of the motion of a solid body moving through a fluid, solving the equations of motion and continuity for flow separation and separation-free flow. Their studies are more in line with the problem presented by this study. They attempted to relate the motion to attached mass, which they explained as follows: "In the calculation of the collision of a floating body with a structure, the attached masses of liquid may play a decisive role, since in the equations of motion they appear as additional components with the mass of the body, increasing the massiveness of the system, and therefore, the forces involved in collision." As the body (or tow) moves toward a rigid barrier (the miter gate), the most important forces are those acting in front of the tow. Kapustanskiĭ and Marchenko (1975) deduced that shape of the body has little effect on the attached mass. This is contrary to drag force theory, which states, in fact, that shape alone governs the coefficient of drag.

Their analysis indicated that it was theoretically impossible to determine specific values of attached mass though they did gain insight on parameters that affect the attached mass. Their results leave experimental findings to fill the void in quantifying attached mass and proper drag relationships.

Limiting velocities and translatory waves

56. A number of studies have been conducted to define the influence of channel cross section on what is termed the limiting velocity of a vessel. Limiting velocity is simply the maximum sailing velocity that could be attained, given adequate horsepower, by a specific size vessel in a specific set of channel dimensions. Jansen and Schijf (1953) and Kooman (1973) discussed the phenomenon of limiting velocity and develop relationships for determination of this velocity. Both sources used the following equation to calculate limiting velocity  $V_L$  :

$$1 - \frac{f}{F} + \frac{V_L^2}{2gh} - \frac{3}{2} \left( \frac{V_L}{gh} \right)^{1/3} = 0 \quad (40)$$

where

$f$  = cross-sectional area of the hull below the water surface

$F$  = cross-sectional area of the channel

$g$  = gravitational constant

$h$  = depth of pool

57. Kooman (1973) described the behavior of ship motion as follows: "A ship in motion causes a water movement around its hull as the water replaced by the bow moves to the stern to fill up the wake. This water movement, the return current, is attended by a drop in the water level as a result of the loss in the velocity head. When there is a uniform sailing speed in a prismatic canal, the waterflow is steady with respect to the ship." Both sources also presented graphical solutions to determine the drop in water surface and the return current. In field observations, Jansen and Schijf (1953) determined that the rear of the ship tended to settle more than the calculated depression and suggested the calculated values be multiplied by a safety factor of 1.4. Similarly, Kooman (1973) added a correction factor due to the sill. The settling of the rear of the ship, especially when crossing the sill, is known as squat (Gelencser 1977). This phenomenon can not only damage the tow and sill from scraping, but it can also dramatically affect the

approaching speed of the tow to such a degree that the tow temporarily stops its forward movement (Maynard 1987).

58. Gelencser (1977), Jansen and Schijf (1953), and Kooman (1973) discussed the merits of deepening channels due to the increase in the limiting velocities that can be obtained. Jansen and Schijf further concluded that increasing the channel cross-sectional depth is more effective than increasing its width to increase the limiting velocity.

59. The sailing speed of vessels rarely approaches the limiting velocity, and Kooman (1973) expanded this to say that it is impossible for normal inland ships or push-tows in prismatic canals to exceed the limiting velocity. Exceptions to this can occur for short durations in a suddenly narrowing section. An example would be a ship entering a comparatively narrow lock at a high speed.

60. The sailing speed of a push-tow in the wide lock approach will in many cases be higher than the limiting speed in the narrow lock chamber. Consequently, a wave forms at the bow of the tow due to the return current being smaller than the quantity of water being replaced by the tow. This generates a positive transitory wave that propagates into the lock chamber ahead of the vessel. Even when the entry speed is lower than the limiting speed, the transitory wave still must adjust to the narrow lock section.

61. The transitory wave generally slows the tow's entry and also makes the entry irregular, because of the continuing backward and forward motions of the wave. Furthermore, a tendency exists for temporary accelerations to occur as the negative wave reflects off the closed miter gates, setting up a temporary water-surface slope in which the bow of the vessel is lowered.

#### Applications of theoretical principles

62. A number of references from abroad presented calculations pertaining to the forces used to calculate impact barriers. Typical of many designs was that resistive energy was defined as force-time displacement of the barrier, and further, the kinetic energy was related to the mass of the vessel moving at an expected velocity such that  $E = (1/2)mV^2$  (Cabelka et al. 1977 and Jackson, Thomson, and Murrer 1978). However, in some references the statement of the problem involved more terms and coefficients. For instance, authors Kozak, Shestakov, and Sadovenko (all from the USSR) included a coefficient in front of the force and energy terms that accounted for additional mass of the water.

63. Kozak (1979) presented kinetic energy of a vessel by the expression

$$E_c = \xi \left( \frac{WV_0^2}{2g} \right) \quad (41)$$

where

$\xi$  = coefficient ranging from 1.1 to 1.15 which allows for the additional mass of water involved, amounting to 10 to 15 percent of the vessel's mass

W = water displacement of the vessel (weight)

$V_0$  = velocity just before collision

g = gravitational constant

64. Sadovenko (1970) presented an equation for the movement of a ship colliding with a barrier as follows:

$$M \frac{dv}{dt} + P + Av^2 = 0 \quad (42)$$

He defined M as "the mass of the vessel together with the added mass of the water, which can constitute 10 to 15 percent of the mass of the vessel." The term P is a function of the barrier's displacement, or the F(y) component. The  $Av^2$  term is the drag force where A is a constant for resistance. Sadovenko related P (or F) as a function of x (or y) to the tension of a flexible cable or chain S (or T), and the half-length of the cable e (or  $\ell$ ), as

$$P = 2S \left( \frac{x}{e} \right) \quad (43)$$

This similarly relates to the equation derived in the section, "In-Place Calibration of the Cable Assembly," such that Equation 2 can be written

$$F = 2T \sin \theta$$

where  $\sin \theta$  can be approximated by  $y/\ell$ .

65. Sadovenko (1968) in his discussion of the design of the resistive system assumed that the mass of the barrier is insignificant, as is the drag

force, and that the vessel is moving in a straight line along the longitudinal axis of the lock. Then, his initial equation (42) can be reduced to

$$P = -M \left( \frac{dv}{dt} \right) \quad (44)$$

which is similar to Equation 8,

$$F = - \Sigma ma$$

66. Shestakov (1973b) also added a coefficient to his equation of motion, which was defined as a coefficient for additional water mass. His equations represented force in the x- and y-axes and that due to a rotational component. He likewise included a drag force component in his equation. Shestakov (1973a) eventually ignored rotation and translation, and assumed

$$P = S_1 \sin \alpha_1 + S_2 \sin \alpha_2 \quad (45)$$

where  $\alpha$  is the angle formed by the cable at impact, which correlates with

$$F = T_1 \sin \theta_1 + T_2 \sin \theta_2 \quad (1 \text{ bis})$$

67. Neither Kozak, Sadovenko, or Shestakov verifies his decision to increase the vessel's mass (Shestakov did not indicate any value for the coefficient), nor did they provide a value for drag or support to ignore it. No studies performed or theory developed in regard to these values were found.

68. These sources do establish that additional mass or attached mass is pertinent to examination of the kinetic energy of a tow in a lock chamber. This concept was also reinforced by a model study by the LaSalle Hydraulic Laboratory (Hausser and Beaudry 1969) in which a fendering system called the Ship Alignment and Mooring System (S.A.M. System) was modeled for locks on the Welland Canal. In the study, the ratio of the braking energy of the fenders to the kinetic energy of the vessel was determined. The braking energy in this study was calculated as the product of the braking force and the distance required for stopping the vessel. It is unclear if the velocities used to calculate the kinetic energy were those produced at precisely the moment of

contact with the fenders, or if it represented the constant velocity of the vessel in the approach. It is suspected to be the latter since the author further discusses the ratios with respect to entry speed. The ratios of braking energy to kinetic energy varied from 0.24 to 2.24. No correlation was found between the entry speed and these ratios. The authors attributed this to several factors including the exact time and location at which the braking force was applied, the variable speed of the ship due to surge patterns in the lock chamber, and the "virtual" (attached mass plus the mass of the ship) mass of the moving vessel. The scope of the S.A.M. study did not include defining the virtual mass, but concluded that "the processes of energy transfer occurring during a maneuver in a lock are of a very complex nature" (Hausser and Beaudry 1969).

#### Empirical solution

69. Very few formulas are presented in this section on hydrodynamic theory. The available literature indicated that although the phenomena of virtual mass and drag contribute to the kinetic energy of a vessel in a lock, values pertaining to these concepts have not been explicitly quantified. This research is designed to measure the increase in kinetic energy, if any, due to the collective effects of attached mass, drag force, and temporary accelerations from translatory waves, such that an empirical solution would lump the unknowns into a relationship

$$E_{TOTAL} = C_E \left( \frac{mV_0^2}{2} \right) \quad (46)$$

where  $E_{TOTAL}$  is energy measured in the model, and  $C_E$  is the coefficient of energy. This research quantifies coefficients that verify or disclaim the use of such a constant, and specifically the value of 1.1 to 1.15 used by several of the authors. The coefficient  $C$  is also determined for force and impulse such that the peak model force is calculated by

$$F_{peak} = -C_F(ma) \quad (47)$$

and the impulse at peak force is calculated by

$$I_{TOTAL} = -C_I(mV_0) \quad (48)$$

Since the constants can be isolated on one side of the equation, then ratios of measured values to computed, or experimental to theoretical, will determine  $C_E$ ,  $C_F$ , and  $C_I$ , the coefficients of energy, force, and impulse, respectively. Furthermore, the product of the coefficient and the mass  $m$  represents the virtual mass of the system or equivalent mass.

## PART IV: TESTING PROGRAM

### Independent Variables

70. A number of independent parameters were set prior to running each series of tests. These parameters included the mass of the tow, the draft of the barges, the configuration of the barges, and the pool depth. Each of these conditions was carefully chosen to best represent actual prototype situations and/or to provide conditions that would support the hypothesis conjectured from the theory.

#### Draft and mass

71. The draft of the barges was chosen based on typical loaded prototype jumbo barges such that 6- and 9-ft drafts, respectively, were represented in the model at 0.24 ft and 0.36 ft. The towboat draft used in the model was set at approximately 0.36 ft. In prototype this boat drafts between 8 and 10 ft. The setting of the drafts consequently led to the ballast of the barges and thereby the mass of each barge and tow. All elements of the barge train including the towboat, ballast, empty barges, and extraneous clamps and appurtenances were carefully weighed on scales before assembly. This ensured accurate representation of the mass of the tow.

#### Configuration

72. Barge configurations were based not only on what is common to the lock represented in this model but also on the relationship of the width of the lead barges to the width of the lock chamber. By testing three different barge train widths, correlations were made concerning the effect of the width on the drag of the tow and ultimately the energy produced by the tow. Six types of configurations were selected. These types are identified in Figure 9.

73. Basically, two-, four-, and six-barge configurations were used. It is possible to lock eight jumbo barges and a tow through the lock at one time. However, the arrangement for lockage is not efficient for river travel. Double lockages are permitted on most of the locks; that is, in a tow larger than eight barges, the towboat can push a section of the barge train into the chamber and then wait in the approach to lock the rest of the barges through. If a tow is traveling through a series of locks, this procedure can greatly increase travel time due to the time-consuming additional lockages. The

six-barge configuration is the most common in prototype and consists of a tow three barges wide by two barges long with the towboat centered behind the barge train. This configuration is optimum in terms of appropriately fitting into the lock chamber without rearranging the tow before lockage or without having to double-lock. The six-barge tows were not rearranged to obtain differing barge widths as this would be redundant to results of the four-barge and two-barge tests. The four-barge configurations provided three different ratios of width of lead barges to width of lock chamber based on one, two and three barge widths, such that the ratio of the width of the barge train to the width of the chamber  $W_B/W_C$  was 0.32 for Type 2, 0.64 for Type 3, and 0.95 for Type 4. It is very unlikely that Type 2 would ever be used during a lockage because it exceeds the length of the chamber, but during travel in open channels the operator may choose such a configuration to minimize drag and increase travel time. The two-barge tows have two types of configurations: essentially, one or two barge widths or  $W_B/W_C$  ratios of 0.32 and 0.64. Again, these configurations were selected primarily to determine the effects, if any, of the tow width on the resultant energy produced by the tow in the chamber. Using two-, four-, and six-barge configurations allowed correlations to be made between mass and the other dependent variables.

#### Pool depths and sill heights

74. Typically, in locks the upstream gates are seated on a miter sill, which is simply a raised concrete section that the gates contact when they are closed. The sill's width and length are sufficient to allow the gates to open into the miter recesses for a vessel's entrance into the chamber and close for the chamber to empty or fill. Because of the expense of construction and operating machinery for miter gates, the height of the sill is generally designed to minimize the height of the miter gate and the static load imposed by the upper pool, while still allowing enough pool for clearance of the tow. Therefore, minimal clearance depths are established based on the minimum upper pool and the submerged depth over the sill. Also, the sill is designed to extend above the approach channel bed to enhance debris and sediment removal and gate operation and maintenance.

75. Several references suggest criteria in regard to sill height. Engineer Manual 1110-2-1604 (Office, Chief of Engineers (OCE), US Army, 1979) dictates the following:

The minimum lock sill depth for shallow draft large locks

should be approximately two times the draft of the tows used in the waterway...the requirement of two times the draft should be available 95% of the time and an absolute minimum of 1.7 times the draft should be available 100% of the time. For a vessel draft of 9 feet, the 95% depth would be 18 feet and the minimum depth 15 feet. Adoption of the above criteria has been based on model studies at the De Voorst Laboratory in the Netherlands and on operating experience at numerous locks in the United States.... For some other type of filling systems (bottom culvert types) the required chamber depth may be less than the minimum sill depth. Where this latter situation occurs a deviation from the above criteria may be considered provided a complete evaluation of the effects of such a change is furnished.

Results from a 1:25 model study of pushtows in locks at the Delft Hydraulics Laboratory (Kooman 1973) suggested that water depths of 1.6 to 1.7 times the draft are optimal for flat-floor locks, while water depths should be roughly 1.5 to 1.6 times the draft in locks with sills.

76. Modifications were made to the model floor and upstream sill to provide two test conditions, shown in Figure 1: a flat-floor condition where the depth of pool does not restrict the tow propeller efficiency, and a raised sill condition that provided minimal clearance for the tow. The lock constructed for this model was designed such that the true model floor, where the fill system was located, was approximately 4 ft below the water-surface elevation. The upstream sill was removed and a false floor was installed, so that the water surface for the tests was 2.6 ft above the false floor. This condition made the submergence depth 7 to 10 times the draft of the test tows. Engineer Manual 1110-2-1604 (OCE 1979) states that gains in tow efficiency do not increase proportionally as sill depth-draft ratios are increased beyond a value of two. Because the depth-draft ratio of the model greatly exceeded the suggested 2.0 ratio, tests could be conducted in which only the geometry imposed by the walls could be isolated by testing variable barge train widths. The results from the flat-floor testing also set a base condition with which to compare tests conducted with an upstream sill in place, thereby determining if the height of the sill had any effect on the testing results.

77. After flat-floor tests were completed, an upstream sill was constructed in the model (Figure 1) with a submergence depth of 0.54 ft, making the submergence-to-draft ratio 1.5. The 1.5 ratio was selected as this was felt to be an extreme condition cited in the references. (This does not

preclude the existence, however, of existing locks that have justified modification of the criteria to lesser ratios.) Logically, if the hydrodynamics were unaffected by this condition, then testing could be discontinued; if appreciable effects did exist, the sill height could be incrementally lowered to determine the relationship between the submergence depth and the hydrodynamics. Testing was stopped after two series of tests were performed with the sill in place. Parts VI and VII compare flat-floor and sill data for the Type 6 barge. With- and without-sill tests were also run for a nine-barge tow, and results are presented in Appendix A.

#### Operation of the Tow

78. The dependent variables to be measured in the testing (i.e., tension and deflection in the cable) were directly affected by the speed of the towboat and the point at which the lead barge contacted the test cable. The tow's speed was not only a function of propeller speed, but also of the mass and configuration of the tow and the geometry of the chamber. The point at which the barge contacted the cable depended on the skill of the radio operator to keep the tow aligned and in the center of the chamber.

79. To determine any correlations between tow velocity and the other parameters, a range of velocities was selected for testing. The objective of this range was to cover velocities in the prototype that were typical as well as extreme. Therefore, the velocities that were used ranged from approximately 0.3 fps to 1.0 fps. Additionally, two velocities were recorded for each test: one at midchamber, the bow of the lead barges being approximately 6.6 ft from the cable, and the other just prior to contact with the cable.

80. The radio control used to operate the model towboat was equipped with two joysticks that controlled the rotational speed of each propeller. The sticks had definite notches in their movement so that approximately 10 different propeller speeds could be obtained. The first two notches (referred to as clicks in the testing records) did not activate the servos that controlled the propellers; therefore, the slowest speed that could be obtained was while operating at three clicks. The two different lock floor dimensions, the configuration of the tows, and the mass of the tows controlled the actual speed obtained while operating the towboat at various clicks. Results of the speed versus the radio control operations are presented in Part VI.

81. The operation of the tow described in the introduction, whereby the tow began at a constant propeller speed from a predetermined starting point and then the propellers were turned off prior to impact, is not necessarily the operation that produces the maximum translatory wave. In fact, revving the propeller speed to coincide with reflection of the wave from the downstream gate would likely propagate the largest wave height. Testing the effects of different operational scenarios, while potentially a worthy topic for future research, was not permissible within the time and scope of this research.

82. As discussed in Part II, the point at which the tow contacted the cable provided the two angle chord lengths,  $l_1$  and  $l_2$ , which were used to define  $\theta_1$  and  $\theta_2$  corresponding to the tension in load cell 1 and load cell 2, respectively. The distance from the cable reaction or hinge point to a mark left by the protruding front of the lead barge on the cable was measured after each test and recorded for use in the data reduction. (The triangular point on the lead barge was coated with lipstick prior to each test, so that it left an identifiable mark on the steel cable.) The distance from the hinge point to the mark was measured with a ruler to within 1/16 in.

#### Dependent Variables

83. The two dependent variables in this testing setup were the tension in the cable and the deflection in the cable during impact. The amount of pretension prior to impact was selected to prohibit the cable from exceeding a maximum deflection of approximately 3.5 in. Since the protruding point on the barge was only 4 in. deep, deflections approaching this value might cause the corners of the barge train to contact the cable assembly or strike the load cells. Conversely, the pretension in the cable had to be set low enough so that minimal deflections did not cause the applied tension to exceed the limits of the load cells. As discussed in Part II, the load cells were zeroed out before the cable was pretensioned. Then the cable was pretensioned and exercised prior to running a set of tests to approximately 350 to 400 lb. Before and after each test, the tension in the cable was measured and recorded.

84. During impact, the changes in tension incurred by both load cells and the position potentiometer were sampled at 200 Hz. By using the measured

values of  $\ell_1$  and  $\ell_2$ , the peak change in tension in each cell, the pretension load in the cable, and the deflection of the cable, the force applied to the cable by the tow could be calculated. Part V describes in detail the formulas and conversions used to acquire these data.

#### Testing Sequence

85. In all, 136 tests were conducted, and 75 are presented in the main report and are briefly described in Table 2. Presented in this table are the test number, data file name, configuration type (Figure 7), total weight of tow, type floor, and midchamber velocity of the approaching tow. Tests 76-136 are presented in Appendix A.

## PART V: DATA REDUCTION

86. This section discusses the analytical techniques used to reduce the data obtained from the instrumentation, and presents the data in graphical as well as table summary form.

### Conversion of Data to Engineering Units

87. Some of the data reduction procedures were common to all the instrumentation. These items include the use of the spreadsheet (Lotus 1-2-3) to perform all calculations, a curve smoothing technique, and a specific method of integration.

88. Data collected for each test by the data acquisition software was directly loaded in Lotus 1-2-3 for reduction and analysis. By using copy commands, formulas could be repeated for a column of numbers. All computations were made with the software and final spreadsheets were saved.

89. The data output provided through the A/D converter reflected the presence of noise. By using a floating point average of the data, a smoothed curve was obtained without sacrificing accuracy. On the data output from load cell 1, load cell 2, the position potentiometer, and the ultrasonic device, every eleven readings were averaged sequentially as follows: 1-11, 2-12, 3-13, etc. This method of curve smoothing made it possible to extract peak values directly from the spreadsheets rather than graphically determining the values.

90. Integration of the  $F_y$  curve and the  $F_t$  curve were accomplished using Simpson's method; that is, average  $y$  values were multiplied by a small change  $d$  along the  $x$ -axis and then summed to give the area under the curve. This procedure was also accomplished by using Lotus 1-2-3.

### Load cells

91. The data collected from each cell prior to impact were averaged to obtain the zero voltage offset. The amplifiers were set such that 1 volt = 200 lb. Then the change in tension of each cell is

$$dT(\text{lb}) = (\text{Voltage in} - \text{zero offset}) \times 200 \text{ lb/volt} \quad (49)$$

Further, the pretension value was added to each  $dT$  such that

$$T(1b) = dT + T_p \quad (23)$$

Position/velocity transducer

92. Likewise, the zero offset on the potentiometer was obtained by averaging the voltages prior to impact. The conversion to feet from volts is then

$$y(\text{ft}) = (\text{Voltage in} - \text{zero offset}) \times 0.67476 \text{ ft/volt} \quad (50)$$

93. The velocity of the cable was obtained from the tachometer voltages by the relationship:

$$V(\text{fps}) = \text{Voltage in} \times 0.8171 \text{ fps/volt} \quad (51)$$

Ultrasonic ranging module

94. The zero offset for the ultrasonic module was defined as the voltage at precisely the moment the tow contacted the cable. This was stated such that the voltage then became the position datum reference point in the y-axis. Then position  $d$  in the y-direction is

$$d(\text{ft}) = (\text{Voltage in} - \text{zero datum offset}) \times 0.4546 \text{ ft/volt} \quad (52)$$

Positive values of  $d$  represent the position of the tow prior to contact; negative values of  $d$  can also be considered as the deflection  $y$  of the cable.

Digital input from light monitors

95. The two light monitors sent a specific digital input "mask," or numerical value, for each on/off sequence. *On* indicated that nothing was prohibiting the light from bouncing off the reflector. *Off* meant that the tow was obstructing the light. If light 1 represented the most upstream light monitor and light 2 the one nearest the cable, then:

<u>Mask</u>	<u>Light 1</u>	<u>Light 2</u>
12	ON	ON
13	OFF	ON
14	ON	OFF
15	OFF	OFF

### Calculation of Force, Energy, and Impulse

96. For each value of  $T_1$ ,  $T_2$ , and  $y$  collected during the sampling (time-step = 0.005 sec), the force was calculated using Equation 1 such that

$$F = T_1 \times \left\{ \sin \left[ \tan^{-1} \left( \frac{y}{\ell_1} \right) \right] \right\} + T_2 \times \left\{ \sin \left[ \tan^{-1} \left( \frac{y}{\ell_2} \right) \right] \right\}$$

Having calculated the force, then the energy is the summation of average force between time-steps times change in displacement  $y$ ; and impulse is the summation of average force between time-steps times 0.005 sec.

### Sample Data Curves

97. Figures 11-17 are sample plots taken from Test 10. Figure 11 shows the total tension exhibited at reaction hinges 1 and 2 versus time. The plot shows how the load cells followed each other during impact. The peaks of each curve are recorded as  $T_1$  and  $T_2$  in the data summary sheet, Table 3. The load, before the curve begins to rise, is the pretension value of the cable prior to impact.

98. The force-time history during impact is displayed in Figure 12. The values of  $F$  on the y-axis were determined by the method described in the section, "Calculation of Force, Energy, and Impulse." Furthermore, the impulse was determined from this graph by calculating the area under the curve. The impulse recorded in Table 3 is that which coincides with the peak of the  $Ft$  curve, labeled as  $I$  in Figure 12.

99. Figure 13 shows the relationship of load and displacement as the cable began to move, reached maximum displacement, and finally returned to its original position. This graph vividly displays the hysteresis of the curve. The arrows drawn on the curve show the movement of the tow into the cable (the rising limb of the  $Ft$  curve) and its retreat into the lock chamber (the falling limb of the  $Ft$  curve). The peak deflection and the peak force can be obtained from this plot.

100. The curve in Figure 14 was obtained by calculating the cumulative area under the force-deflection curve for each value of deflection. The value on the y-axis corresponding to the peak deflection is the value of  $E$

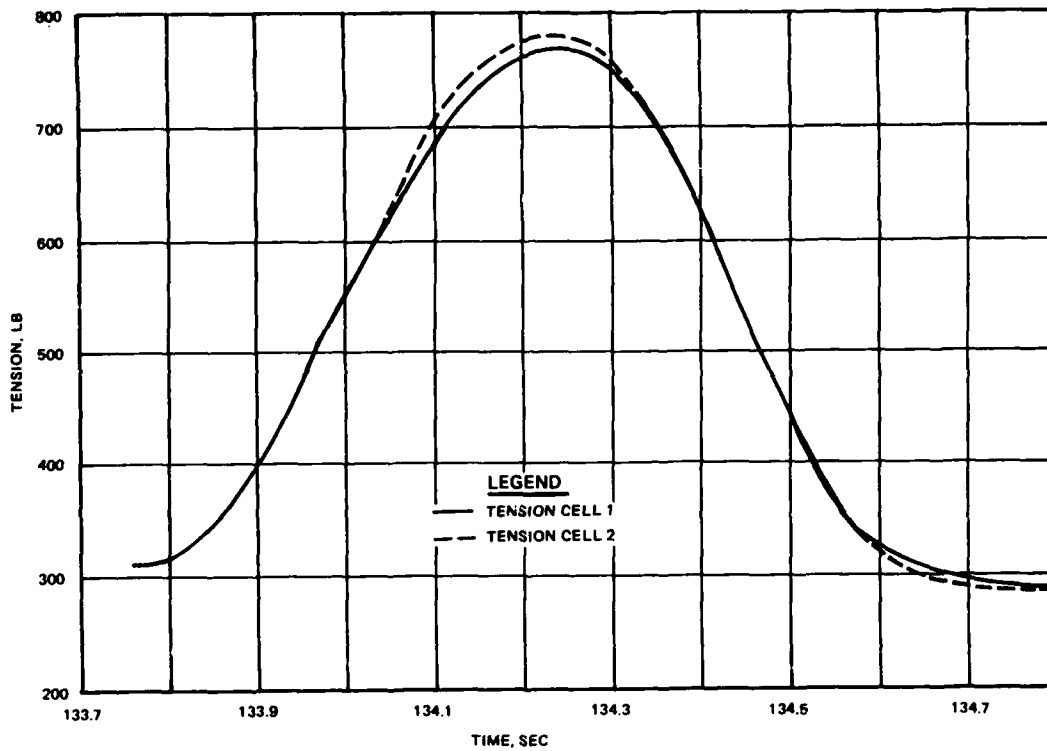


Figure 11. Cable tension, Test 10

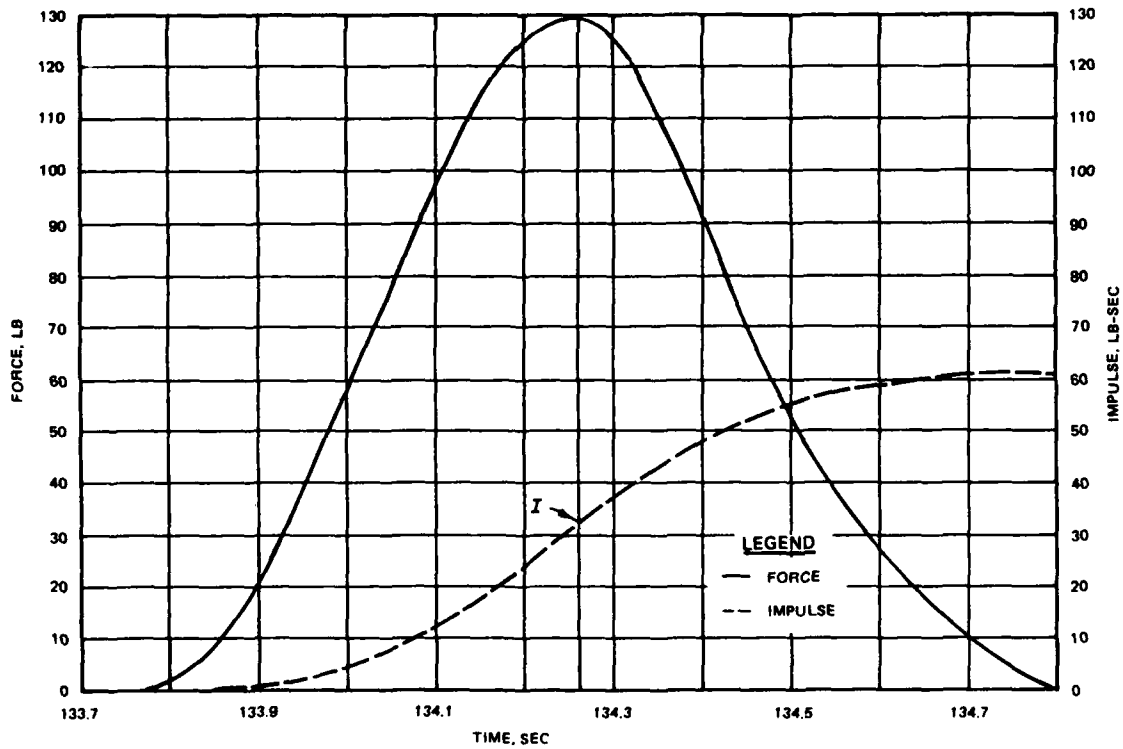


Figure 12. Force and impulse, Test 10

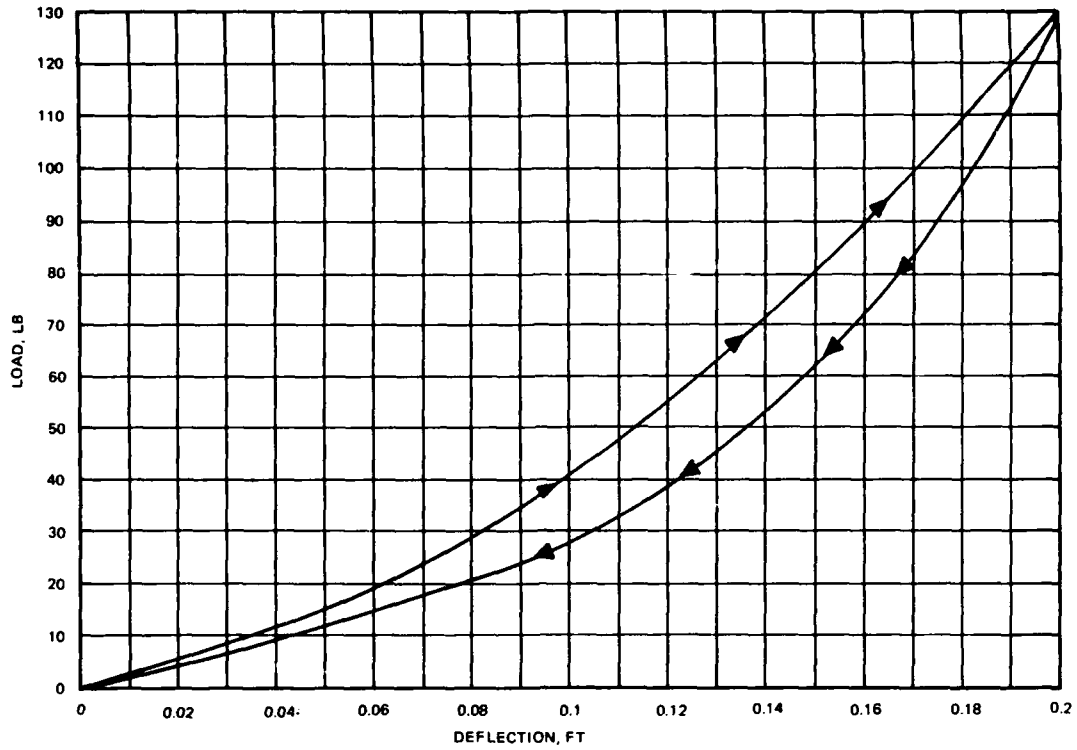


Figure 13. Force-deflection curve, Test 10

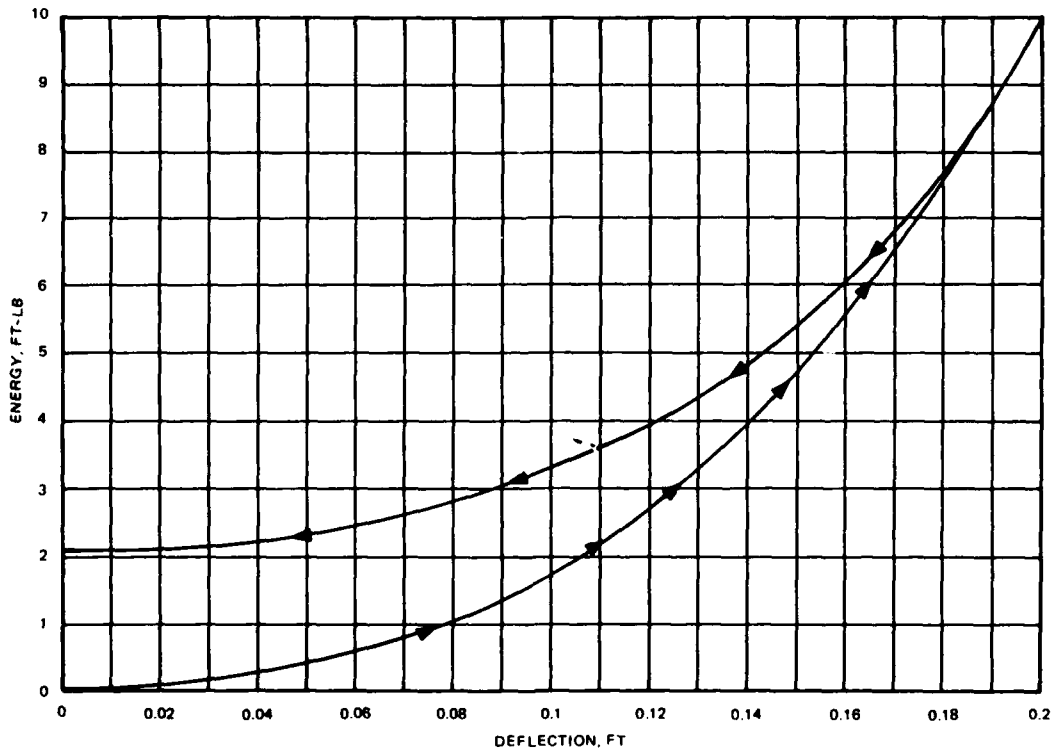


Figure 14. Energy-deflection curve, Test 10

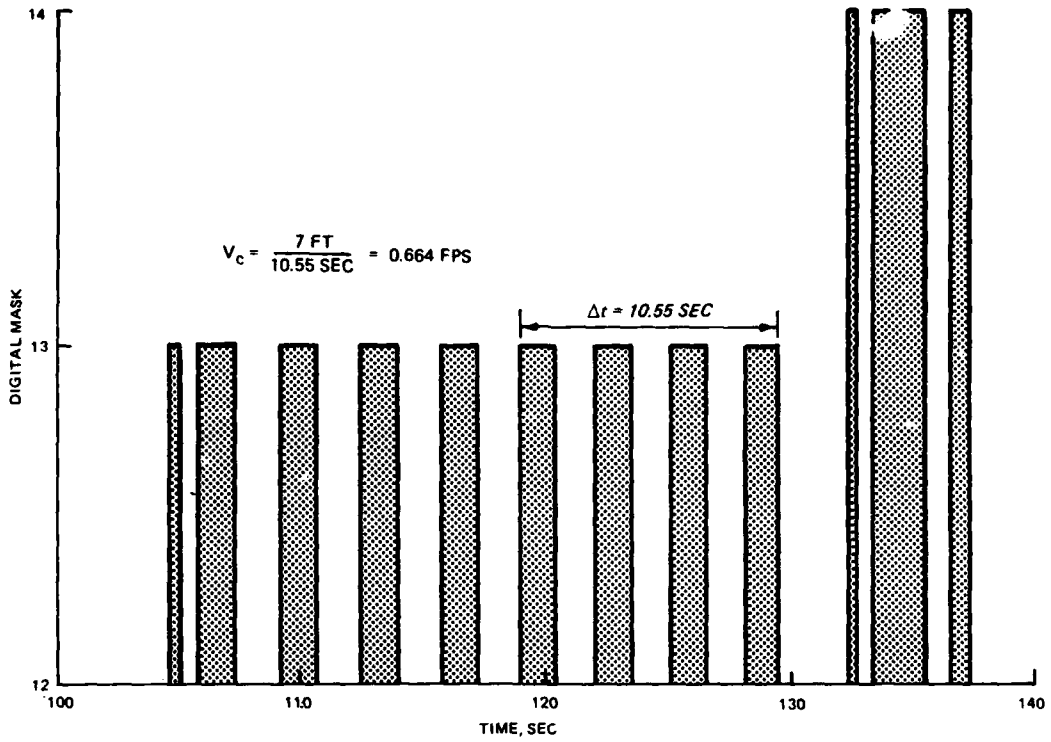


Figure 15. Midchamber tow velocity, Test 10

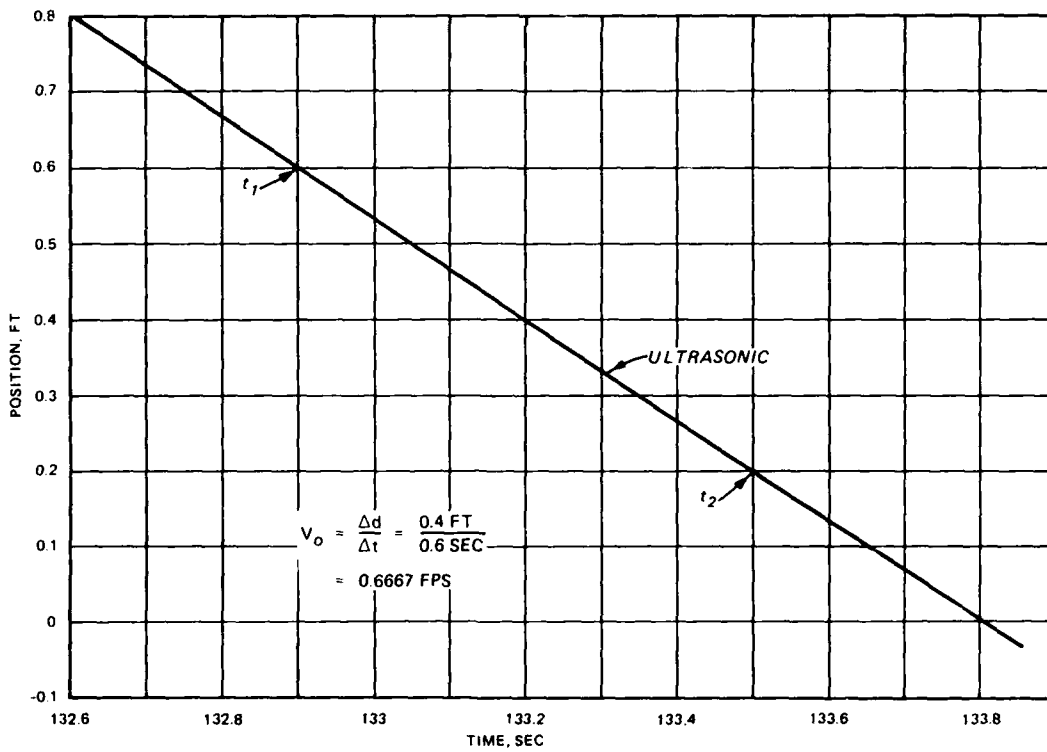


Figure 16. Approach velocity  $V_0$ , Test 10

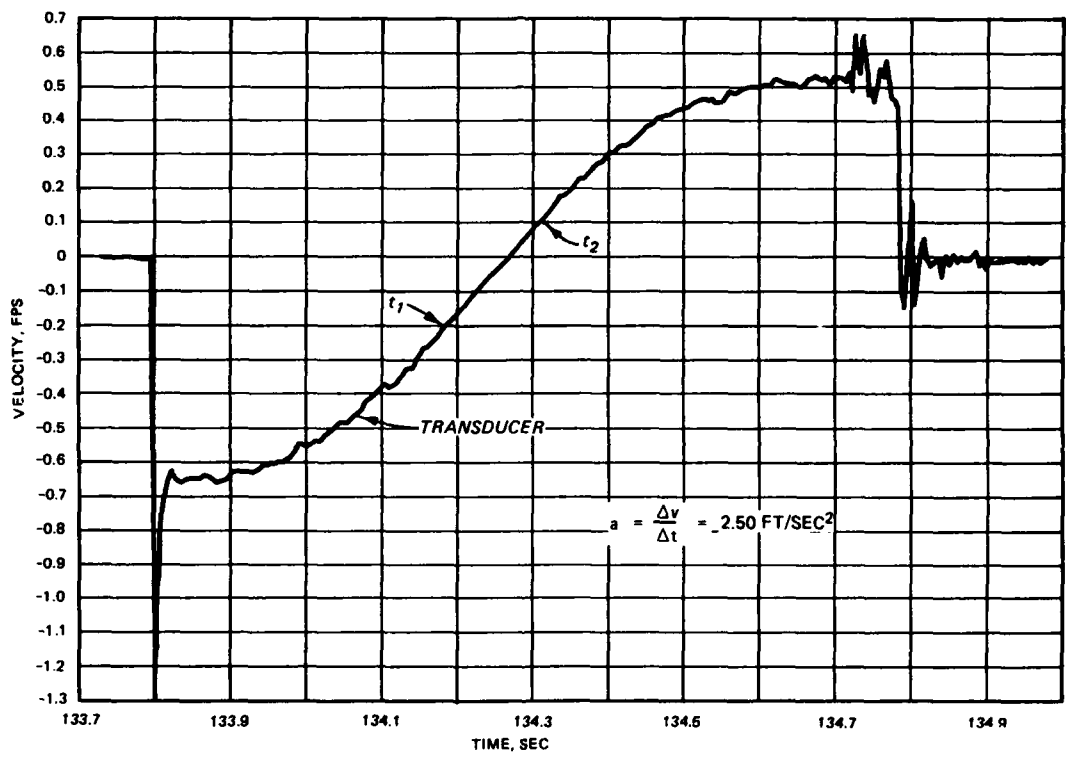


Figure 17. Cable velocity, Test 10

recorded in Table 3. As can be seen by the plot, energy was lost during the reaction due to the hysteretic damping of the cable. The value at the ordinate represents the area contained by the loop in the force-deflection curve. Again the arrows are drawn to show the sequence in which the values were plotted.

101. Figure 15 is a plot of the digital bit response of the light monitors versus time. Since the mask sequence has already been explained, it can simply be stated that the velocity was determined by graphically taking the time lapse as the last four panels on the barge passed the light monitor and dividing it into the total number of 1-ft panels and spaces. This is shown on the graph and used to define the average speed of the tow at midchamber  $V_c$ .

102. Position of the tow (in feet) versus time is plotted in Figure 16, as obtained from the ultrasonic device, such that positive values of feet represent the position of the tow before it impacted the cable. Velocity is obtained by taking the slope of the line produced by this plot. The linearity indicates that the velocity was relatively constant prior to contact. An example calculation is provided on the plot.

103. The cable velocity versus time is shown in Figure 17. Values of zero before and after the impact show that the cable returned to a quiescent state. Negative values of velocity represent the cable velocity from initial contact in the +y-direction until zero velocity occurred at maximum displacement of the cable. Positive values of velocity indicate the speed of movement of the cable back to its original position. The acceleration is the slope of the curve as it passes through zero. An example of this procedure is shown on the plot. Note on the curve that the velocity tended to oscillate due to vibration of the cable as the tow was rejected from it.

#### Summary Data of Peak Results

104. Table 3 is a summary spreadsheet containing all available data from Tests 1-75. Included in the table are the test number, weight of the tow,  $l_1$ ,  $l_2$ , maximum deflection, velocity at cable or initial velocity  $V_0$ , midchamber velocity  $V_c$ , acceleration  $a$ , initial tension in cable  $T_p$ , peak tension cell 1  $T_1$ , peak tension cell 2  $T_2$ , peak force  $F$ , energy  $E$ , and impulse  $I$ .

## PART VI: COMPARISON OF EXPERIMENTAL DATA

105. By comparing experimental results, several questions have been resolved on how the independent variables of mass, barge width, and lock floor geometry relate to the dependent variables of force and energy. Additionally, observations are made concerning the effects of the same independent variables on the tow speed in the chamber. Most of the conclusions have been drawn from graphical representations of the data presented in Table 3.

### Force and Energy Versus Velocity for Variable Mass

106. Both force and energy are directly related to mass. Figure 18 shows the relationship between velocity and force for three different mass tows; Figure 19, the relationship between velocity and energy. Obviously, for a given velocity, as mass increases, so do the force and energy.

### Force and Energy Versus Velocity for Variable Barge Widths

107. Figures 20 and 21 show the force-velocity curves for tests with four barges ( $mg = 1,180$  lb) and tests with two barges ( $mg = 694$  lb) in a flat lock floor, respectively (where  $mg$  is the mass times the gravitational constant). For differing  $W_B/W_C$  ratios there was no apparent change in the relationship between force and velocity. This indicates that the width of the barge train has negligible influence on its applied force for a given velocity. Figures 22 and 23 display the energy-velocity curves for the same conditions. There seems to be a slight shift in the energy as the velocity exceeds 0.6 fps for the Type 3 configuration, but the data for Types 2 and 4 are represented by virtually the same curve. There is no explanation for this shift, but the author still concludes that the width does not appear to affect the energy applied by the tow to the cable system. However, the barge widths had dramatic effects on the speed of the tow relative to a particular propeller speed of the towboat engines (see the section, "Effects of Tow Operation on Velocity").

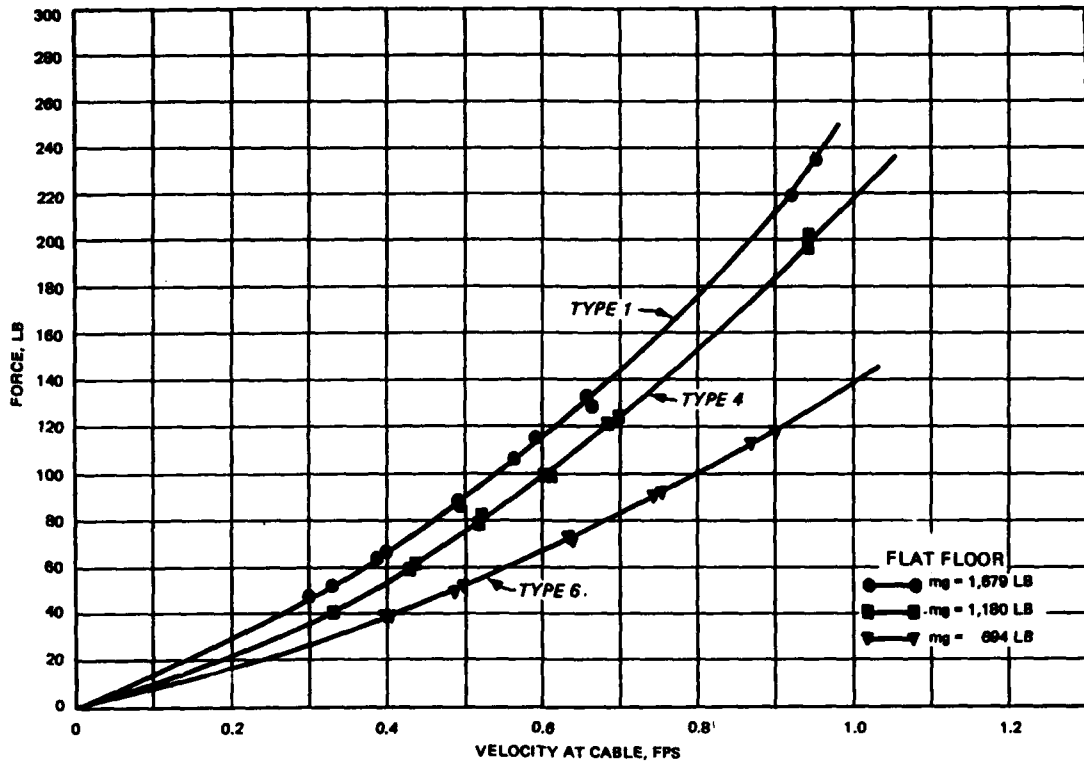


Figure 18. Force-velocity curve, variable mass

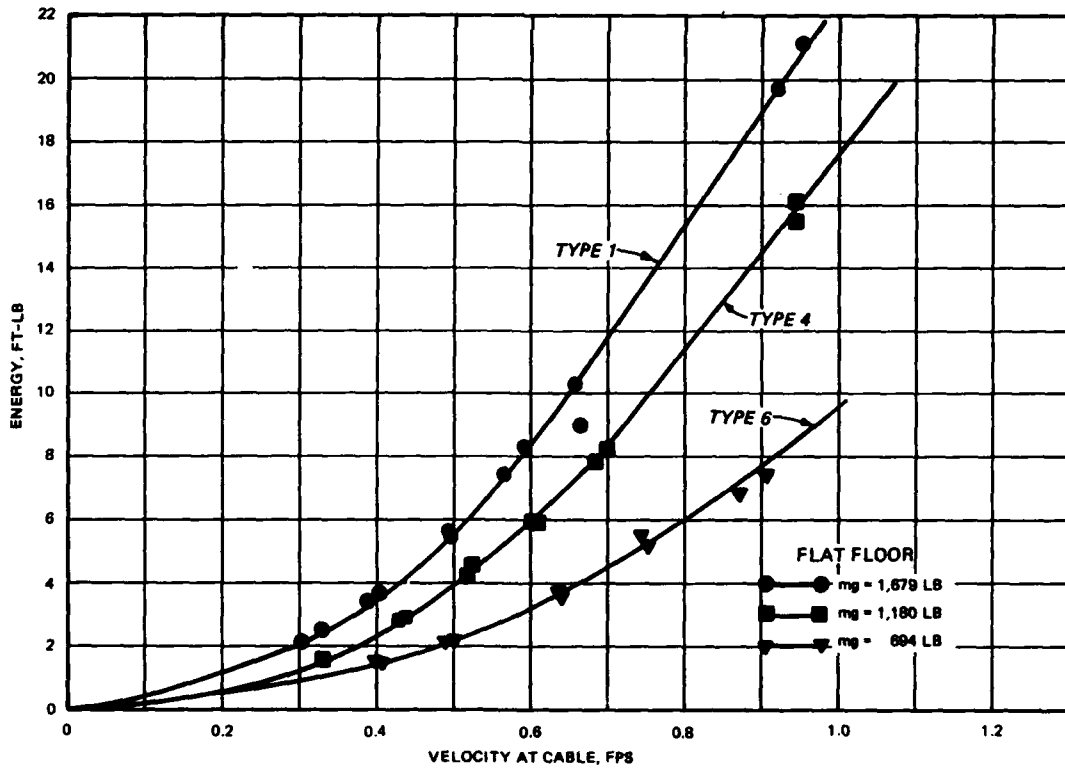


Figure 19. Energy-velocity curve, variable mass

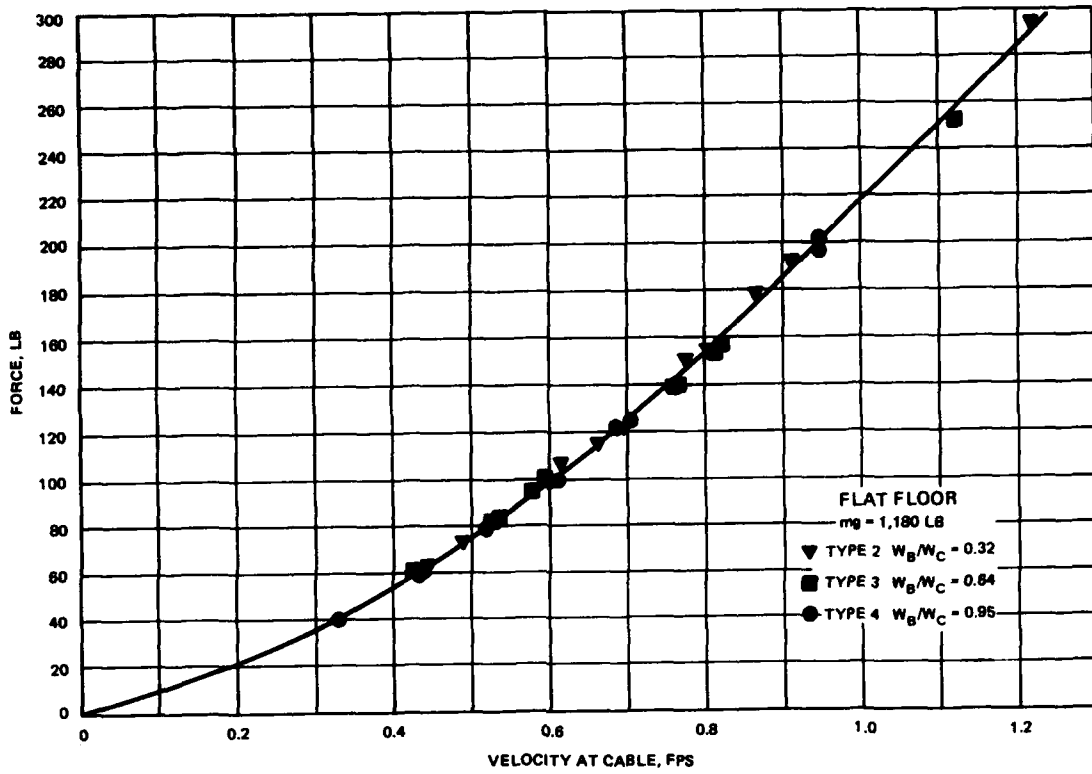


Figure 20. Force-velocity curve,  $m_g = 1,180 \text{ lb}$

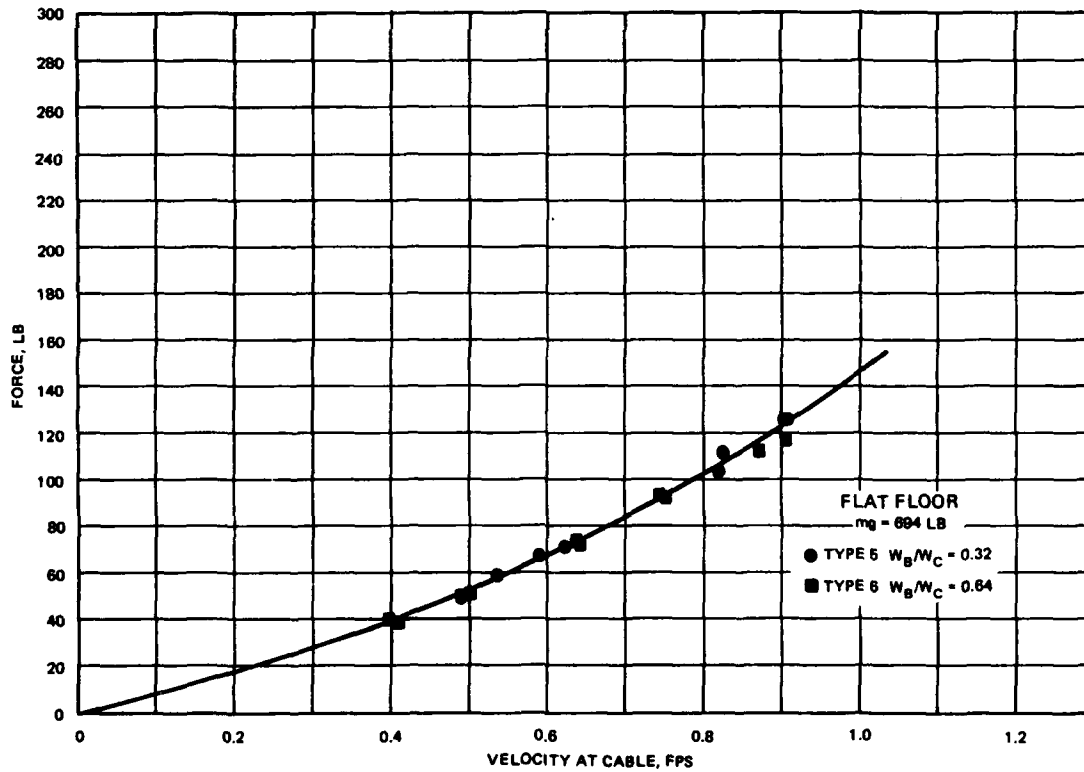


Figure 21. Force-velocity curve,  $m_g = 694 \text{ lb}$

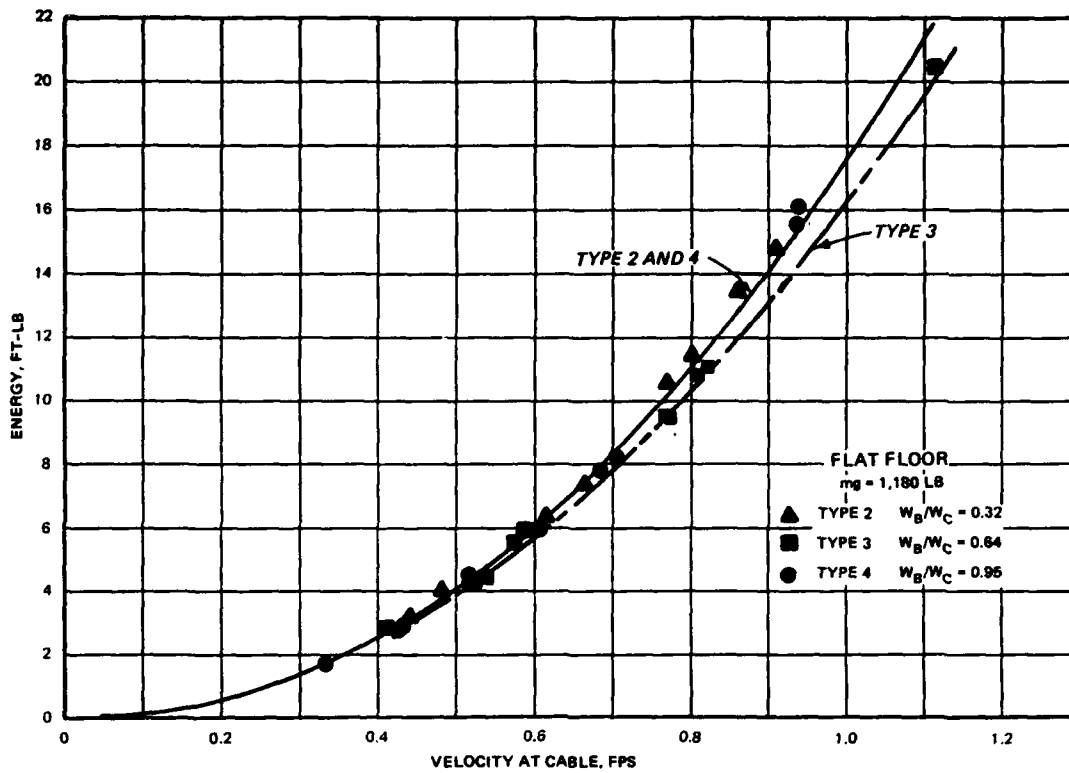


Figure 22. Energy-velocity curve,  $m_g = 1,180$  lb

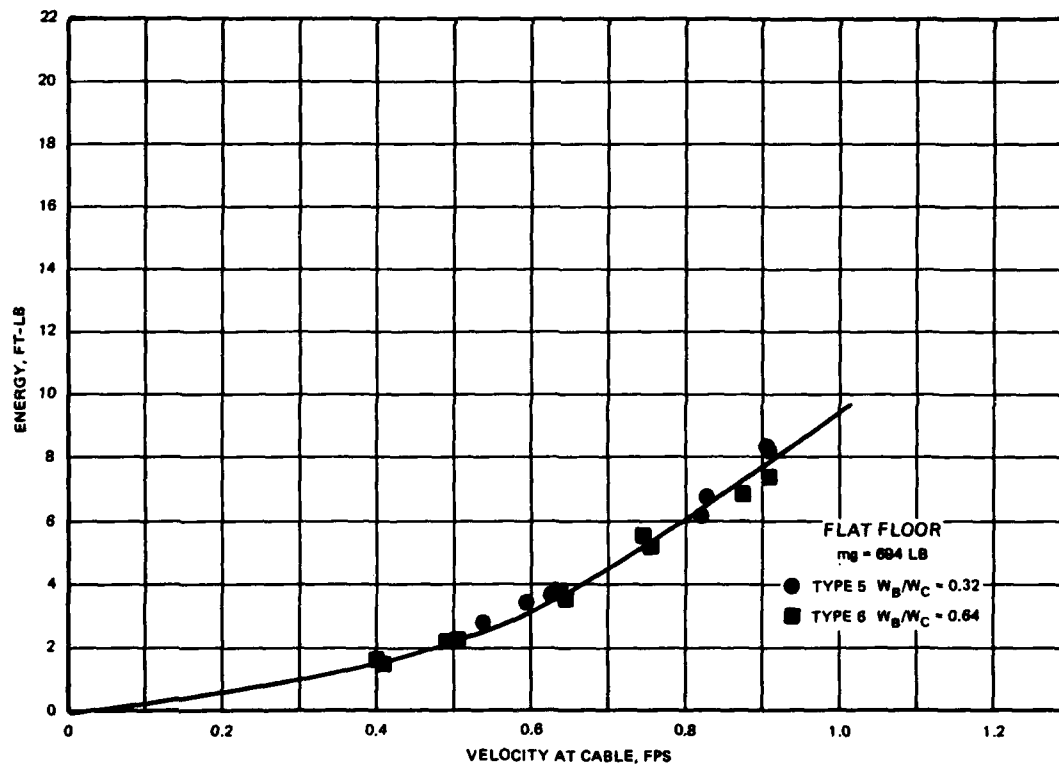


Figure 23. Energy-velocity curve,  $m_g = 694$  lb

## Force and Energy Versus Velocity for Flat Floor and Sill

108. For a given  $V_0$ , mass, and configuration, the applied force was unaffected by the sill (Figure 24); neither was the energy (Figure 25). While the tow speed was fairly constant through the chamber for the flat floor condition, it varied with the sill in place (see the section, "Effects of Tow Operation on Velocity") such that as the tow was crossing the sill, it slowed down; and as it passed the sill, it tended to surge forward at an increased velocity. To give some indication of this phenomenon, Figures 26 and 27 show the midchamber velocity as it relates to force and energy. As can be seen by these curves, for a given midchamber velocity, the force and energy are higher with the sill in place. The following section presents relationships developed between  $V_0$  and  $V_c$ .

### Effects of Tow Operation on Velocity

109. Figure 28 shows a bar graph relating the different propeller operations (clicks on the radio control) to the  $V_0$  values obtained from testing. This graph is intended to show trends, not absolute relationships, between increasing propeller speeds and the geometry of variable  $W_B/W_C$  ratios, variable draft and mass, and with- and without-sill conditions. Absolute relationships between these parameters could not be determined for several reasons. For one, tachometer readings were not available to relate the radio clicks to propeller speed. Also, each bar represents an average speed obtained from one to three data points. Another complication was that the radio operation was limited, in that a linear increase in propeller speed could not be obtained between each click on the control. In fact, between clicks 7 and 8, the apparent velocity of the tow increased between 0.2 and 0.3 fps, as opposed to approximate increments of 0.1 fps for clicks 3 through 7. This accounts for the gaps that are sometimes displayed in the data curves.

110. Upon examination of this bar graph, several trends can be deduced relative to geometric effects on velocity of the tow. Bars 3-5 and 6-7 on each increasing propeller speed show how velocity decreases as barge width increases for four-barge and two-barge configurations, respectively. Bars 1 and 2 show that velocity of the tow is lower for tests conducted with the

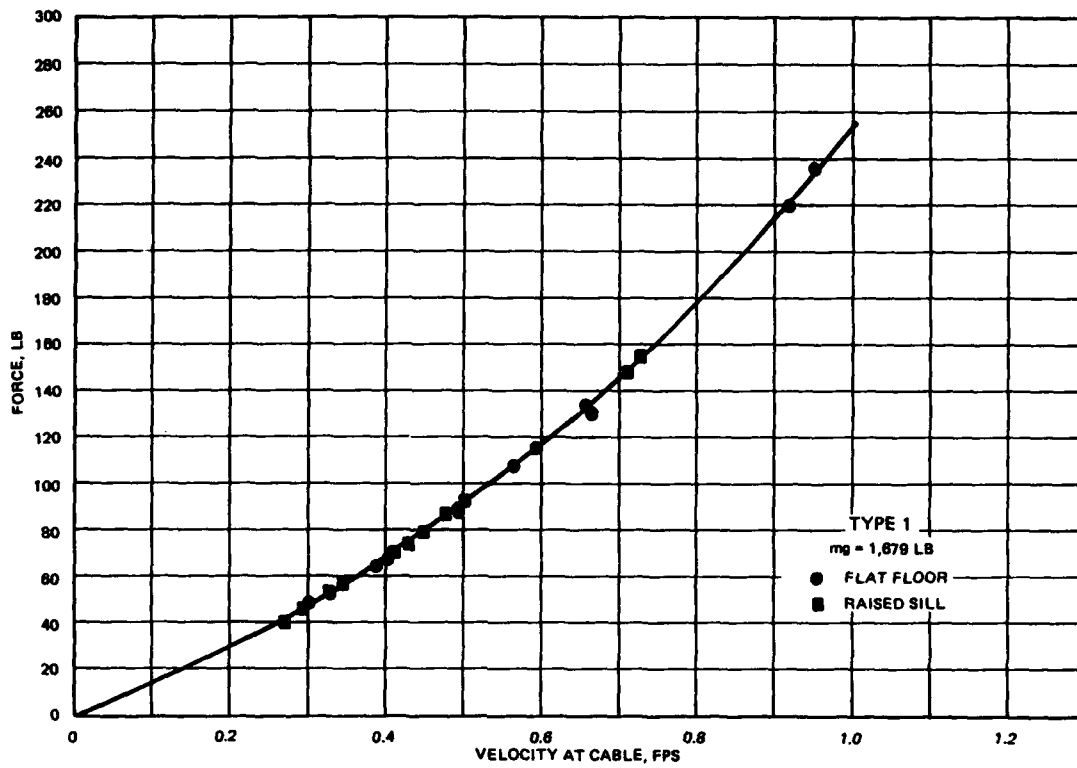


Figure 24. Force-velocity curve, mg = 1,679 lb

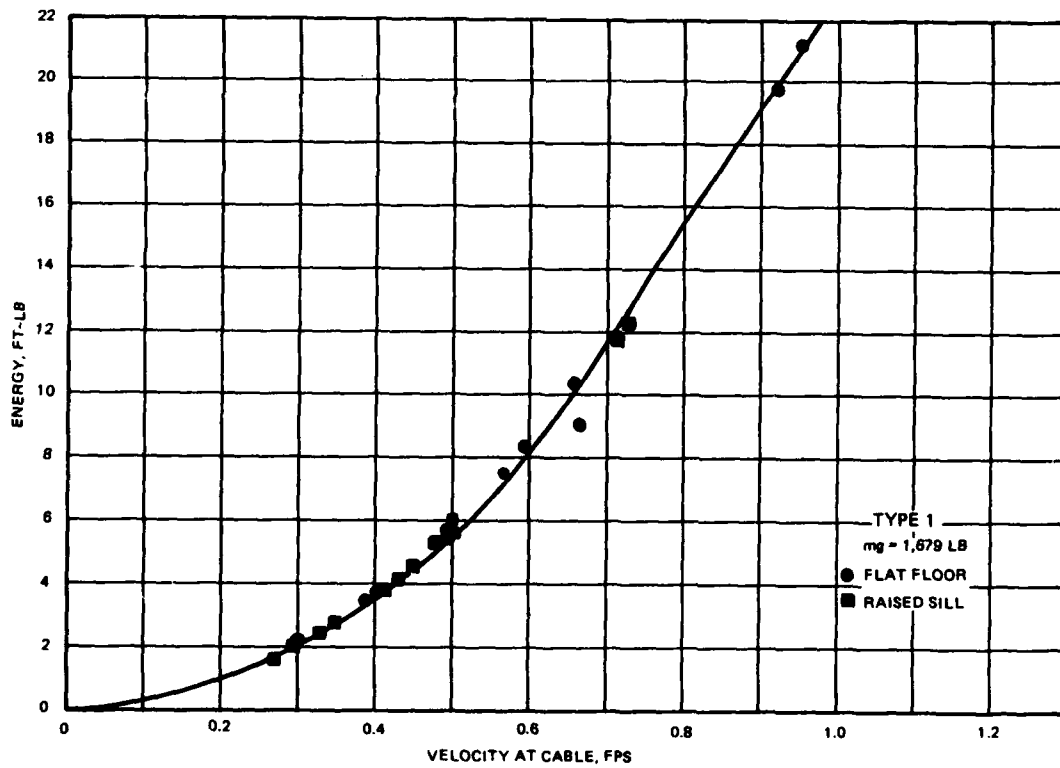


Figure 25. Energy-velocity curve, mg = 1,679 lb

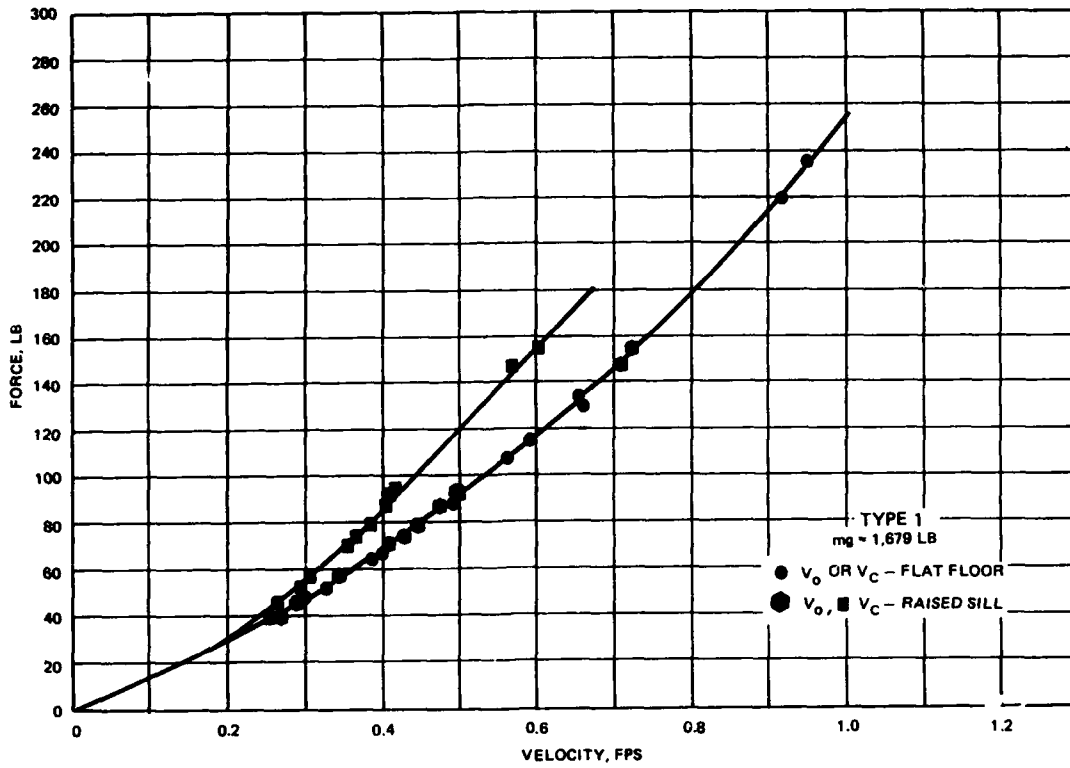


Figure 26. Force-velocity curve,  $V_0$  and  $V_c$

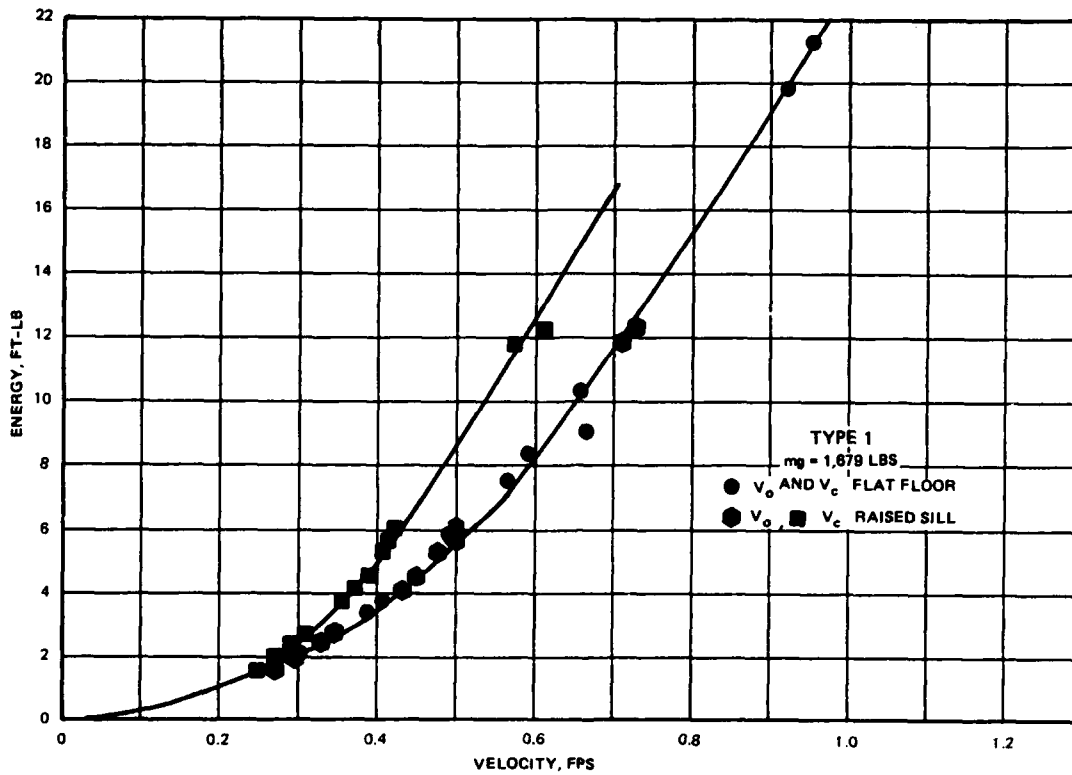


Figure 27. Energy-velocity curve,  $V_0$  and  $V_c$

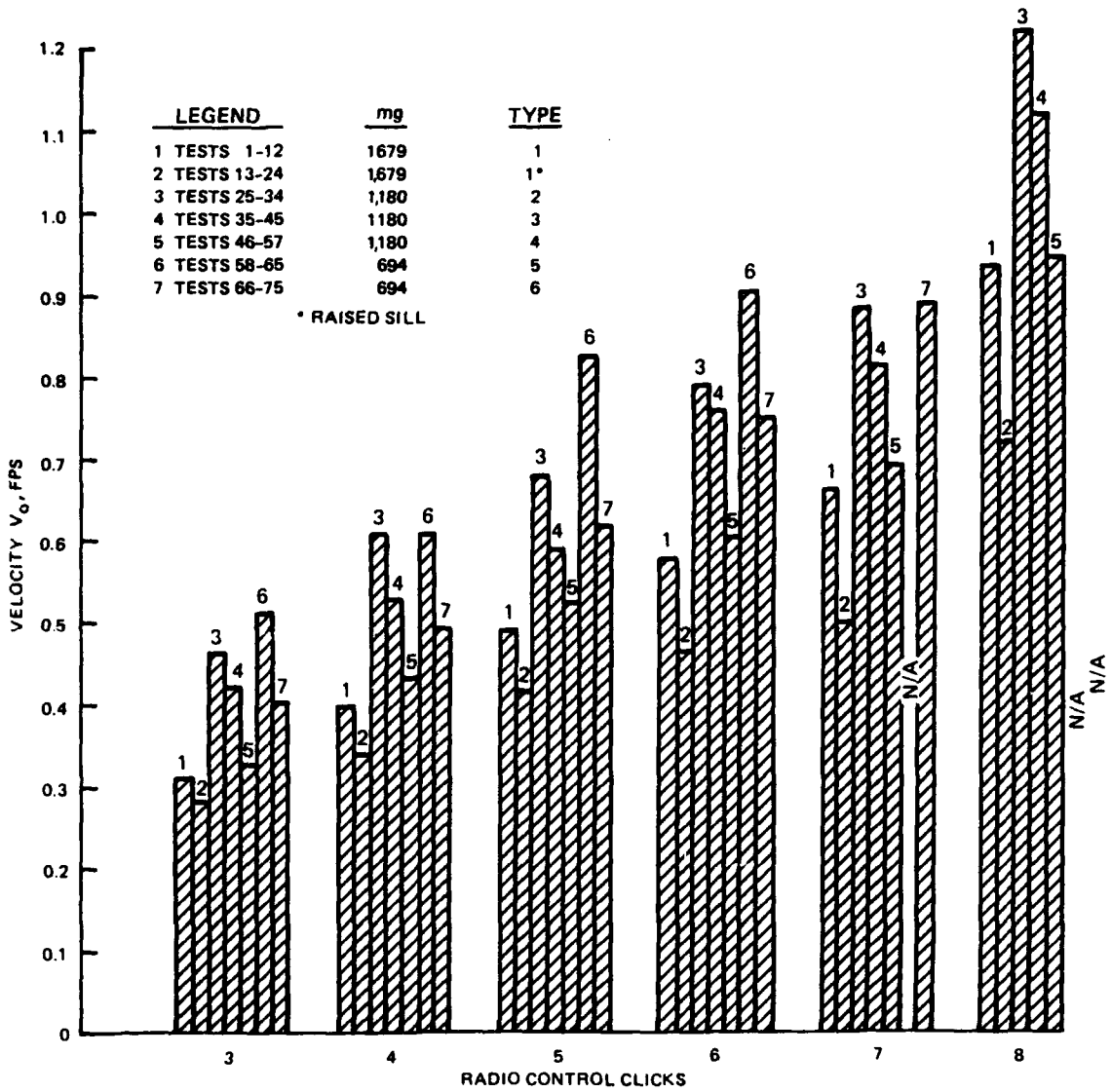


Figure 28. Trends in velocity due to tow operation

raised sill in place. Finally, increasing the mass of the tow decreases its velocity.

111. Figures 29-31 display the relationship between velocity at mid-chamber versus the velocity of the tow just prior to impact. All flat floor conditions produced slopes, or ratios of  $V_c$  to  $V_0$ , of approximately 1. The relationship in Figure 31 displaying the with- and without-sill conditions shows that the sill lowers this ratio and has a dramatic effect on the movement of the tow in the chamber.

### Results

112. The data plots indicate that force and energy are not affected by the geometric constraints of the lock chamber if the velocity at impact is used. When force-velocity curves were compared for conditions just prior to impact for a given mass with an unrestricted depth of pool condition (Figures 20 and 21), the different barge widths caused no apparent shift to the curves. In fact the data plotted tightly along the curves. The energy curves for variable barge widths were also similar with only minor shifts in the curves for high velocities. When force and energy versus  $V_0$  were plotted for the two test series with and without the sill (Figures 24 and 25), for the same mass and configuration, differences were negligible. Configuration and floor conditions did play a vital role in the resulting tow velocity (Figure 28).

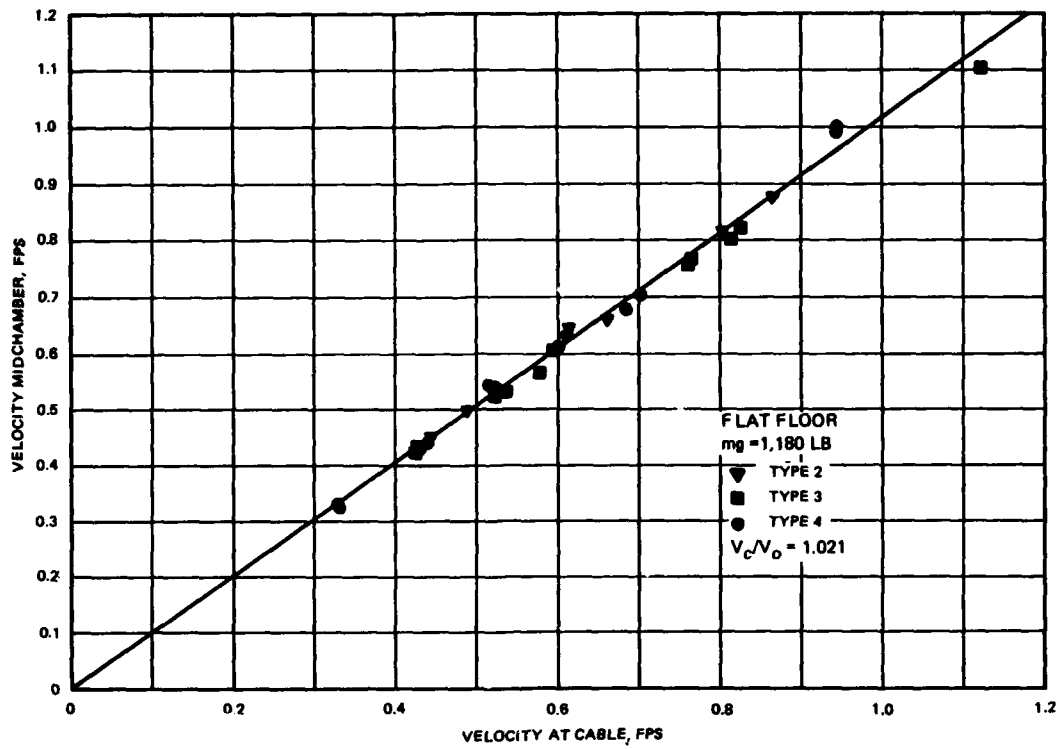


Figure 29.  $V_0$  versus  $V_c$ ,  $mg = 1,180 \text{ lb}$

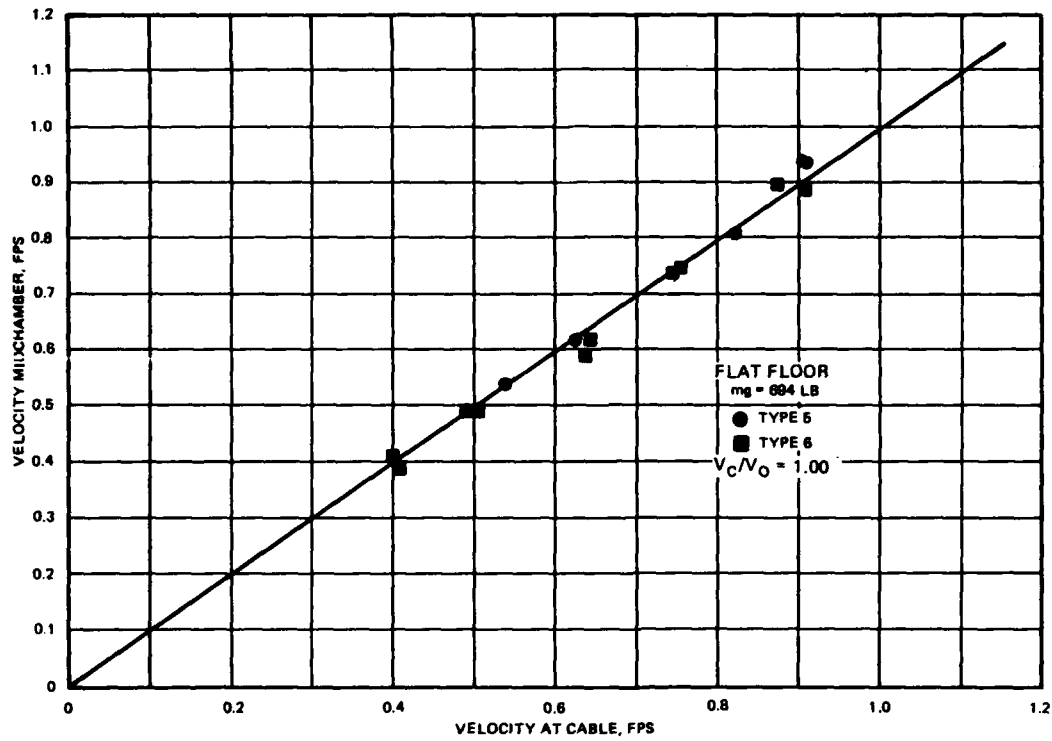


Figure 30.  $V_0$  versus  $V_c$ ,  $mg = 694 \text{ lb}$

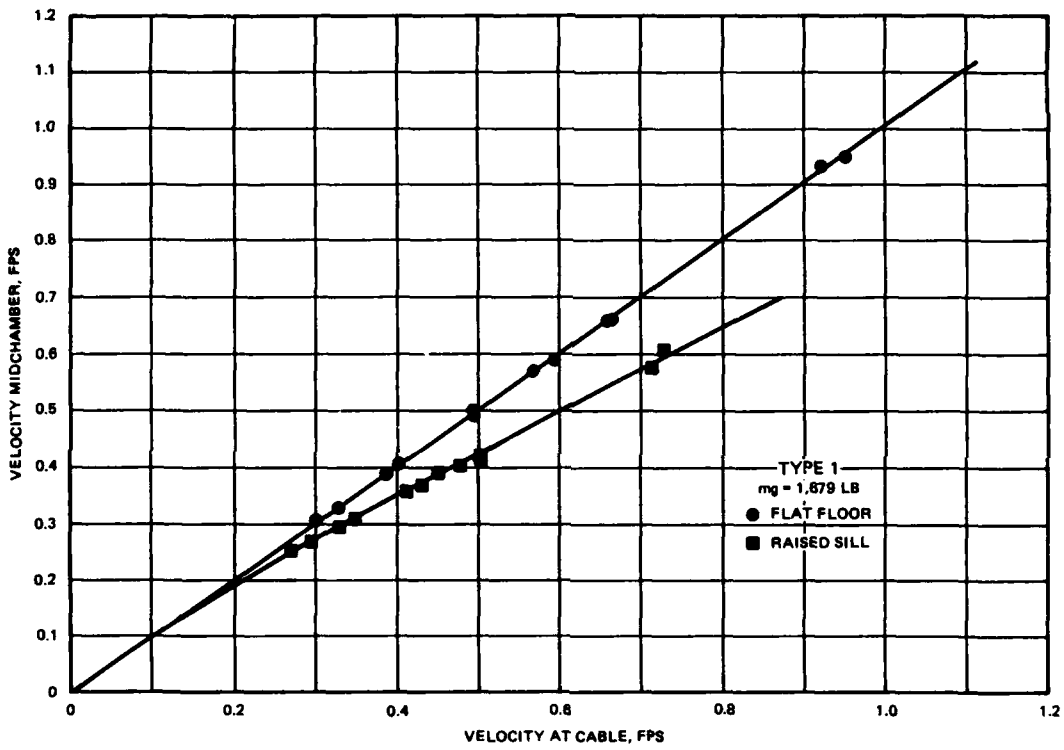


Figure 31.  $V_0$  versus  $V_c$ , mg = 1,679 lb

## PART VII: COMPARISON OF THEORETICAL TO EXPERIMENTAL RESULTS

### Force Comparisons

113. Force is related to mass by Equation 47, where  $a$  is the derivative of velocity versus time or the slope of this curve at peak impact. The term  $F_{\text{peak}}$  is the peak force formed at maximum deflection of the cable and is taken from the experimental data where  $F_{\text{peak}}$  equals  $T_1 \sin \theta_1 + T_2 \sin \theta_2$ . Empirically assessing the ratio of the experimental force to that calculated theoretically by the product of  $m$  and  $a$ , Equation 47 can be arranged such that

$$C_F = \frac{F_{\text{peak}}}{-ma} \quad (53)$$

or

$$C_F = \frac{F_M}{F_T} \quad (54)$$

Where  $F_M$  and  $F_T$  are the model and theoretical forces, respectively. Values for  $C_F$  are derived by the slope of the plots of  $F_M$  versus  $F_T$  (Figures 32-37). (Table 4 lists the data used to obtain these plots as well as those related to energy and impulse.)

### Energy Comparisons

114. If kinetic energy is calculated by Equation 16, in which  $E = (1/2)mV_0^2$ , and is represented in the model as the integral of  $F dy$ , then Equation 46 can be rearranged in terms of  $C_E$  where

$$C_E = \frac{E_{\text{TOTAL}}}{\frac{1}{2} mV_0^2} \quad (55)$$

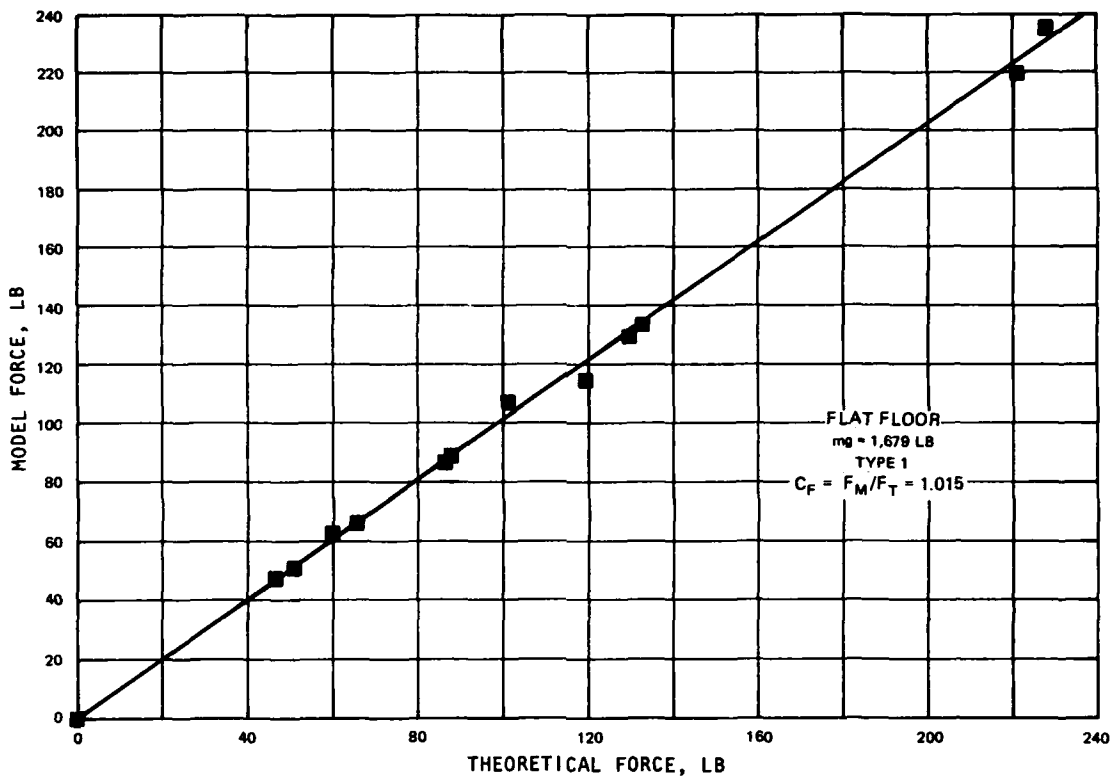


Figure 32. Comparison of experimental to theoretical results,  $C_F$ , flat floor, type 1 tow

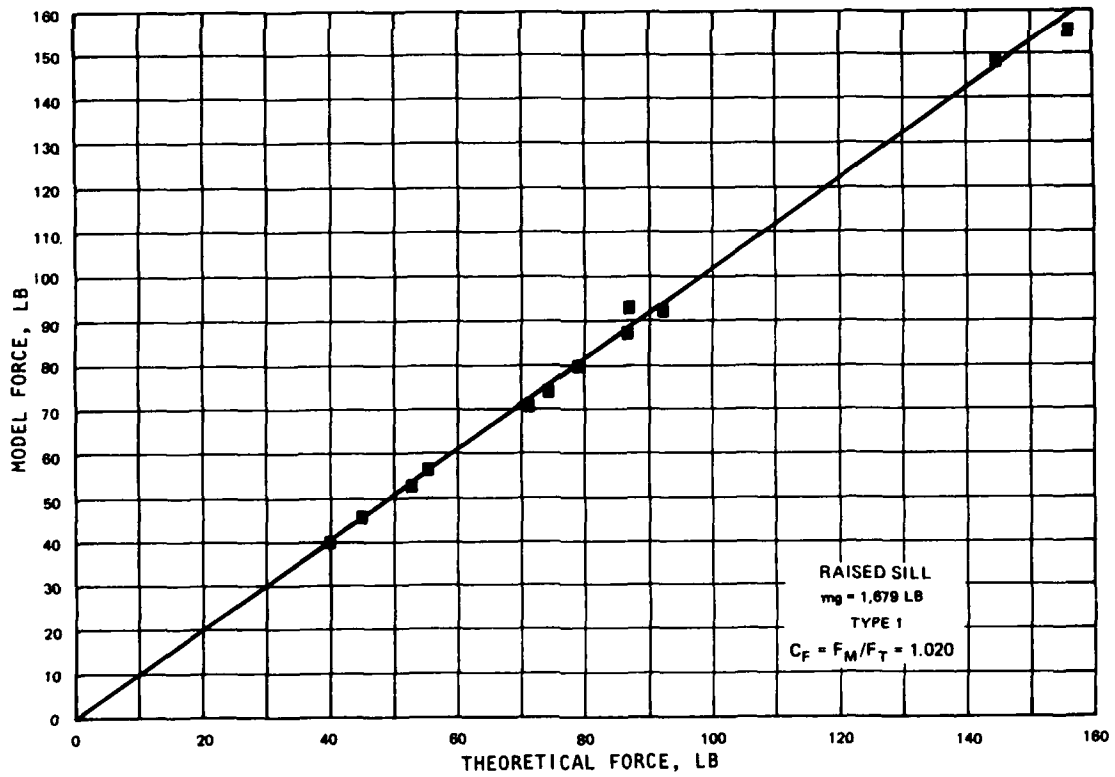


Figure 33. Comparison of experimental to theoretical results,  $C_F$ , raised sill, type 2 tow

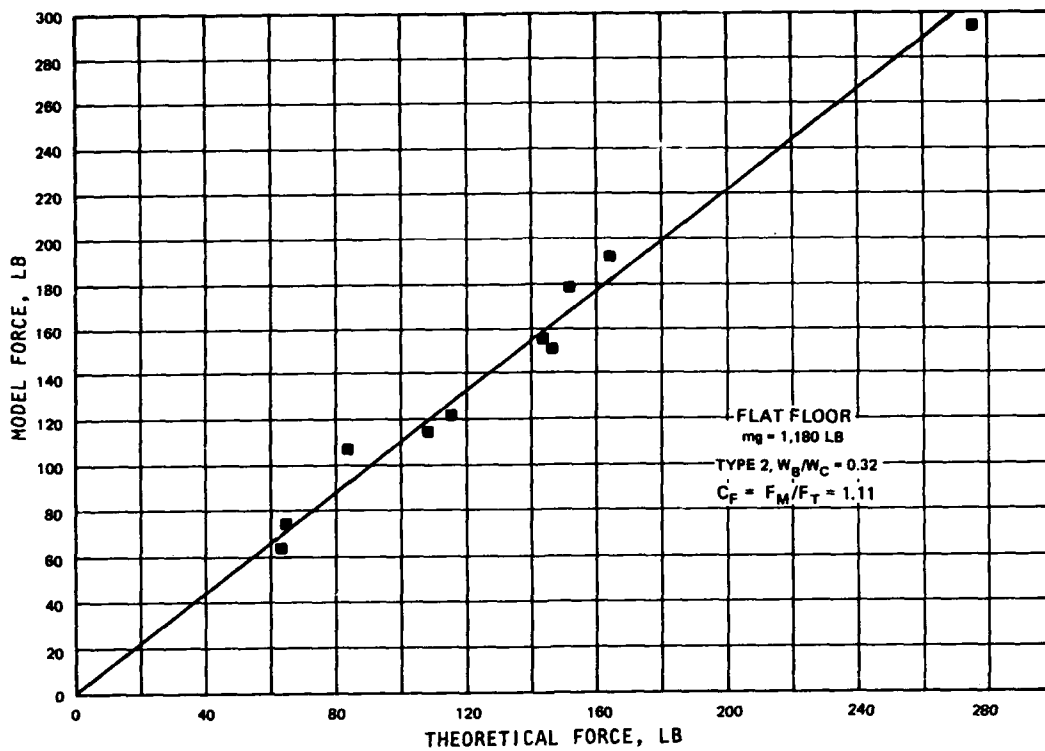


Figure 34. Comparison of experimental to theoretical results,  $C_F$ , type 2 tow

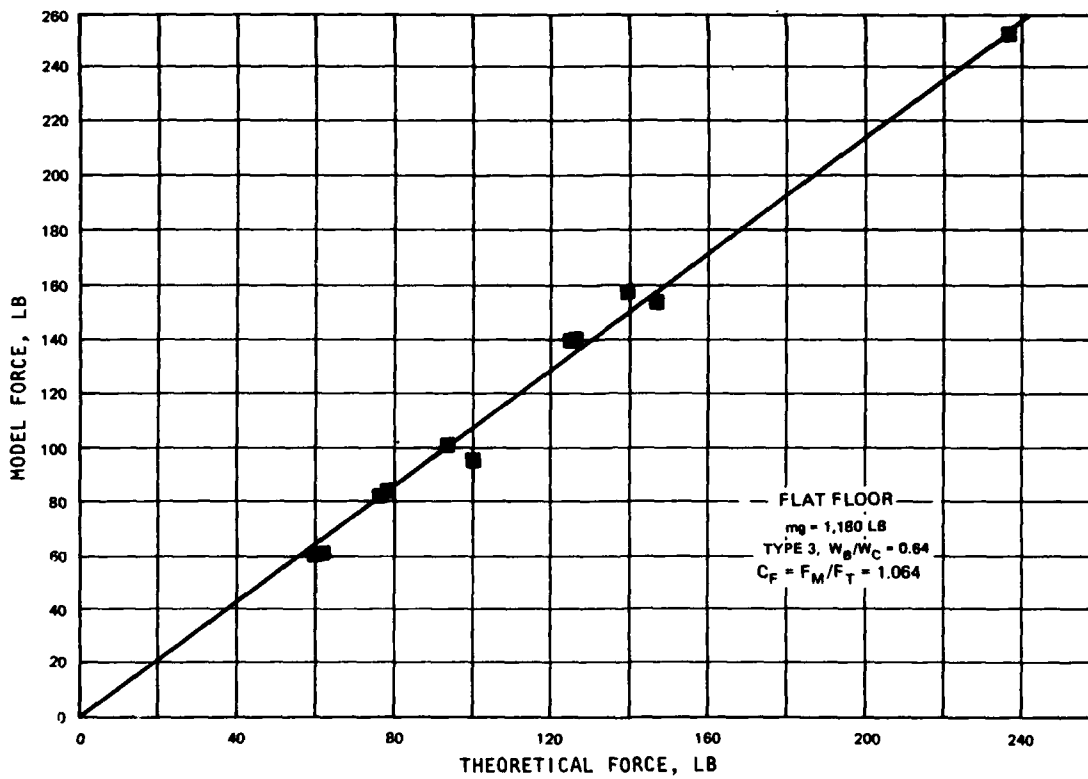


Figure 35. Comparison of experimental to theoretical results,  $C_F$ , type 3 tow

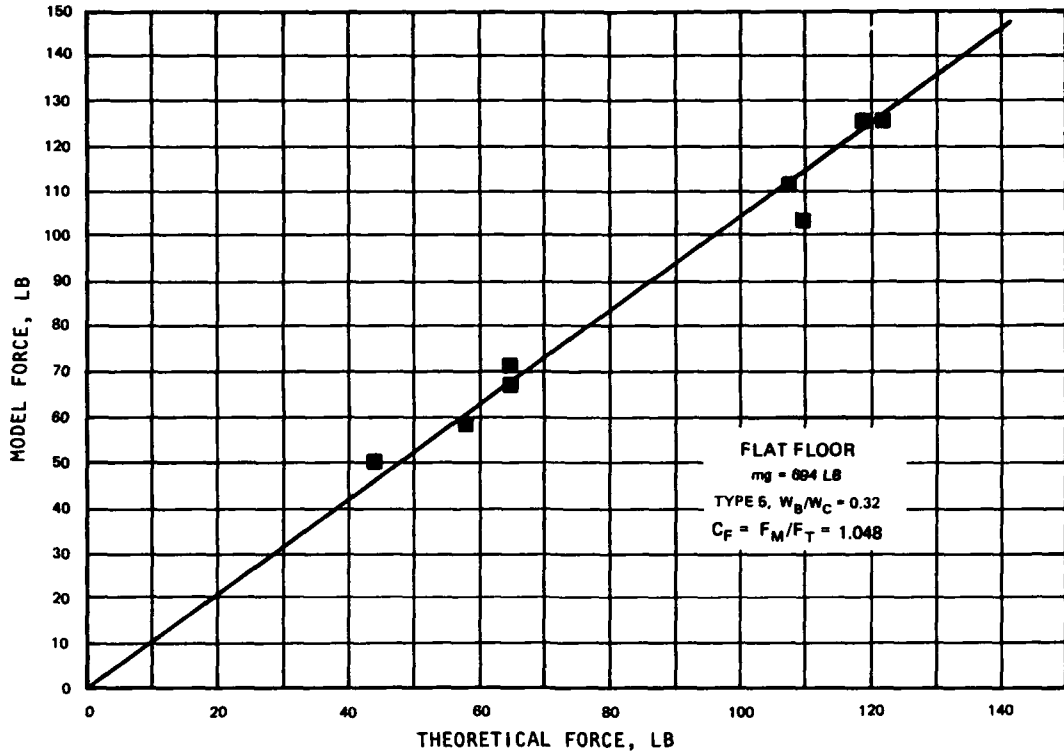


Figure 36. Comparison of experimental to theoretical results,  $C_F$ , type 5 tow

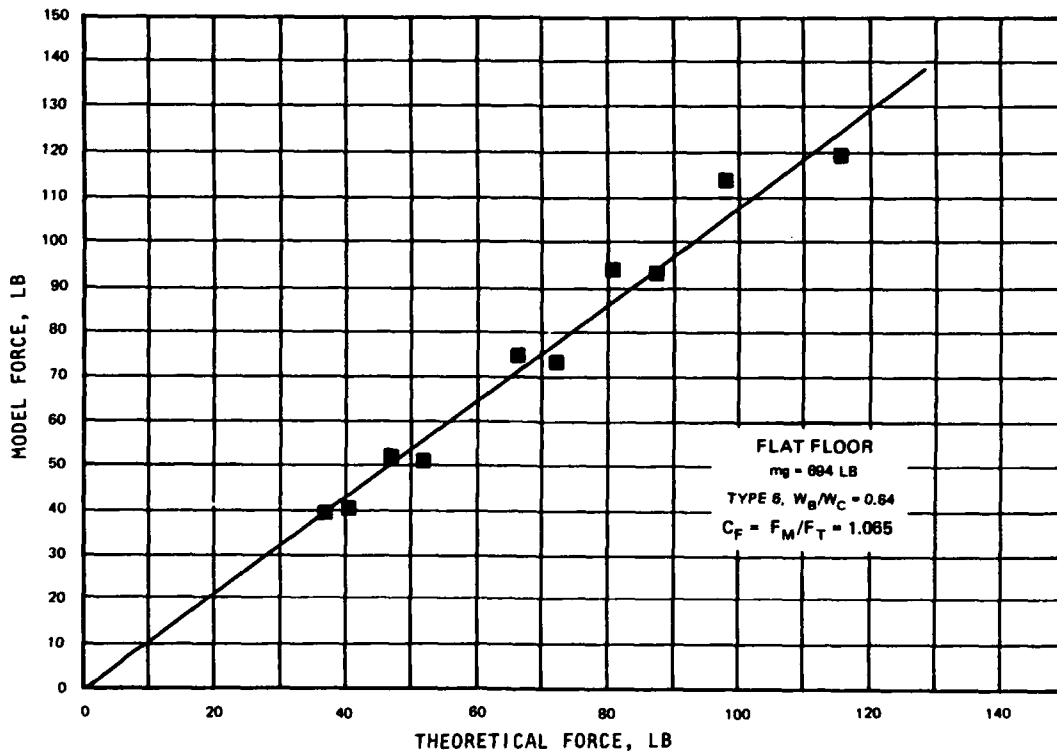


Figure 37. Comparison of experimental to theoretical results,  $C_F$ , type 6 tow

or

$$C_E = \frac{E_M}{E_T} \quad (56)$$

where  $E_M$  and  $E_T$  are the model and theoretical forces, respectively. The coefficient  $C_E$  was taken from Figures 38-44.

#### Impulse Comparisons

115. From Equation 22, theoretical impulse is the product of the mass and the initial velocity. The impulse from the model is the integral of the force-time curve. Then  $C_I$  taken from Equation 48 is

$$C_I = \frac{I_{TOTAL}}{-mV_0} \quad (57)$$

or

$$C_I = \frac{I_M}{I_T} \quad (58)$$

where  $I_M$  and  $I_T$  are the model and theoretical impulses, respectively. Values of  $C_I$  can be found in Figures 45-51.

#### Results

116. Table 5 presents the values of  $C_F$ ,  $C_E$ , and  $C_I$  obtained from the plots in Figures 32-51. There does not appear to be any particular trend in these coefficients for variations in mass, configuration, or floor conditions. The coefficient  $C_F$  tended to have the highest average coefficient (approximately 1.05); the impulse coefficient  $C_I$  was next with an average value of approximately 0.94; the energy comparisons resulted in the lowest coefficients with an average  $C_E$  value of 0.90. The low value of  $C_E$  would suggest that the energy actually produced by the tow was lower than the calculated kinetic energy. This would disprove the theory of attached mass

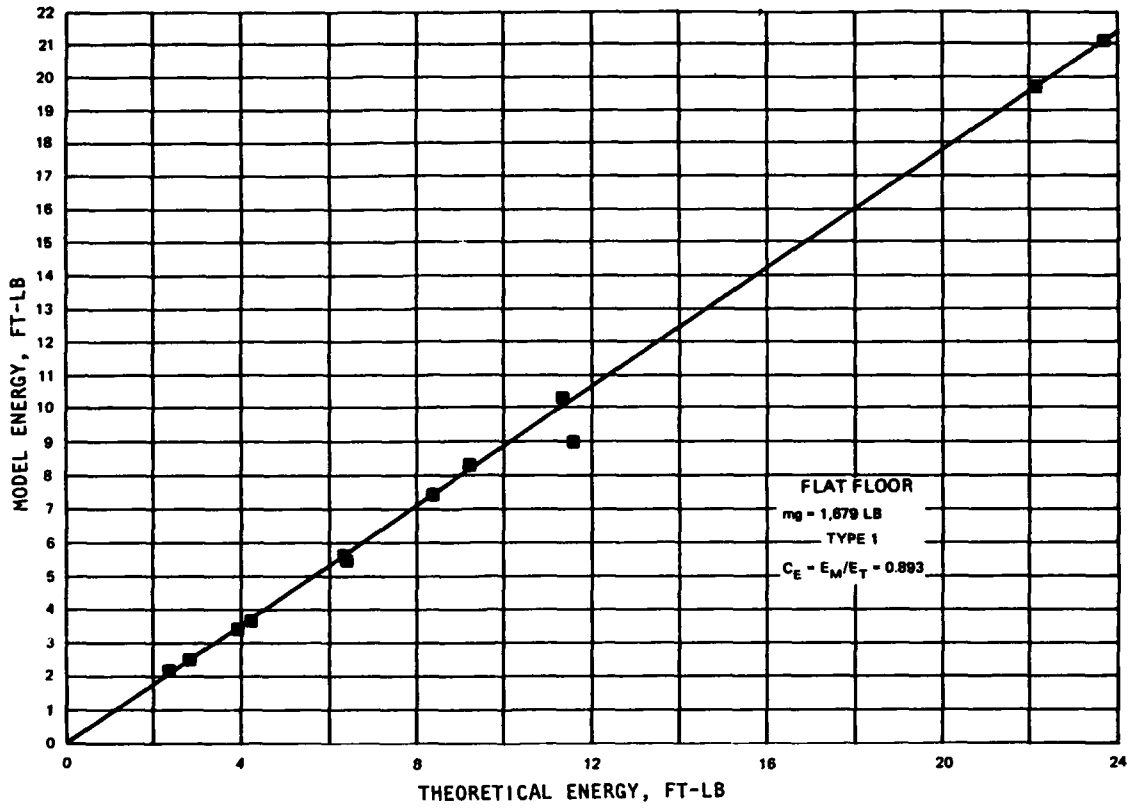


Figure 38. Comparison of experimental to theoretical results,  $C_E$ , flat floor, type 1 tow

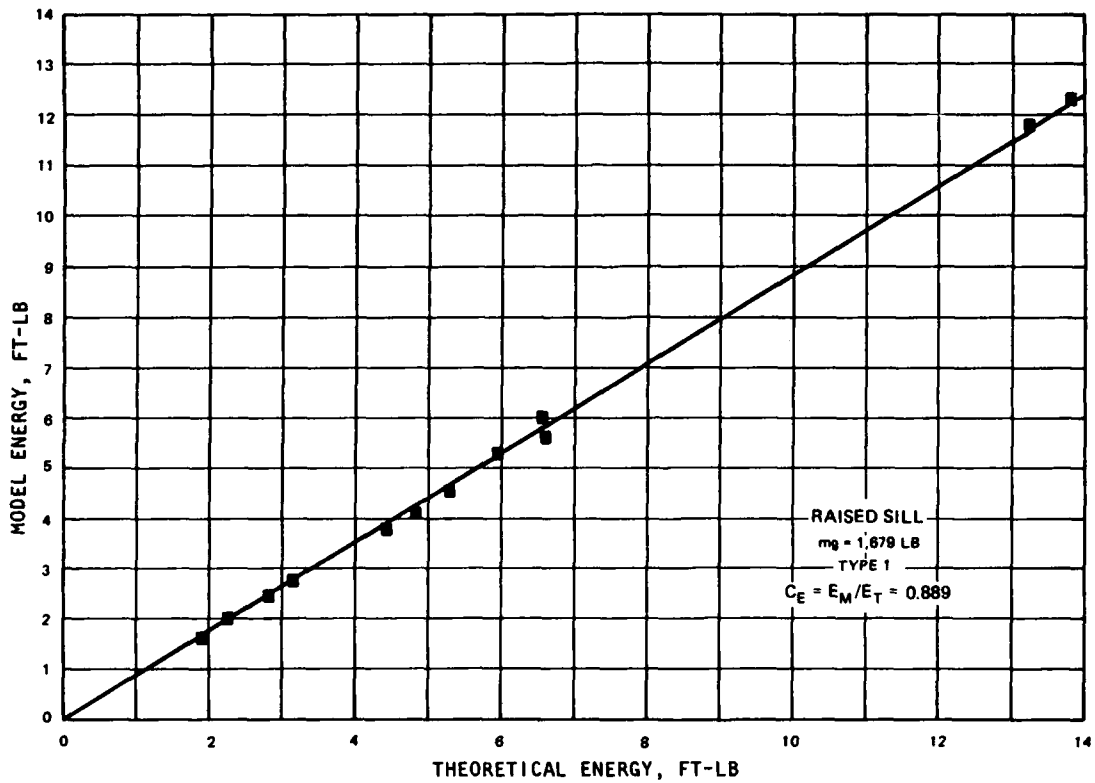


Figure 39. Comparison of experimental to theoretical results,  $C_E$ , raised sill, type 1 tow

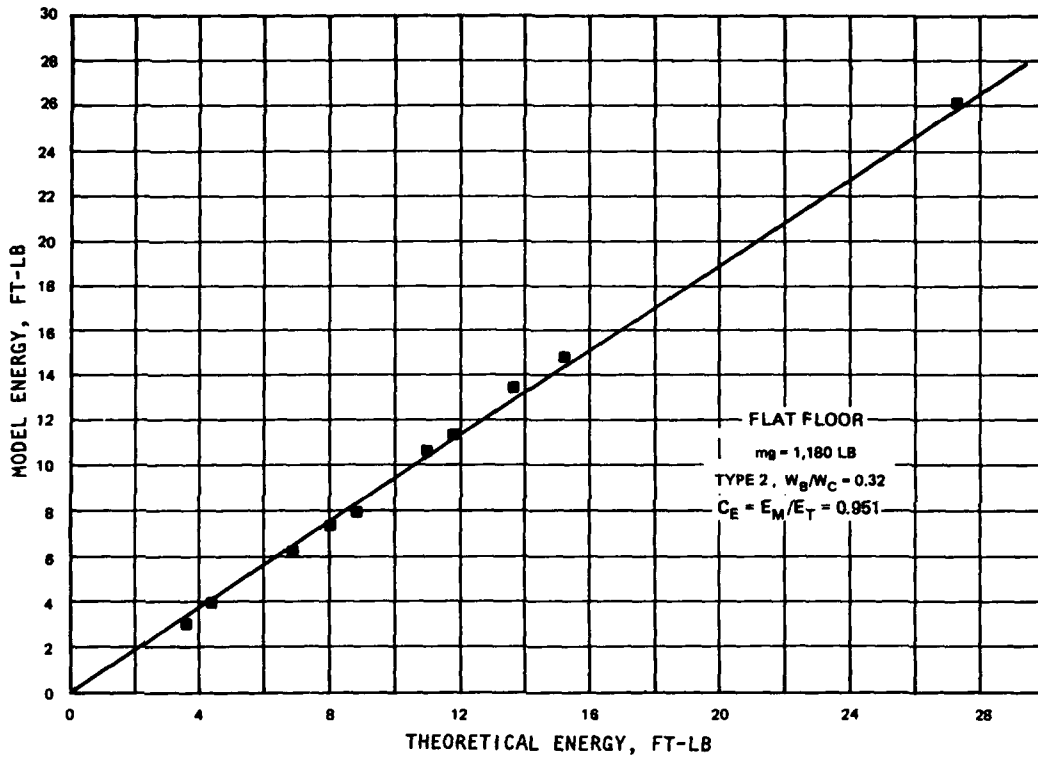


Figure 40. Comparison of experimental to theoretical results,  $C_E$ , type 2 tow

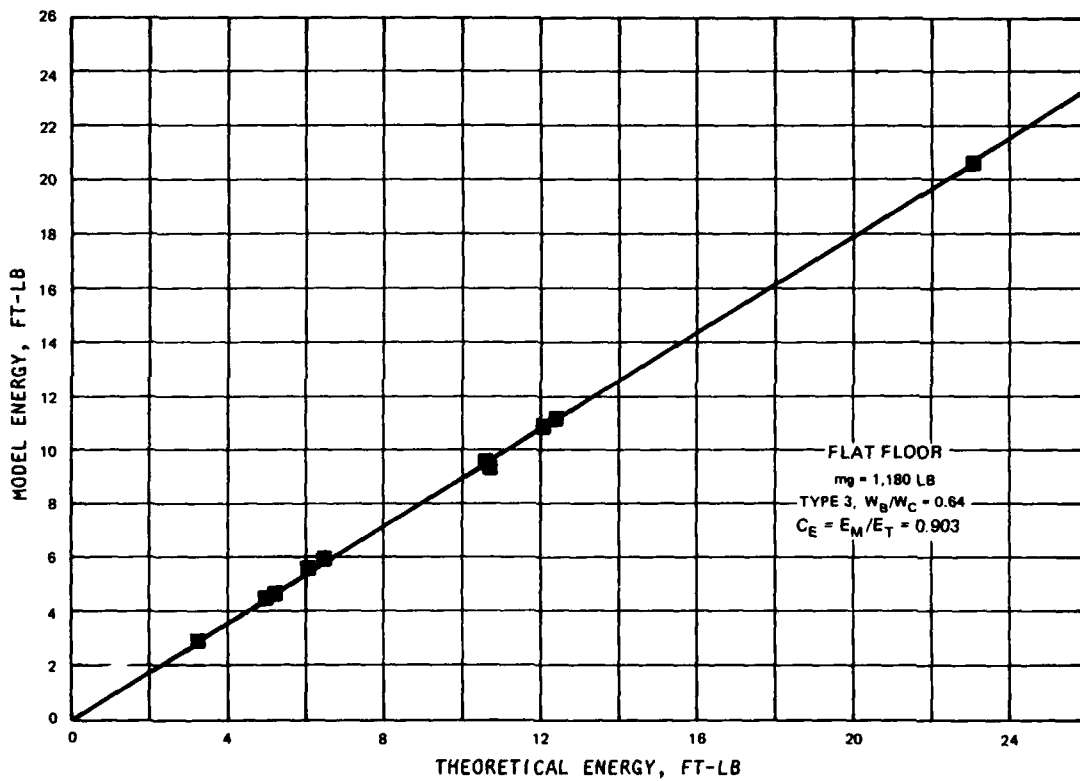


Figure 41. Comparison of experimental to theoretical results,  $C_E$ , type 3 tow

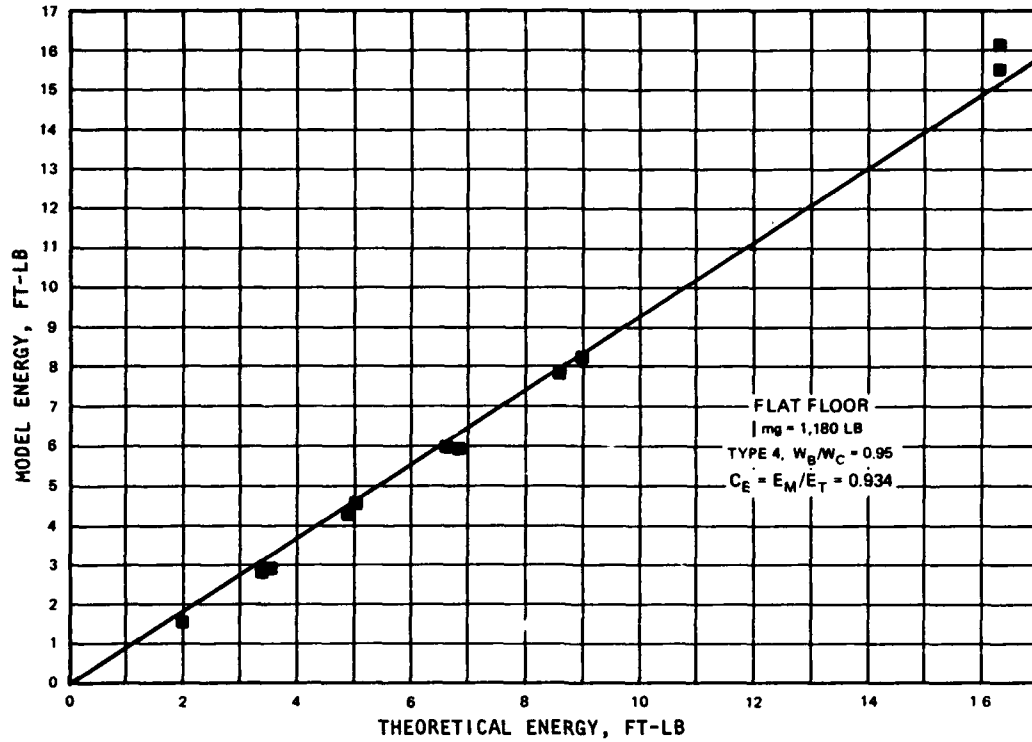


Figure 42. Comparison of experimental to theoretical results,  $C_E$ , type 4 tow

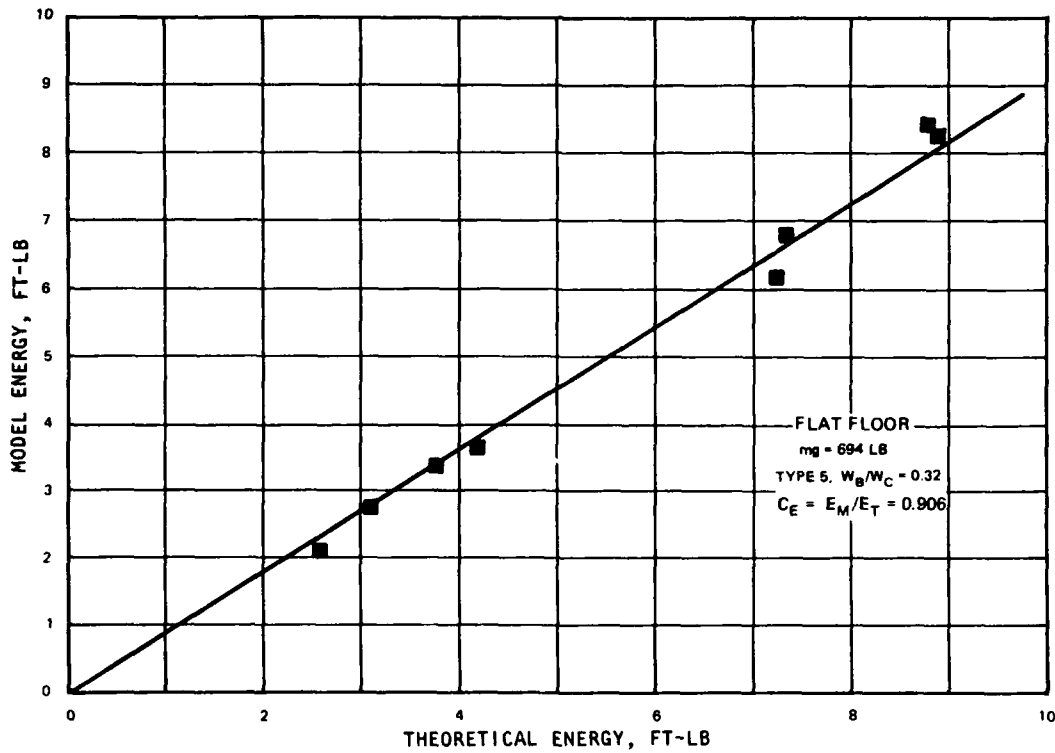


Figure 43. Comparison of experimental to theoretical results,  $C_E$ , type 5 tow

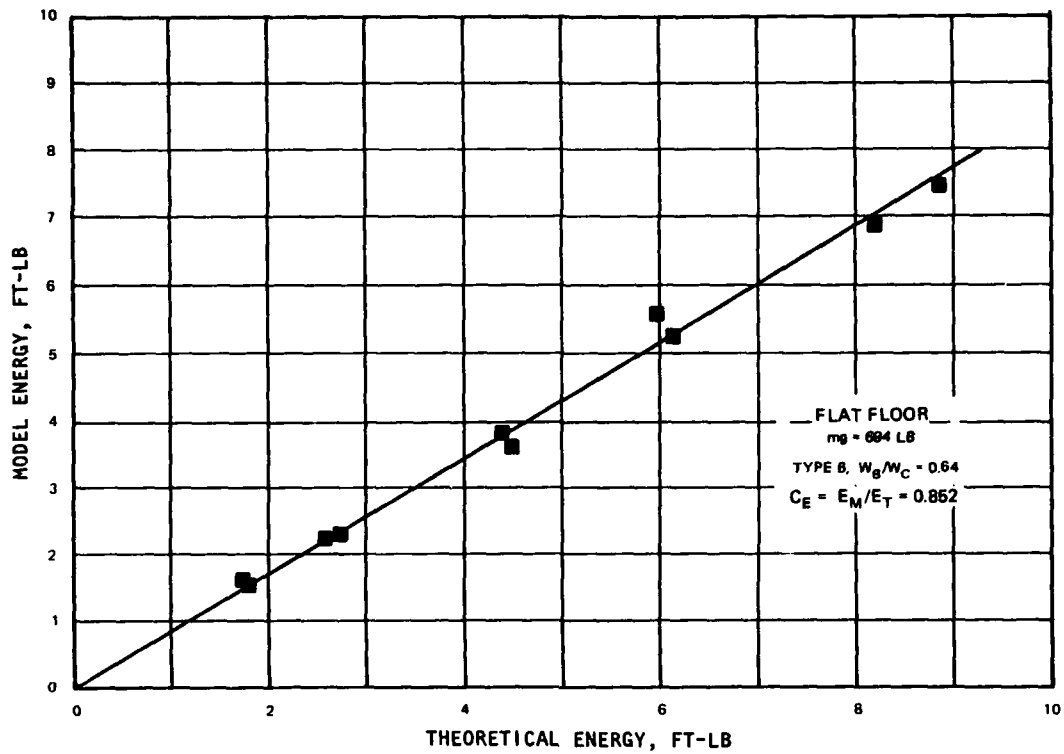


Figure 44. Comparison of experimental to theoretical results,  $C_E$ , type 6 tow

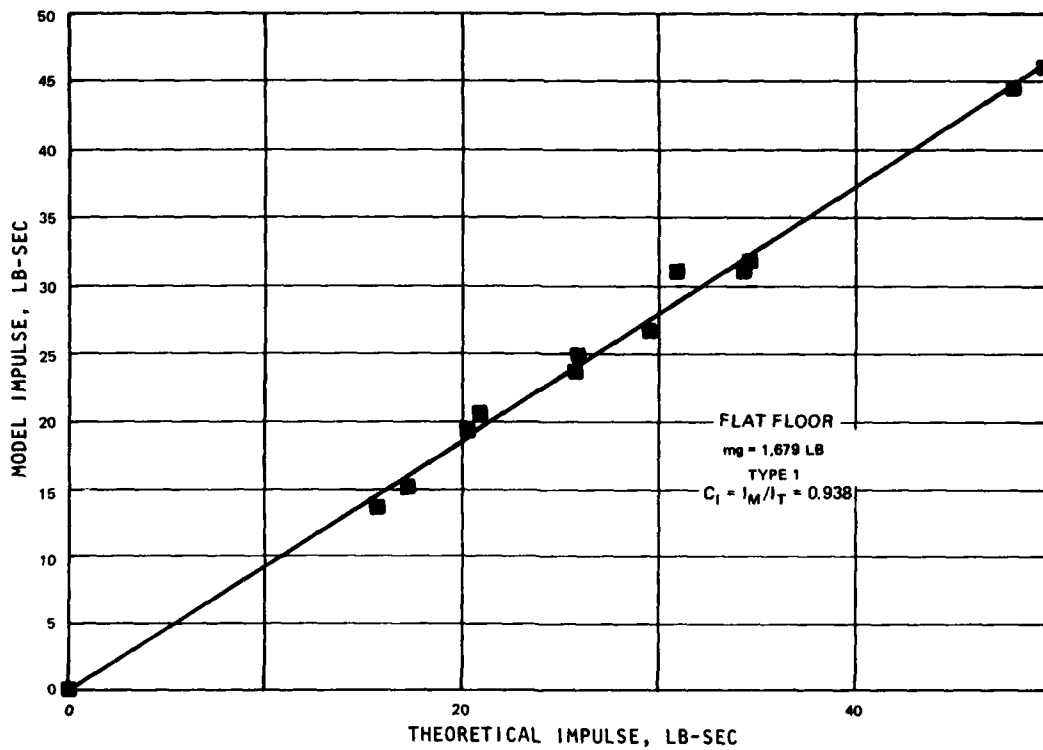


Figure 45. Comparison of experimental to theoretical results,  $C_I$ , flat floor, type 1 tow

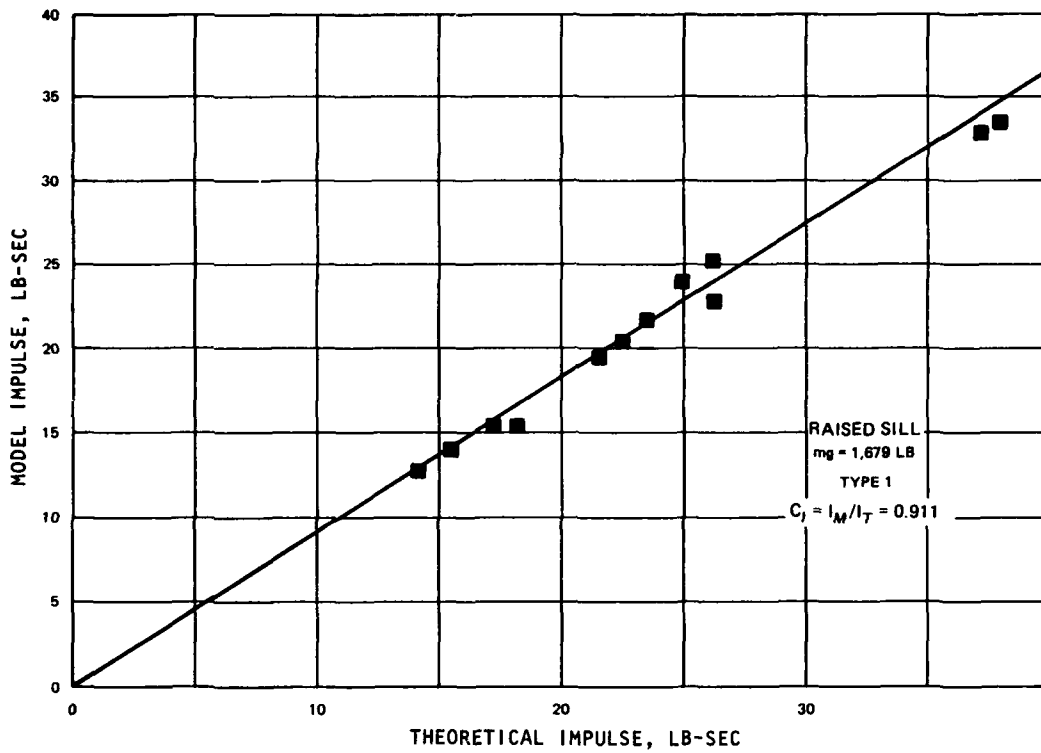


Figure 46. Comparison of experimental to theoretical results,  $C_I$ , raised sill, type 1 tow

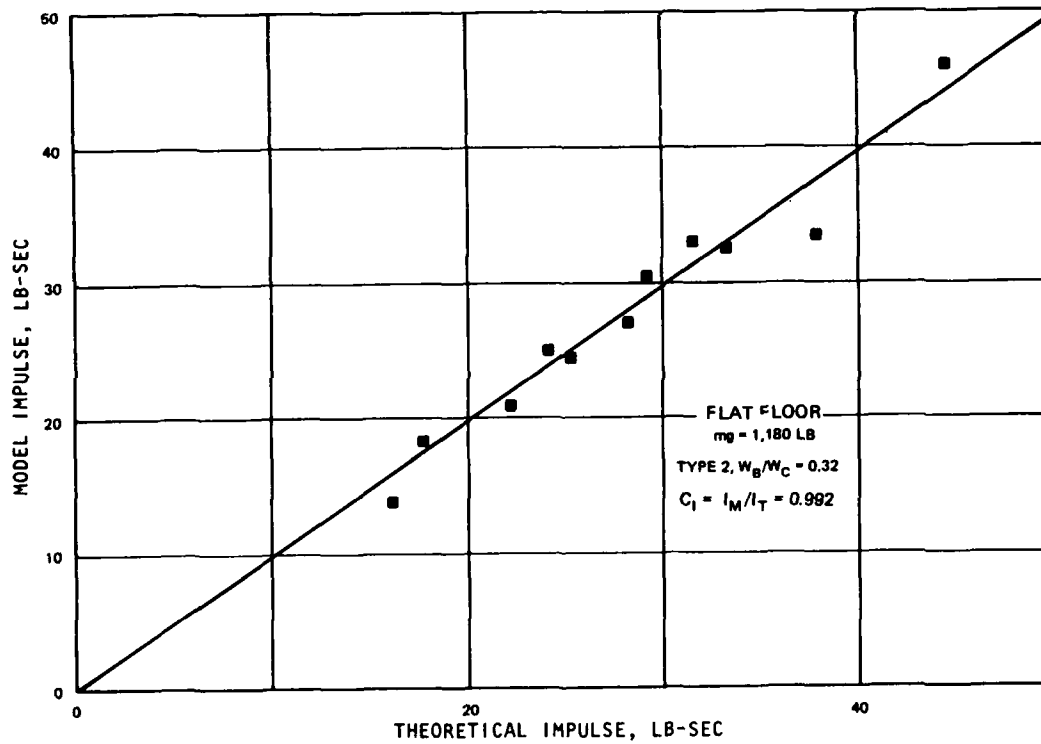


Figure 47. Comparison of experimental to theoretical results,  $C_I$ , type 2 tow

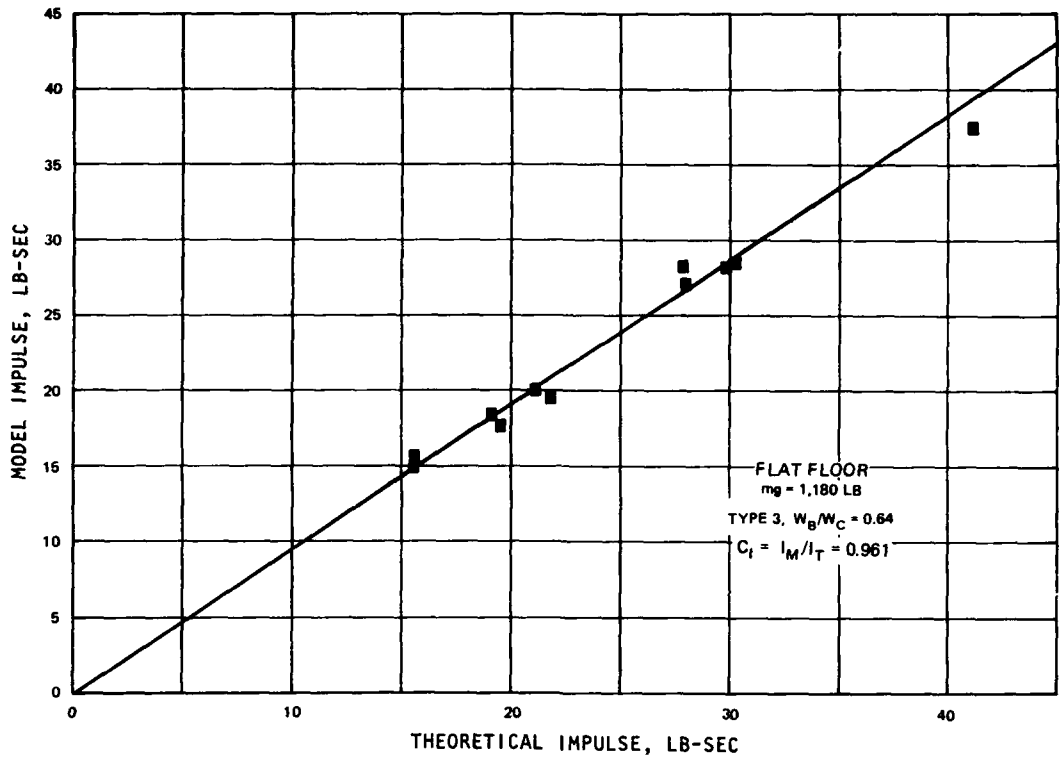


Figure 48. Comparison of experimental to theoretical results,  $C_I$ , type 3 tow

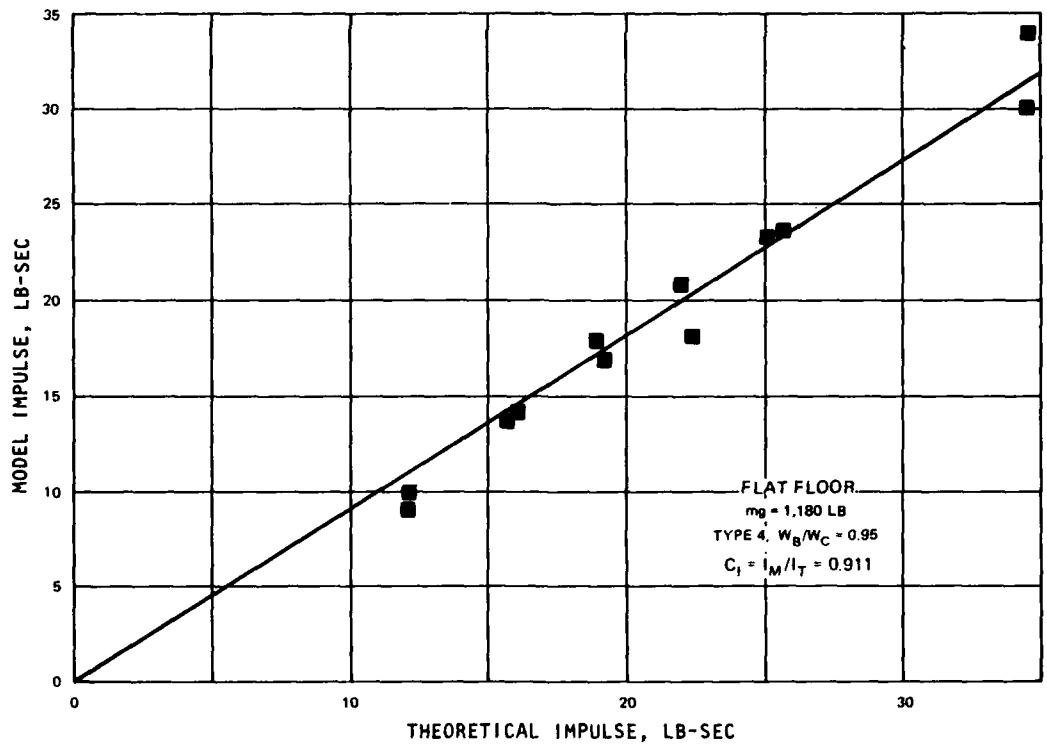


Figure 49. Comparison of experimental to theoretical results,  $C_I$ , type 4 tow

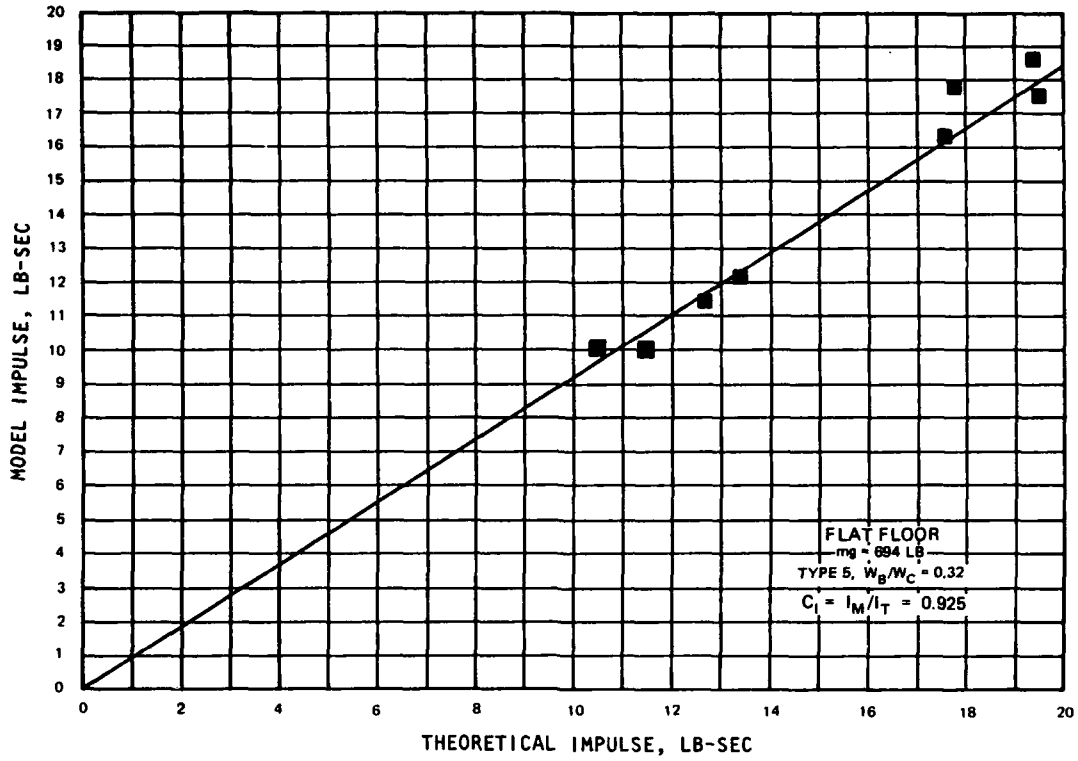


Figure 50. Comparison of experimental to theoretical results,  $C_I$ , type 5 tow

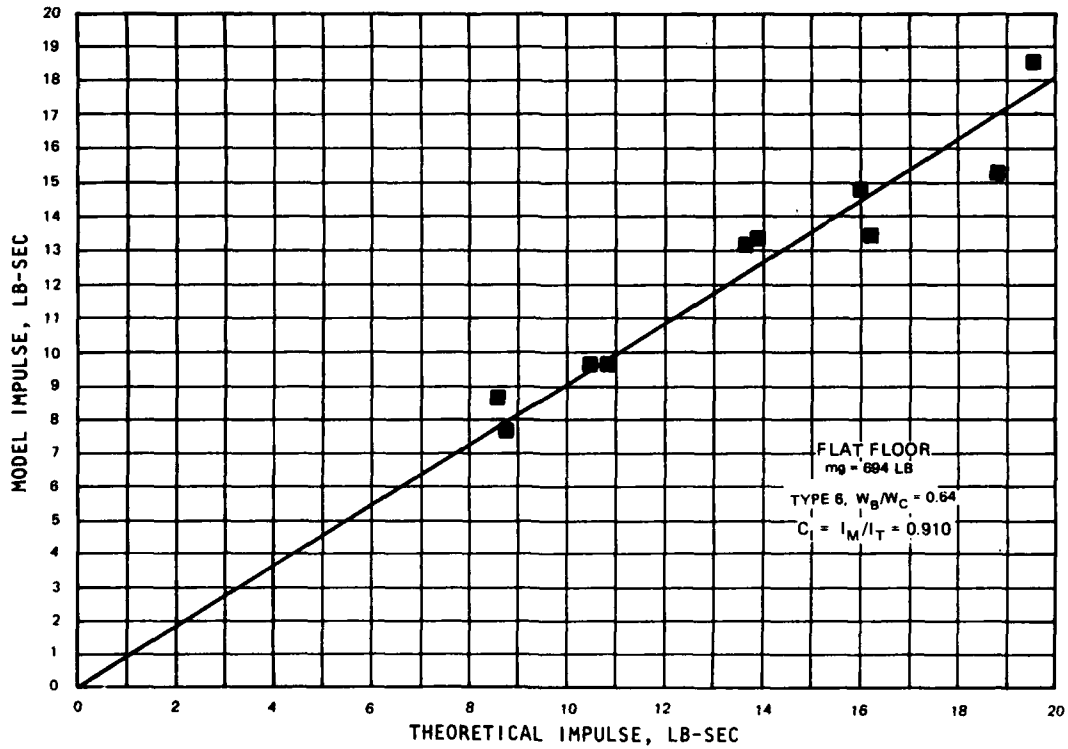


Figure 51. Comparison of experimental to theoretical results,  $C_I$ , type 6 tow

increasing a tow's energy by 10 to 15 percent. The value may be offset due to the increased amount of drag present in the model. It is not expected, however, that the drag could reduce the energy by as much as 20 to 25 percent, which would be implied if the condition of attached mass were valid. The variation in the coefficients may also be explained by possible errors in the data collection and the extraction of parameters such as  $a$  and  $V_0$  for calculation of the theoretical values. If the coefficients times the mass can be assumed to represent an equivalent mass (where the average of the coefficients determined from force, energy, and impulse is 0.96), then equivalent mass would be approximately 96 percent of the tow's mass. Further, assuming the 4 percent offset is due to the model drag, which appears to be a more representative value of these effects, then it can be concluded that the coefficient is closer to 1, and equivalent mass is simply the actual mass of the tow. Based on these comparisons, it must be concluded that energy can be approximated by the theoretical equation of energy  $(1/2)mV_0^2$ .

## PART VIII: CONCLUSIONS

117. The test results indicate that the kinetic energy of the vessel, under the prescribed circumstances of testing, can be calculated directly from the mass of the vessel  $m$  and the expected velocity  $V_0$  at impact by the equation

$$E = \frac{1}{2} mV_0^2 \quad (59)$$

This assumes the coefficient of attached mass equals 1 and does not support increasing the virtual mass by 10 to 15 percent or by any other percentage. The average values of  $C_F$ ,  $C_E$ , and  $C_I$  are, respectively, 1.05, 0.90, and 0.94. These results do not suggest, however, that the mass be decreased according to the coefficient  $C_E$ , since this may falsely represent the phenomenon. Due to the slightly higher drag components typically exhibited in scaled-down models, it is felt that the use of this coefficient may adversely affect the design safety factor.

118. Then, the energy that determines structural design of a barrier to prevent impact to a miter gate can be approximated by the kinetic energy of the tow, provided the design mass and speed just prior to impact are known. Mass is readily quantified since the geometry of locks and/or waterways dictate a maximum size and draft of tow (OCE 1980). As stated before, a vast majority of US locks are filled by a six-barge configuration at a 9-ft draft. Some waterways, such as the Columbia River in the northwest United States, allow for 14-ft drafts and have lock chambers that are 86 ft wide by 650 ft long. In any case, mass can be determined by transportation statistics for a particular lock or waterway.

119. Velocity, on the other hand, is a somewhat more elusive quantity. It has been shown that geometry plays a vital role in the kinematics of the tow. In the model, velocity at precisely the moment of contact could be measured with a high degree of accuracy. Conversely, values of this velocity in the prototype precisely at the gate or precisely at the location of a barrier are unknown. Typical values of tow velocities in channels and statistics on transit times in waterways and through locks are available through several data bases. Ideally, a relationship between tow speed in the channel approach

and tow speed at impact would provide a more feasible estimation of velocity for design, since ranges of the tow speed in the approach do exist. In this model, the length of the approach was insufficient for the tow to obtain a constant sailing speed before entering the lock, preventing the determination of such a relationship. Therefore, only the velocity at impact was used to relate speed to energy and to force. Selection of a design velocity is also theoretically influenced by the limiting velocity, and influenced by issues concerning allowable or permissible entry speeds.

120. Calculated values of force and energy should be used cautiously and in thorough comprehension of the limitations imposed by the test conditions in this model study, listed as follows:

- a. The test cable may or may not be critically located in the chamber to cause a coincidental occurrence of the maximum refracted wave (off the closed miter gates) with the bow of the barge upon contact with the cable.
- b. The angle of approach formed by the tow with the cable, as well as any rotational component of force, was ignored in the model study. These conditions have negligible effects on the resulting force in as much as the typical tows cannot create angles of significance in the lock chamber. Ignoring the angle of approach would not be appropriate in an area where large angular attacks of the bow with the cable could be obtained. A case in point is perhaps in an approach where the guide and guard walls are flared from the lock entrance and where a barrier is being designed at this entrance.
- c. Finally, concluding that the coefficient of attached mass equals 1 is valid only for the drafts, configuration, and ranges of velocities covered in this testing program.

121. It is felt, however, that the force, energy, and impulse exhibited by these tests are representative of true prototype conditions. The selection of the model characteristics, as reiterated from the background and testing procedures chapters, were based on replication of actual conditions relative to chamber dimensions, tow velocities, tow operation, mass and configuration, and the location of the cable with respect to the downstream gate.

122. Testing performed in this model study confirms results obtained from the literature related to the motion of a tow in a confined channel. The wave phenomenon resulting from variable geometric condition can cause the tow to slow and/or surge. Although the transitory wave was not precisely defined in these tests, the relationship of barge widths to chamber width, as well as the lock floor conditions, had a dramatic influence on the speed of the vessel

in the chamber. At the same propeller rotations or tow operation, wider barge trains and installation of the upstream sill resulted in slower impacting speeds than those exhibited by flat floor conditions and narrower barge train widths. The conclusions related to motion were, in fact, similar to those in the literature (Kooman 1973) whereby three basic phenomena were observed:

- a. Small tows are hardly affected by the lock.
- b. High sills slow down the tow.
- c. Entry speeds are irregular with the sill in place.

123. In summary, geometry affects only the kinetic energy of the tow inasmuch as the velocity decreases as the barge width increases, and likewise decreases with a sill in place. The relationship of kinetic energy to the velocity and to the mass of the tow remains intact, such that if attached mass, caused by the translatory wave, does exist, it is either negligible or is negated by resistance forces. Then, the study concludes that the coefficient of attached mass approximates 1; and variable geometric conditions of the lock and barges affect the movement and velocity of the tow in the lock chamber.

## REFERENCES

- Biggs, John M. 1964. Introduction to Structural Dynamics, McGraw-Hill, New York.
- Cabelka, Jaroslav, Cabelka, Jan, Pozimek, J., and Zaruba, J. 1977. "Modern Equipment of Locks Raising the Traffic Capacity and Security of Navigation on Inland Waterways in Czechoslovakia," Proceedings of the 24th International Navigation Congress, Permanent International Association of Navigation Congresses, Leningrad, Section 1, Subject 1, pp 57-74.
- Gelencser, G. J. 1977. "Improving the Effective Capacity of a Navigation System," Proceedings of the 24th International Navigation Congress, Permanent International Association of Navigation Congresses, Leningrad, Section 1, Subject 1, pp 21-40.
- Hausser, R., and Beaudry, J. P. 1969 (Apr). "Welland Canal Lock No. 7, Model Study of the S.A.M. Project," LHL-509, LaSalle Hydraulic Laboratory, LTD, Canada.
- Henderson, F. M. 1966. Open Channel Hydraulics, Macmillan, New York.
- Hibbeler, R. C. 1974. Engineering Mechanics: Dynamics, Macmillan, New York.
- Jackson, J. P., Thomson, A., and Murrer, E. W. 1978 (Sep). "A Ship Arrester System for the Protection of Lock Gates," Proceedings of the 5th International Fluid Power Symposium, British Hydraulic Research Association, Durham, England, No. E3, pp 33-62.
- Jansen, P. Ph., and Schijf, J. B. 1953. Proceedings of the 18th International Navigation Congress, Permanent International Association of Navigation Congresses, Rome, Section 1, Inland Navigation, Communication 1.
- Kapustanskii, S. M., and Marchenko, D. V. 1975. "Theoretical Recommendations for Determination of Attached Masses of Water as Ships Move through a Canal," Translated from the Russian, Trudy LPI, No. 346, Gidroenergetika i Vodnoe Khoziaistvo, pp 63-67.
- Kooman, Ir. C. 1973. "Navigation Locks for Push Tows," No. 16, Rijkswaterstaat Communications, Government Publishing Office, The Hague, The Netherlands.
- Kozak, G. I. 1979 (Nov). "Design of Protective Devices for Navigation Lock-Gates, Employing Hydraulic Shock Dampers," Translated from Gidrotekhnicheskoe Stroitel'stvo, No. 11, pp 30-35.
- Martin, Sandra K. "Interim Guidance on Lock Gate Barrier Systems" (in preparation), REMR Tech Note, US Army Engineer Waterways Experiment Station, Vicksburg, MS.
- \_\_\_\_\_. 1986 (Sep). "Protection of Lock Gates from Vessel Impact," REMR Bulletin, Vol 3, No. 2, US Army Engineer Waterways Experiment Station, Vicksburg, MS.
- \_\_\_\_\_. 1987b (Nov). "Streamlining Data Acquisition and Model Control on a 1:25 Scale Lock Model," Proceedings of the 5th National Conference on Microcomputers in Civil Engineering, University of Central Florida, College of Extended Studies, Orlando, FL.

Maynord, Stephen T. 1987 (Apr). "Safe Navigation Speeds and Clearance at Lower Sill, Temporary Lock 52, Ohio River," Technical Report HL-87-3, US Army Engineer Waterways Experiment Station, Vicksburg, MS.

Office, Chief of Engineers, US Army. 1979 (Apr). "Hydraulic Design of Navigation Locks" (Draft), Engineer Manual 1110-2-1604, US Government Printing Office, Washington, DC.

\_\_\_\_\_. 1980 (Dec). "Layout and Design of Shallow-draft Waterways," Engineer Manual 1110-2-1611, US Government Printing Office, Washington, DC.

Sadovenko, V. V. 1968. "Design of Safety Barriers in Locks," Translated from Russian Rechnoy Transport, No. 5, pp 32-33, Moscow.

\_\_\_\_\_. 1970. "A Study of the Work of Protective Barrages in Front of Navigation Lock Gates," Abstract of M.S. thesis, Translated from Russian, Leningrad Institute of Water Transport, Leningrad.

Shestakov, A. S. 1973a. "Calculation of a Safety Device in the Form of a Flexible Barrier Equipped with Hydraulic Dampers, for Use when Loading Ships," Translated from Russian, Leningrad Institute of Water Technology, No. 140, pp 248-260.

\_\_\_\_\_. 1973b. "Theoretical and Experimental Research into the Operation of Safety Systems to Protect the Gates of Navigational Locks from Vessel Collisions," Master of Technical Sciences thesis, Translated from Russian, Leningrad Institute of Water Transport, Leningrad.

Steidel, Robert F., Jr. 1971. An Introduction to Mechanical Vibrations, Wiley, New York.

Timoshenko, S. P., and Gere, J. M. 1972. Mechanics of Materials, Litton Educational, New York.

Table 1  
Angular Approach

<u>Number of Barges</u>	<u>Configuration</u>	<u>Maximum Offset Angle deg</u>	$\frac{F_y}{F_r}$ <u>cos &lt;</u>
6	Type 1	0.7	0.9999
4	Type 2	4.5	0.9969
4	Type 3	4.1	0.9974
4	Type 4	1.5	0.9997
2	Type 5	7.7	0.9910
2	Type 6	11.9	0.9785

Table 2  
Description of Model Tests

Test No.	File Name	Type of Configuration*	Tow Weight lb	Pool Type**	Midchamber Tow Speed fps
1	B6D9V3A	1	1679.0	Flat	0.3098
2	B6D9V3B	1	1679.0	Flat	0.3326
3	B6D9V4A	1	1679.0	Flat	0.3879
4	B6D9V4B	1	1679.0	Flat	0.4071
5	B6D9V5A	1	1679.0	Flat	0.5019
6	B6D9V5B	1	1679.0	Flat	0.4913
7	B6D9V6A	1	1679.0	Flat	0.5715
8	B6D9V6B	1	1679.0	Flat	0.5883
9	B6D9V7A	1	1679.0	Flat	0.6605
10	B6D9V7B	1	1679.0	Flat	0.6636
11	B6D9V8A	1	1679.0	Flat	0.9397
12	B6D9V8B	1	1679.0	Flat	0.9525
13	SB6D9V3A	1	1679.0	Sill	0.2532
14	SB6D9V3B	1	1679.0	Sill	0.2688
15	SB6D9V4A	1	1679.0	Sill	0.2960
16	SB6D9V4B	1	1679.0	Sill	0.3098
17	SB6D9V5A	1	1679.0	Sill	0.3704
18	SB6D9V5B	1	1679.0	Sill	0.3581
19	SB6D9V6A	1	1679.0	Sill	0.3911
20	SB6D9V6B	1	1679.0	Sill	0.4047
21	SB6D9V7A	1	1679.0	Sill	0.4155
22	SB6D9V7B	1	1679.0	Sill	0.4218
23	SB6D9V8A	1	1679.0	Sill	0.5762
24	SB6D9V8B	1	1679.0	Sill	0.6088
25	B14D9V3A	2	1176.0	Flat	0.4519
26	B14D9V3B	2	1176.0	Flat	0.5000
27	B14D9V4A	2	1176.0	Flat	0.6495
28	B14D9V5A	2	1176.0	Flat	0.6976
29	B14D9V5B	2	1176.0	Flat	0.6606
30	B14D9V6A	2	1176.0	Flat	0.7929
31	B14D9V6B	2	1176.0	Flat	0.8194
32	B14D9V7A	2	1176.0	Flat	0.8779
33	B14D9V7B	2	1176.0	Flat	0.9333
34	B14D9V8A	2	1176.0	Flat	1.2492
35	B22D9V3A	3	1182.0	Flat	0.4351

(Continued)

Note: The barge draft for each test was 0.36 ft.

\* Shown in Figure 9.

\*\* Upstream Sill, Pool Depth to Draft Ratio = 1.5; Flat Floor, Pool Depth to Draft Ratio = 7.3.

Table 2 (Concluded)

Test No.	File Name	Type of Configuration	Tow Weight lb	Pool Type	Midchamber Tow Speed fps	
36	B22D9V3B	3	1182.0	Flat	0.4247	
37	B22D9V4A	↓	1182.0	↓	0.5261	
38	B22D9V4B		1182.0		0.5328	
39	B22D9V5A		0.6075			
40	B22D9V5B		0.5689			
41	B22D9V6A		0.7712			
42	B22D9V6B		0.7609			
43	B22D9V7A		0.8061			
44	B22D9V7B		0.8255			
45	B22D9V8A		1.1076			
46	B4D9V3A		4		1176.0	↓
47	B4D9V3B	↓	↓	0.3275		
48	B4D9V4A			0.4411		
49	B4D9V4B			0.4308		
50	B4D9V5A			0.5429		
51	B4D9V5B			0.5401		
52	B4D9V6A			0.6152		
53	B4D9V6B			0.6364		
54	B4D9V7A			0.6832		
55	B4D9V7B			0.7070		
56	B4D9V8A			↓	↓	0.9925
57	B4D9V8B	1.0019				
58	B2D9V3A	5	693.0			0.4941
59	B2D9V3B	↓	↓			0.5429
60	B2D9V4A					0.6197
61	B2D9V4B					0.6007
62	B2D9V5A					0.8390
63	B2D9V5B					0.8140
64	B2D9V6A					0.9423
65	B2D9V6B					0.9393
66	B21D9V3A			6	694.5	0.4134
67	B21D9V3B			↓	↓	0.3872
68	B21D9V4A					0.4863
69	B21D9V4B	0.4877				
70	B21D9V5A	0.6225				
71	B21D9V5B	0.5929				
72	B21D9V6A	0.7402				
73	B21D9V6B	0.7481				
74	B21D9V7A	0.8911				
75	B21D9V7B	0.8982				

Table 3  
Data Summary, Tests 1-75

Test No.	Weight of the Tow lb	Length of Cable, ft		Maximum y ft	Velocity, fps		T <sub>p</sub>	Tension, lb		Peak Force F lb	Energy E ft-lb	Impulse I lb-sec
		ℓ <sub>1</sub>	ℓ <sub>2</sub>		V <sub>0</sub>	V <sub>c</sub>		T <sub>1</sub>	T <sub>2</sub>			
1	1,679.0	2.4427	2.3073	0.1089	0.3019	0.3098	330.9	523.7	524.9	48.0	2.20	13.74
2		2.4115	2.3385	0.1148	0.3302	0.3326	329.4	541.0	542.6	52.1	2.53	15.20
3		2.4271	2.3229	0.1311	0.3887	0.3879	325.7	577.4	582.7	63.8	3.44	19.48
4		2.3958	2.3542	0.1351	0.4034	0.4071	324.2	587.8	594.7	66.7	3.69	20.85
5		2.3542	2.3958	0.1602	0.4931	0.5019	323.6	654.0	666.5	88.6	5.65	23.69
6		2.3750	2.3750	0.1587	0.4954	0.4913	319.6	649.7	666.4	86.9	5.53	24.92
7		2.4271	2.3229	0.1788	0.5668	0.5715	319.6	707.5	724.5	107.3	7.49	26.69
8		2.3542	2.3958	0.1859	0.5941	0.5883	318.4	734.9	745.8	115.1	8.35	31.19
9		2.4062	2.3438	0.2016	0.6592	0.6605	315.5	783.1	797.3	133.4	10.34	31.22
10		2.3750	2.3750	0.1997	0.6667	0.6636	313.8	771.8	781.9	129.5	9.05	32.08
11		2.3542	2.3958	0.2535	0.9218	0.9397	312.9	1,021.2	1,050.3	219.3	19.77	44.68
12		2.4427	2.3073	0.2623	0.9532	0.9525	297.0	1,059.7	1,088.1	235.3	21.18	45.98
13		2.4167	2.3333	0.0923	0.2709	0.2532	361.8	517.3	517.4	40.0	1.62	12.75
14		2.3438	2.4062	0.1015	0.2959	0.2688	360.0	540.7	542.6	46.2	2.01	14.00
15		2.4010	2.3490	0.1114	0.3297	0.2960	355.9	569.9	567.7	52.9	2.46	15.47
16		2.4375	2.3125	0.1167	0.3488	0.3098	351.6	582.9	583.6	57.2	2.77	15.41
17		2.4375	2.3125	0.1372	0.4314	0.3704	349.6	642.3	652.2	74.4	4.14	20.50
18		2.4062	2.3438	0.1333	0.4128	0.3581	348.4	630.0	633.8	70.8	3.81	19.49
19		2.2812	2.4688	0.1438	0.4508	0.3911	347.0	655.4	666.4	79.8	4.56	21.77
20		2.3542	2.3958	0.1526	0.4781	0.4047	343.9	678.5	690.3	87.3	5.32	24.00
21		2.3854	2.3646	0.1560	0.5040	0.4155	342.9	702.4	712.6	92.7	5.64	22.88
22		2.2927	2.4583	0.1606	0.5020	0.4218	341.6	691.0	700.9	93.3	6.05	25.31
23		2.3646	2.3854	0.2069	0.7129	0.5762	340.7	845.3	865.2	148.5	11.80	32.95

(Continued)

Note: N/A indicates that instrumentation was not sampled for Tests 46-57.

Table 3 (Continued)

Test No.	Weight of the Tow lb	Length of Cable, ft		Maximum y ft	Velocity, fps		a	Tension, lb		Peak Force F lb	Energy E ft-lb	Impulse I lb-sec	
		l <sub>1</sub>	l <sub>2</sub>		V <sub>0</sub>	V <sub>c</sub>		T <sub>p</sub>	T <sub>1</sub>				T <sub>2</sub>
24	1,679.0	2.4167	2.3333	0.2112	0.7278	0.6088	3.000	334.6	866.9	887.7	155.5	12.34	33.56
25	1,176.0	2.3699	2.4166	0.1182	0.4443	0.4519	1.729	399.5	646.2	648	63.8	3.13	13.89
26		2.7449	2.0416	0.1285	0.4889	0.5000	1.773	400.5	688.1	691.3	75.1	3.99	18.43
27		3.0209	1.7656	0.1517	0.6132	0.6495	2.292	389.0	784.4	792.0	107.4	6.28	20.86
28		2.4636	2.3229	0.1708	0.6954	0.6976	3.152	400.5	854.7	864.2	122.5	7.97	24.49
29		2.4896	2.2969	0.1657	0.6632	0.6606	2.958	400.5	836.7	843.8	115.6	7.35	25.21
30		2.4844	2.3021	0.1892	0.7754	0.7929	4.000	400.5	950.0	963.2	151.2	10.60	27.19
31		2.4792	2.3073	0.1942	0.8031	0.8194	3.930	400.5	963.7	975.0	156.4	11.31	30.60
32		2.7657	2.0208	0.2048	0.8651	0.8779	4.140	400.5	1,019.8	1,032.9	179.5	13.48	33.00
33		2.7136	2.0729	0.2133	0.9127	0.9333	4.490	400.5	1,055.0	1,070.0	192.4	14.83	32.60
34		2.5574	2.2291	0.2617	1.2216	1.2492	7.540	389.0	1,335.0	1,363.0	294.3	26.10	46.00
35	1,182.0	2.3230	2.4635	0.1162	0.4252	0.4351	1.686	398.0	619.9	635.4	60.6	2.96	15.84
36		2.2709	2.5156	0.1154	0.4237	0.4247	1.633	398.0	629.2	629.3	60.6	2.92	15.09
37		2.5938	2.1927	0.1353	0.5227	0.5261	2.100	397.3	727.5	719.0	81.9	4.45	18.52
38		2.6094	2.1771	0.1368	0.5367	0.5328	2.165	396.5	725.8	736.3	84.2	4.58	17.74
39		2.1407	2.6458	0.1516	0.5962	0.6075	2.552	398.0	781.9	806.2	101.3	5.98	19.66
40		2.4063	2.3802	0.1486	0.5775	0.5689	2.733	402.2	771.4	769.3	95.5	5.62	20.22
41		2.0990	2.6875	0.1785	0.7649	0.7712	3.455	404.9	927.2	936.8	140.2	9.44	27.28
42		2.5834	2.2031	0.1813	0.7616	0.7609	3.403	403.6	916.9	923.6	139.6	9.57	28.41
43		2.4063	2.3802	0.1900	0.8144	0.8061	4.000	402.3	961.4	988.0	154.1	10.89	28.38
44		2.7397	2.0469	0.1901	0.8255	0.8255	3.800	401.2	964.4	991.1	158.0	11.20	28.67
45		2.2605	2.5260	0.2398	1.1217	1.1076	6.468	389.9	1,244.4	1,287.3	252.7	20.59	37.60
46		2.4636	2.3229	0.0865	0.3316	0.3323	N/A	416.5	564.0	560.0	40.5	1.59	9.96
47	1,176.0	2.4428	2.3437	0.0859	0.3303	0.3275	N/A	416.5	562.0	559.0	40.1	1.54	9.02
48		2.5261	2.2604	0.1129	0.4396	0.4411	N/A	416.5	648.8	645.6	61.1	2.93	14.16
49		2.4428	2.3437	0.1114	0.4295	0.4308	N/A	416.5	637.7	635.5	59.1	2.84	13.73
50		2.4428	2.3437	0.1323	0.5174	0.5429	N/A	416.5	711.0	712.0	78.3	4.28	17.96

(Continued)

Table 3 (Concluded)

Test No.	Weight of the Tow lb	Length of Cable, ft		Maximum y ft	Velocity, fps		a	Tension, lb			Peak Force F lb	Energy E ft-lb	Impulse I lb-sec
		l <sub>1</sub>	l <sub>2</sub>		V <sub>0</sub>	V <sub>c</sub>		T <sub>p</sub>	T <sub>1</sub>	T <sub>2</sub>			
51	1,176.0	2.4115	2.375	0.1364	0.5252	0.5401	N/A	416.5	720.3	720.6	81.9	4.58	16.99
52		2.4219	2.3646	0.1511	0.6013	0.6152	N/A	416.5	787.2	790.7	99.3	5.98	20.83
53		2.4896	2.2969	0.1501	0.6121	0.6364	N/A	416.5	794.5	796.3	99.7	5.96	18.15
54		2.4115	2.3750	0.1693	0.6857	0.6832	N/A	416.5	858.7	861.2	121.3	7.87	23.4
55		2.4636	2.3229	0.1705	0.7015	0.7070	N/A	416.5	873.9	880.3	124.7	8.28	23.67
56		2.4532	2.3333	0.2157	0.9444	0.9925	N/A	416.5	1,088.3	1,105.4	196.9	15.57	30.14
57		2.3594	2.4271	0.2196	0.9450	1.0019	N/A	416.5	1,095.9	1,119.2	202.2	16.22	34.01
58	693.0	2.9239	1.8626	0.0970	0.4894	0.4941	2.050	402.0	592.7	590.3	50.5	2.12	10.06
59		2.5629	2.2236	0.1111	0.5370	0.5429	2.706	402.0	631.5	628.5	58.7	2.76	10.01
60		2.7501	2.0364	0.1244	0.6245	0.6197	3.016	400.0	672.1	677.7	71.7	3.66	12.24
61		2.5834	2.2031	0.1214	0.5920	0.6007	3.018	400.0	659.0	662.9	67.5	3.39	11.48
62		2.6407	2.1458	0.1604	0.8270	0.8390	5.000	400.0	823.4	832.8	111.9	6.79	17.78
63		2.3959	2.3906	0.1537	0.8210	0.8140	5.100	400.0	807.0	816.4	103.9	6.18	16.36
64		2.4844	2.3021	0.1731	0.9048	0.9432	5.667	400.0	869.8	882.1	126.4	8.41	18.64
65		2.4532	2.3333	0.1729	0.9098	0.9393	5.538	400.0	867.9	879.2	126.1	8.27	17.55
66	694.5	2.5782	2.2083	0.0875	0.3997	0.4134	1.869	386.5	534.3	535.4	40.5	1.58	8.67
67		2.1719	2.6146	0.0863	0.4078	0.3872	1.701	385.9	533.5	536.7	38.7	1.49	7.70
68		2.1251	2.6614	0.1033	0.5035	0.4863	2.188	384.6	583.4	591.7	51.4	2.27	9.68
69		2.3751	2.4114	0.1029	0.4894	0.4877	2.407	383.9	580.7	589.0	50.1	2.19	9.67
70		2.2761	2.5104	0.1268	0.6441	0.6225	3.353	383.9	674.6	690.3	72.3	3.59	13.41
71		2.7761	2.0104	0.1269	0.6376	0.5929	3.088	383.9	669.9	683.9	73.4	3.79	13.32
72		2.0157	2.7708	0.1445	0.7451	0.7402	3.750	382.9	742.4	764.1	92.9	5.53	14.86
73		2.6094	2.1771	0.1450	0.7545	0.7481	4.063	381.9	749.2	763.7	92.3	5.21	13.47
74		2.2240	2.5625	0.1670	0.9076	0.8911	5.385	381.1	830.2	858.5	117.5	7.41	18.59
75		1.9844	2.8021	0.1592	0.8733	0.8982	4.560	380.4	810.5	841.5	112.7	6.84	15.31

Table 4  
Experimental to Theoretical Comparisons

Test No.	Force, lb		Energy, ft-lb		Impulse, lb-sec	
	Theory	Model	Theory	Model	Theory	Model
	$F_T$	$F_M$	$E_T$	$E_M$	$I_T$	$I_M$
1	46.82	48.0	2.38	2.20	15.74	13.74
2	51.67	52.1	2.84	2.53	17.22	15.20
3	60.02	63.8	3.94	3.44	20.27	19.48
4	66.06	66.7	4.24	3.69	21.03	20.85
5	87.70	88.6	6.34	5.65	25.71	23.69
6	87.08	86.9	6.40	5.53	25.83	24.92
7	101.42	107.3	8.38	7.49	29.55	26.69
8	119.62	115.1	9.20	8.35	30.98	31.19
9	133.54	133.4	11.33	10.34	34.37	31.22
10	130.36	129.5	11.59	9.05	34.76	32.08
11	221.19	219.3	22.15	19.77	48.07	44.68
12	228.12	235.3	23.69	21.18	49.70	45.98
13	40.31	40.0	1.91	1.62	14.13	12.75
14	45.10	46.2	2.28	2.01	15.43	14.00
15	53.08	52.9	2.83	2.46	17.19	15.47
16	55.58	57.2	3.17	2.77	18.19	15.41
17	74.51	74.4	4.85	4.14	22.49	20.50
18	71.59	70.8	4.44	3.81	21.52	19.49
19	79.36	79.8	5.30	4.56	23.51	21.77
20	86.92	87.3	5.96	5.32	24.93	24.00
21	92.40	92.7	6.62	5.64	26.28	22.88
22	87.08	93.3	6.57	6.05	26.18	25.31
23	145.01	148.5	13.25	11.80	37.17	32.95
24	156.43	155.5	13.81	12.34	37.95	33.56
25	63.15	63.8	3.60	3.13	16.23	13.89
26	64.75	75.1	4.36	3.99	17.86	18.43
27	83.71	107.4	6.87	6.28	22.40	20.86
28	115.12	122.5	8.83	7.97	25.40	24.49
29	108.03	115.3	8.03	7.35	24.22	25.21
30	146.09	151.2	10.98	10.60	28.32	27.19
31	143.53	156.4	11.78	11.31	29.33	30.60
32	151.20	179.5	13.67	13.48	31.59	33.00
33	163.98	192.5	15.21	14.83	33.33	32.60
34	275.37	294.3	27.25	26.10	44.61	46.00
35	61.89	60.6	3.32	2.96	15.61	15.84
36	59.94	60.6	3.29	2.92	15.55	15.09
37	77.09	81.9	5.01	4.45	19.19	18.52
38	79.47	84.2	5.29	4.58	19.70	17.74

(Continued)

Note: N/A indicates that instrumentation was not sampled for Tests 46-57.

Table 4 (Concluded)

Test No.	Force, lb		Energy, ft-lb		Impulse, lb-sec	
	Theory	Model	Theory	Model	Theory	Model
	$F_T$	$F_M$	$E_T$	$E_M$	$I_T$	$I_M$
39	93.68	101.3	6.52	5.98	21.89	19.66
40	100.32	95.5	6.12	5.62	21.20	20.22
41	126.83	140.2	10.74	9.44	28.08	27.28
42	124.92	139.6	10.65	9.57	27.96	28.41
43	146.83	154.1	12.17	10.89	29.90	28.38
44	139.49	158.0	12.51	11.20	30.30	28.67
45	237.43	252.7	23.09	20.59	41.18	37.60
46	N/A	40.5	2.01	1.59	12.11	9.96
47	N/A	40.1	1.99	1.54	12.06	9.02
48	N/A	61.1	3.53	2.93	16.05	14.16
49	N/A	59.1	3.37	2.84	15.69	13.73
50	N/A	78.3	4.89	4.28	18.90	17.96
51	N/A	81.9	5.04	4.58	19.18	16.99
52	N/A	99.3	6.60	5.98	21.96	20.83
53	N/A	99.7	6.84	5.96	22.35	18.15
54	N/A	121.3	8.59	7.87	25.04	23.40
55	N/A	124.7	8.99	8.28	25.62	23.67
56	N/A	196.9	16.29	15.57	34.49	30.14
57	N/A	202.2	16.31	16.22	34.51	34.01
58	44.12	50.5	2.58	2.12	10.53	10.06
59	58.24	58.7	3.10	2.76	11.56	10.01
60	64.91	71.7	4.20	3.66	13.44	12.24
61	64.95	67.5	3.77	3.39	12.74	11.48
62	107.61	111.9	7.36	6.79	17.80	17.78
63	109.76	103.9	7.25	6.18	17.67	16.36
64	121.96	126.4	8.81	8.41	19.47	18.64
65	119.19	126.1	8.91	8.27	19.58	17.55
66	40.31	40.5	1.72	1.58	8.62	8.67
67	36.69	38.7	1.79	1.49	8.80	7.70
68	47.19	51.4	2.73	2.27	10.86	9.68
69	51.91	50.1	2.58	2.19	10.56	9.67
70	72.32	72.3	4.47	3.59	13.89	13.41
71	66.60	73.4	4.38	3.79	13.75	13.32
72	80.88	92.9	5.99	5.53	16.07	14.86
73	87.63	92.3	6.14	5.21	16.27	13.47
74	116.15	117.5	8.88	7.41	19.58	18.59
75	98.35	112.7	8.22	6.84	18.84	15.31

Table 5  
Summary of Empirical Coefficients

<u>Sill</u>	<u>mg, lb</u>	<u><math>W_B/W_C</math></u>	<u><math>C_F</math></u>	<u><math>C_E</math></u>	<u><math>C_I</math></u>
NO	1,679	0.95	1.015	0.893	0.938
YES	1,679	0.95	1.020	0.889	0.911
NO	1,180	0.32	1.110	0.951	0.992
NO	1,180	0.64	1.064	0.903	0.961
NO	1,180	0.95	N/A*	0.934	0.911
NO	694	0.32	1.048	0.906	0.925
NO	694	0.64	1.065	0.852	0.910

---

\* The velocity tachometer was not in operation during this set of tests; therefore, acceleration was not calculated.

APPENDIX A: SUPPLEMENTARY DATA

1. This appendix contains data that was obtained during the model testing but not included in the main report. Data from Tests 76-136 are included in summary Tables A1-A3. In Tests 76-108 the testing apparatus was identical to that described in the main report and shown in Figure 5. The only difference between these tests and those performed in Tests 1-75 is that the draft of the barges was 0.24 ft, consequently affecting their ultimate mass.

2. In Tests 109-136 a different type barge configuration was tested; that is, a nine-barge tow as depicted by Type 7 in Figure A1. Due to the increase in the mass using this barge configuration, a new cable and cell assembly was installed in the model. The primary difference between this assembly and that in the main report is that the cable size and the load cells are larger.

3. Conclusions drawn from these tests reiterate those found in the main report. Table A4, displaying the empirical coefficients obtained from these tests, confirms results presented in Table 5 in the main report.

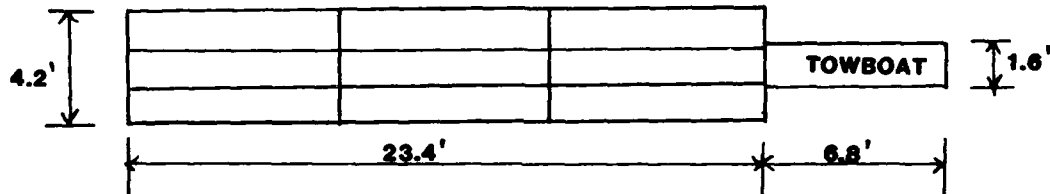


Figure A1. Type 7 barge configuration

Table A1  
Description of Model Tests

Test No.	File Name	Barge Draft ft	Type of Configuration*	Tow Weight lb	Pool Type**	Midchamber Tow Speed fps
76	B32D6V3B	0.24	1	1,124.0	FLAT	0.4155
77	B32D6V3C					0.4317
78	B32D6V4A					0.5137
79	B32D6V4B					0.5092
80	B32D6V5A					0.6364
81	B32D6V5B					0.6605
82	B32D6V5C					0.6061
83	B32D6V6A					0.7036
84	B32D6V6B					0.7779
85	B32D6V7A					0.8188
86	B32D6V7B	0.36	4	803.0	FLAT	0.7823
87	B32D7V7C					0.8046
88	B32D6V8A					1.1767
89	B4D6V3A					0.4001
90	B4D6V3B4					0.4561
91	B4D6V4A4					0.5908
92	B4D6V4B4					0.5129
93	B4D6V5A4					0.7071
94	B4D6V5B4					0.7036
95	B4D6V6A4					0.8001
96	B4D6V6B4	0.36	5	477.0	FLAT	0.7780
97	B4D6V7A4					0.9035
98	B4D6V7B4					0.9092
99	B2D6V3A4					0.6279
100	B2D6V3B4					0.6574
101	B2D6V4A4					0.7780
102	B2D6V4B4					0.7822
103	B2D6V5A4					1.0073
104	B2D6V5B4					1.0221
105	B2D6V6A4					1.1477
106	B2D6V6B4	1.1767				
107	B2D6V7A4	1.3210				
108	B2D6V7B4	1.3087				
109	B9D9V3A6	0.36	7	2,361.0	FLAT	0.2532
110	B9D9V3B6					0.2893
111	B9D9V4A6					0.3407
112	B9D9V4B6					0.3432
113	B9D9V5A6					0.4094
114	B9D9V5B6					0.4131
115	B9D9V6A6					0.4636

(Continued)

\* Shown in Figure 9.

\*\* Upstream Sill, Pool Depth to Draft Ratio = 1.5; Flat Floor, Pool Depth to Draft Ratio = 7.3.

Table A1 (Concluded)

Test No.	File Name	Barge Draft ft	Type of Configuration	Tow Weight lb	Pool Type	Midchamber Tow Speed fps
116	B9D9V6B6	0.36	7	2,361.0	FLAT	0.4862
117	B9D9V7A6	↓	↓	↓	↓	0.5556
118	B9D9V7B	↓	↓	↓	↓	0.5304
119	B9D9V8A	↓	↓	↓	↓	0.7911
120	B9D9V8B	↓	↓	↓	↓	0.7693
121	B9D9V9A	↓	↓	↓	↓	0.8751
122	SB9D9V3A	↓	↓	↓	SILL	0.2006
123	SB9D9V3B	↓	↓	↓	↓	0.1926
124	SB9D9V4A	↓	↓	↓	↓	0.2191
125	SB9D9V4B	↓	↓	↓	↓	0.2212
126	SB9D9V5A	↓	↓	↓	↓	0.2677
127	SB9D9V5B	↓	↓	↓	↓	0.2657
128	SB9D9V6A	↓	↓	↓	↓	0.3366
129	SB9D9V6B	↓	↓	↓	↓	0.3318
130	SB9D9V7A	↓	↓	↓	↓	0.3590
131	SB9D9V7B	↓	↓	↓	↓	0.3618
132	SB9D9V8A	↓	↓	↓	↓	0.5264
133	SB9D9V8B	↓	↓	↓	↓	0.5129
134	SB9D9V9A	↓	↓	↓	↓	0.6335
135	SB9D910A	↓	↓	↓	↓	0.7652
136	SB9D9VWA	↓	↓	↓	↓	1.0372

Table A2  
Data Summary, Tests 76-136

Test No.	Weight of the Tow lb	Length of Cable, ft		Maximum y ft	Velocity, fps		T <sub>p</sub>	Tension, lb		Peak Force F lb	Energy E ft-lb	Impulse I lb-sec
		l <sub>1</sub>	l <sub>2</sub>		V <sub>0</sub>	V <sub>c</sub>		a	T <sub>1</sub>			
76	1,124.0	2.4453	2.3047	0.1076	0.4032	0.4155	1.573	389.3	599.2	54.5	2.48	13.10
77		2.3828	2.3672	0.1206	0.4231	0.4317	1.688	388.8	614.2	62.2	3.15	15.09
78		2.4193	2.3307	0.1319	0.5085	0.5137	2.156	386.8	676.7	75.5	4.03	16.28
79		2.4661	2.2839	0.1282	0.4983	0.5092	2.050	380.8	661.6	71.1	3.74	17.31
80		2.4089	2.3412	0.1565	0.6281	0.6364	2.754	380.8	741.3	96.9	6.14	21.75
81		2.3750	2.3750	0.1577	0.6387	0.6605	2.889	381.3	747.0	99.5	6.24	20.11
82		2.4557	2.2943	0.1534	0.5849	0.6061	2.635	383.3	722.1	93.0	5.71	19.91
83		2.4713	2.2787	0.1671	0.6894	0.7036	3.234	383.3	790.1	112.1	7.38	22.83
84		2.3750	2.3750	0.1795	0.7570	0.7779	3.773	383.3	843.0	128.2	8.78	22.71
85		2.4193	2.3307	0.1938	0.8090	0.8188	4.257	381.3	882.1	145.2	10.72	26.38
86		2.3750	2.3750	0.1854	0.7781	0.7823	4.059	379.4	864.7	135.4	9.57	25.36
87		2.4297	2.3202	0.1967	0.7667	0.8046	3.850	342.2	817.6	134.9	10.02	26.23
88		2.4870	2.2630	0.2377	1.1400	1.1767	6.384	379.4	1,091.3	220.1	19.30	34.98
89	803.0	2.4349	2.3151	0.0945	0.3846	0.4001	1.600	331.0	496.9	39.4	1.61	8.42
90		2.3750	2.3750	0.1067	0.4430	0.4561	1.918	328.0	525.0	47.2	2.12	10.21
91		2.4219	2.3281	0.1261	0.5497	0.5908	2.563	330.0	594.5	63.1	3.23	12.44
92		2.4479	2.3021	0.1186	0.5067	0.5129	2.213	330.0	572.5	57.5	2.76	10.71
93		2.4531	2.2969	0.1506	0.6673	0.7071	3.388	330.0	666.6	85.0	5.13	13.56
94		2.4375	2.3125	0.1575	0.6890	0.7036	3.400	329.5	683.7	91.3	5.71	15.83
95		2.3906	2.3594	0.1681	0.7808	0.8001	4.282	329.5	738.3	104.8	6.83	16.84
96		2.4219	2.3281	0.1627	0.7273	0.7780	3.792	330.0	708.5	97.9	6.23	16.19
97		2.4115	2.3385	0.1828	0.8670	0.9035	4.853	330.0	786.0	121.9	8.51	19.00
98		2.3854	2.3646	0.1817	0.8523	0.9092	4.871	327.5	785.5	120.7	8.35	20.95
99	477.0	2.3072	2.4427	0.1112	0.6129	0.6279	3.500	339.5	553.1	51.8	2.40	7.80
100	477.0	2.3854	2.3646	0.1133	0.6297	0.6574	3.778	336.0	563.7	53.7	2.53	8.32

(Continued)

Table A2 (Continued)

Test No.	Weight of the Tow lb	Length of Cable, ft		Maximum y ft	Velocity, fps			Tension, lb		Peak Force F lb	Energy E ft-lb	Impulse I lb-sec	
		l <sub>1</sub>	l <sub>2</sub>		V <sub>0</sub>	V <sub>c</sub>	a	T <sub>p</sub>	T <sub>1</sub>				T <sub>2</sub>
101	447.0	2.4167	2.3333	0.1349	0.7822	0.7780	5.093	336.0	642.8	650.2	73.2	3.93	10.00
102		2.3490	2.4010	0.1360	0.7578	0.7822	4.857	337.5	630.7	636.3	72.3	3.99	10.00
103		2.5938	2.1563	0.1603	0.9779	1.0073	6.376	337.5	730.0	742.0	99.6	6.24	13.80
104		2.5104	2.2396	0.1626	N/A	1.0221	6.806	337.5	736.5	748.2	101.8	6.53	12.98
105		2.3542	2.3958	0.1838	1.1431	1.1477	8.452	337.5	800.4	807.1	123.8	8.91	15.73
106		2.3646	2.3854	0.1830	1.1341	1.1767	8.519	338.5	800.3	804.6	123.1	8.79	15.49
107		2.5729	2.1771	0.1958	1.3194	1.3210	9.476	338.5	889.5	902.4	148.2	10.72	17.67
108		2.5833	2.1667	0.2045	1.3469	1.3087	10.223	340.0	915.2	926.2	159.2	12.07	18.75
109	2,361.0	2.2603	2.2812	0.0827	0.2687	0.2532	0.748	581.5	796.0	795.6	57.3	2.18	18.56
110		2.2707	2.2708	0.0884	0.2898	0.2893	0.838	576.0	814.3	815.2	62.4	2.56	20.00
111		2.2135	2.3280	0.1056	0.3506	0.3407	1.046	574.0	879.8	876.2	80.1	3.81	25.05
112		2.2340	2.3075	0.1063	0.3523	0.3432	1.096	574.0	876.8	873.4	81.9	3.87	22.86
113		2.2135	2.3280	0.1239	0.4175	0.4094	1.326	570.0	946.5	944.5	102.8	5.49	27.19
114		2.2499	2.2916	0.1246	0.4242	0.4131	1.425	567.5	954.3	952.8	103.3	5.61	28.43
115		2.2603	2.2812	0.1354	0.4737	0.4636	1.622	567.0	1,006.6	996.1	118.7	6.84	32.20
116		2.2707	2.2708	0.1398	0.4932	0.4862	1.707	566.0	1,029.9	1,019.4	125.0	7.37	33.30
117		2.2551	2.2864	0.1591	0.5700	0.5556	2.156	565.0	1,129.5	1,121.4	155.4	10.20	42.50
118		2.2395	2.3020	0.1508	0.5455	0.5304	1.940	559.5	1,093.4	1,081.9	143.0	8.91	35.20
119		2.2655	2.2760	0.2046	0.8077	0.7911	3.500	559.0	1,455.4	1,434.6	258.4	19.99	54.20
120		2.2603	2.2812	0.2018	0.7779	0.7693	3.281	541.5	1,415.2	1,398.4	248.4	18.75	51.70
121		2.2655	2.2760	0.2375	0.9206	0.8751	4.286	435.5	1,594.3	1,564.8	327.3	26.31	63.30
122		2.2290	2.3125	0.0669	0.2051	0.2006	0.564	528.5	679.3	689.2	40.3	1.24	13.43
123		2.1874	2.3541	0.0671	0.2039	0.1926	0.543	527.5	684.0	688.6	40.5	1.26	13.64
124		2.2186	2.3229	0.0729	0.2249	0.2191	0.633	524.5	707.6	711.7	45.4	1.50	13.74
125		2.2707	2.2707	0.0749	0.2341	0.2212	0.622	519.5	704.2	706.6	46.0	1.59	16.83

(Continued)

Table A2 (Concluded)

Test No.	Weight of the Tow lb	Length of Cable, ft		Maximum y ft	Velocity, fps			Tension, lb			Peak Force F lb	Energy E ft-lb	Impulse I lb-sec
		l <sub>1</sub>	l <sub>2</sub>		V <sub>0</sub>	V <sub>c</sub>	a	T <sub>p</sub>	T <sub>1</sub>	T <sub>2</sub>			
126	2,361.0	2.2499	2.2916	0.0908	0.2829	0.2677	0.814	519.5	755.9	755.5	60.4	2.45	18.44
127		2.2342	2.3073	0.0890	0.2783	0.2657	0.765	519.5	745.3	749.5	58.4	2.34	19.25
128		2.2395	2.3020	0.1099	0.3471	0.3366	1.096	519.5	811.2	823.4	78.9	3.81	22.35
129		2.2499	2.2916	0.1086	0.3495	0.3318	1.065	519.0	812.3	823.1	78.0	3.70	21.40
130		2.2290	2.3125	0.1168	0.3737	0.3590	1.150	517.0	837.9	849.5	85.8	4.39	24.44
131		2.1717	2.3698	0.1141	0.3726	0.3618	1.120	514.5	837.8	850.4	84.1	4.16	24.57
132		2.2499	2.2916	0.1580	0.5357	0.5264	1.932	502.5	1,016.3	1,009.9	141.1	9.08	35.00
133		2.2290	2.3125	0.1546	0.5163	0.5129	1.795	495.5	985.8	981.1	133.1	8.41	34.28
134		2.2707	2.2708	0.1708	0.5993	0.6335	2.192	491.5	1,075.6	1,058.7	159.7	10.87	37.50
135		2.2499	2.2916	0.1964	0.7317	0.7652	2.910	485.0	1,244.5	1,252.8	215.4	15.99	46.32
136		2.1769	2.3646	0.2131	0.8077	1.0362	3.226	467.5	1,355.3	1,364.1	252.7	20.01	51.67

Table A3  
Experimental to Theoretical Comparisons

Test No.	Force, lb		Energy, ft-lb		Impulse, lb-sec	
	Theory	Model	Theory	Model	Theory	Model
	$F_T$	$F_M$	$E_T$	$E_M$	$I_T$	$I_M$
76	54.91	54.50	2.84	2.48	14.07	13.10
77	58.92	62.20	3.12	3.15	14.77	15.09
78	75.26	75.50	4.51	4.03	17.75	16.28
79	71.56	71.10	4.33	3.74	17.39	17.31
80	96.13	96.90	6.89	6.14	21.92	21.75
81	100.85	99.50	7.12	6.24	22.29	20.11
82	91.98	93.00	5.97	5.71	20.42	19.91
83	112.89	112.10	8.30	7.38	24.06	22.83
84	131.70	128.20	10.00	8.78	26.42	22.71
85	148.60	145.20	11.42	10.72	28.24	26.38
86	141.69	135.40	10.57	9.57	27.16	25.36
87	134.39	134.90	10.26	10.02	26.76	26.23
88	222.85	220.10	22.68	19.30	39.79	34.98
89	39.90	39.40	1.84	1.61	9.59	8.42
90	47.83	47.20	2.45	2.12	11.05	10.21
91	63.92	63.10	3.77	3.23	13.71	12.44
92	55.19	57.50	3.20	2.76	12.64	10.71
93	84.49	85.00	5.55	5.13	16.64	13.56
94	84.79	91.30	5.92	5.71	17.18	15.83
95	106.78	104.80	7.60	6.83	19.47	16.84
96	94.56	97.90	6.60	6.23	18.14	16.19
97	121.02	121.90	9.37	8.51	21.62	19.00
98	121.47	120.70	9.06	8.35	21.25	20.95
99	51.85	51.80	2.78	2.40	9.08	7.80
100	55.97	53.70	2.94	2.53	9.33	8.32
101	75.45	73.20	4.53	3.93	11.59	10.00
102	71.95	72.30	4.25	3.99	11.23	10.00
103	94.45	99.60	7.08	6.24	14.49	13.80
104	100.82	101.80	0.00	6.53	0.00	12.98
105	125.21	123.80	9.68	8.91	16.93	15.73
106	126.20	123.10	9.53	8.79	16.80	15.49
107	140.37	148.20	12.89	10.72	19.55	17.67
108	151.44	159.20	13.44	12.07	19.95	18.75
109	54.85	57.30	2.65	2.18	19.70	18.56
110	61.44	62.40	3.08	2.56	21.25	20.00
111	76.70	80.10	4.51	3.81	25.71	25.05
112	80.36	81.90	4.55	3.87	25.83	22.86
113	97.23	102.80	6.39	5.49	30.61	27.19
114	104.49	103.30	6.60	5.61	31.10	28.43
115	118.93	118.70	8.23	6.84	34.73	32.20

(Continued)

Table A3 (Concluded)

Test No.	Force, lb		Energy, ft-lb		Impulse, lb-sec	
	Theory	Model	Theory	Model	Theory	Model
	$F_T$	$F_M$	$E_T$	$E_M$	$I_T$	$I_M$
116	125.16	125.00	8.92	7.37	36.16	33.30
117	158.08	155.40	11.91	10.20	41.79	42.50
118	142.25	143.00	10.91	8.91	40.00	35.20
119	256.63	258.40	23.92	19.99	59.22	54.20
120	240.57	248.40	22.18	18.75	57.04	51.70
121	314.26	327.30	31.07	26.31	67.50	63.30
122	41.35	40.30	1.54	1.24	15.04	13.43
123	39.81	40.50	1.52	1.26	14.95	13.64
124	46.41	45.40	1.85	1.50	16.49	13.74
125	45.61	46.00	2.01	1.59	17.16	16.83
126	59.68	60.40	2.93	2.45	20.74	18.44
127	56.09	58.40	2.84	2.34	20.41	19.25
128	80.36	78.90	4.42	3.81	25.45	22.35
129	78.09	78.00	4.48	3.70	25.63	21.40
130	84.32	85.80	5.12	4.39	27.40	24.44
131	82.12	84.10	5.09	4.16	27.32	24.57
132	141.66	141.10	10.52	9.08	39.28	35.00
133	131.61	133.10	9.77	8.41	37.86	34.28
134	160.72	159.70	13.17	10.87	43.94	37.50
135	213.37	215.40	19.63	15.99	53.65	46.32
136	236.54	252.70	23.92	20.01	59.22	51.67

Table A4  
Summary of Empirical Coefficients

<u>Sill</u>	<u>mg, lb</u>	<u><math>\frac{W_B}{W_C}</math></u>	<u><math>C_F</math></u>	<u><math>C_E</math></u>	<u><math>C_I</math></u>
NO	1,124	0.95	0.995	0.917	0.935
NO	803	0.95	1.013	0.920	0.900
NO	477	0.32	1.023	0.913	0.920
NO	2,361	0.95	1.027	0.849	0.937
YES	2,361	0.95	1.017	0.839	0.887

APPENDIX B: NOTATION

Symbol	Definition
a	Acceleration
A	Cross-sectional area
$A_c$	Cross-sectional area of cable
$A_s$	Cross-sectional area of swivel
$C_E$	Coefficient of energy
$C_F$	Coefficient of force
$C_I$	Coefficient of impulse
d	Position of the tow with respect to the cable
dT	Change in tension as a function of cable elongation
E	Energy; modulus of elasticity
$E_M$	Model energy
$E_T$	Theoretical energy
$E_{TOTAL}$	Energy measured in model
F	Force in y-direction
$F_M$	Model force
$F_{peak}$	Peak model force, $F_M$
$F_r$	Resultant force formed by translation angle
$F_T$	Theoretical force
$F_y$	Force in the y-direction or F
I	Impulse
$I_M$	Model impulse
$I_T$	Theoretical impulse
$I_{TOTAL}$	Impulse at peak force
KE	Kinetic energy
$l$	Half-length of cable
$l_1$	Length of cable from contact point to reaction hinge at cell 1

<u>Symbol</u>	<u>Definition</u>
$l_2$	Length of cable from contact point to reaction hinge at cell 2
$l_x$	Length of cell and swivel assembly
$l_{1x}, l_{2x}$	Length of cable from contact point to end of swivel
$m$	Mass of vessel
PE	Potential energy
$t$	Time
$t_0$	Time when tow initially contacts the cable
$t_1$	Time when the peak force occurs
T	Tension
$T_1$	Tension corresponding to cell 1
$T_2$	Tension corresponding to cell 2
$T_p$	Pretension in cable
$v$	Velocity
$v_c$	Midchamber velocity of vessel
$v_0$	Velocity of vessel just prior to impact
$v_1$	Velocity at peak displacement
W	Work
$W_B$	Width of barge train
$W_c$	Width of chamber
$y$	Deflection or displacement
$\dot{y}$	First derivative of displacement
$\ddot{y}$	Second derivative of displacement
$\delta_c$	Elongation in the cable only
$\delta_s$	Elongation in the swivel only
$\delta_t$	Total elongation of cable assembly
$\theta$	Angle formed by cable at impact

<u>Symbol</u>	<u>Definition</u>
$\theta_1$	Angle formed by cable corresponding to cell 1
$\theta_2$	Angle formed by cable corresponding to cell 2